NASA TECHNICAL MEMORANDUM

NASA TM X-62,171

NASA TM X-62,171

WIND–SENSITIVITY STUDIES OF A NON–RETURN WIND TUNNEL, WITH A 216– BY 432–MM (8.5– BY 17.0–IN) TEST SECTION – PHASE I

William T. Eckert, Kenneth W. Mort, and J. E. Piazza

Ames Research Center
and
U.S. Army Air Mobility R&D Laboratory
Moffett Field, Calif. 94035

September 1972

110p

NOTATION

B	semiwidth of model test section, mm
C	center direction probe
C_P,CP	test-section pressure coefficient, $\frac{P_{T_o} \text{ or } P_{S_o} - P_{S_w}}{Q_o}$
H	semiheight of model test section, mm
lc	contraction length: distance from inlet lip to test section (see figure 2(a)), cm
P	port direction probe
P_{S_o}	test-section static pressure, mm of water
P_{S_w}	wind static pressure, mm of water
P_{T_o}	test-section total pressure, mm of water
P_{T_w}	wind total pressure, mm of water
Q_o,QO	test-section dynamic pressure, (average P_{T_o}) - (average P_{S_o}), mm of water
Q_w,QW	wind dynamic pressure, $P_{T_w} - P_{S_w}$, mm of water
R	radius
S	starboard direction probe
TH.S	test-section sideflow angle, θ_s (positive for air from port), deg
TH.U	test-section upflow angle, θ_u, deg
V	test-section velocity, knots
V_w	wind velocity, knots
Y	horizontal distance from test-section center line (positive starboard), mm
Z	vertical distance from test-section center line (positive up), mm

ΔP total tunnel pressure loss; average static pressure rise across the fans (increment from no-wind condition), mm of water

ΔP_I inlet pressure loss, (P_{S_w}) - (average P_{T_o}), mm of water

$\frac{\Delta Q_*}{Q_o}$ test section dynamic pressure variation over 75% of B and H, $(C_{P_{total}} - C_{P_{static}})_{Q_w \neq 0} - (C_{P_{total}} - C_{P_{static}})_{Q_w = 0}$ local maximum, with the faired curved shifted such that $\frac{\Delta Q_*}{Q_o}$ was defined as zero when $Q_w = 0$

Δu maximum deviation from the mean axial velocity over 75% of the width on the horizontal center line and of the height on the vertical center line of the test section; the wind off value is subtracted from the wind on value, $\frac{V}{2} \frac{\Delta Q_*}{Q_o}$, knots

Δv maximum lateral velocity on the center line; the wind off value is subtracted from the wind on value, positive to the starboard, $V \frac{\theta_s}{57.3}$, knots

Δw maximum vertical velocity on the center line; the wind off value is subtracted from the wind on value, positive up, $V \frac{\theta_u}{57.3}$, knots

θ_s test-section sideflow angle (positive for air from port), deg

θ_u test-section upflow angle, deg

ψ azimuth angle of model center line with respect to wind axis (positive for wind from port), deg

WIND-SENSITIVITY STUDIES OF A NON-RETURN WIND TUNNEL WITH A 216- BY 432-MM (8.5- BY 17.0-IN) TEST SECTION - PHASE I

William T. Eckert, Kenneth W. Mort, and J. E. Piazza

Ames Research Center

and

U.S. Army Air Mobility Research & Development Laboratory

SUMMARY

The purpose of this study was to develop inlet and exit treatments which would minimize the effect of external wind on the test-section flow quality of a non-return wind tunnel. The investigation was conducted in the Ames Research Center 40- by 80-Foot Wind Tunnel which served as the wind source. Several inlets and two exits were tested at wind directions ranging from 0 to 180 degrees and at wind-to-test-section velocity ratios between zero and one.

For the best inlet configuration the flow quality was good, with a velocity deviation in each of the three directions generally less than ½ knot (0.26 m/sec) for wind velocities of 15 knots (7.7 m/sec) or less. The loss in total pressure due to the inlet treatment was low: about 0.03 of the test-section dynamic pressure.

INTRODUCTION

The NASA has been investigating the usefulness and practicability of a new full-scale V/STOL wind tunnel. During these studies the feasibility of using a non-return wind tunnel configuration was established.

There are two advantages that a non-return wind tunnel has over a closed-circuit tunnel: (1) no purging of contaminants such as engine exhaust gases and heated tunnel air is required; and (2) the structural cost is potentially less.

Non-return tunnels can be made to have good power efficiency (ref. 1). However, because of the open ends, the flow quality may be adversely affected by external winds. It has been generally found that although shielding can be used at the ends to significantly reduce the effects of winds, this treatment caused large losses in power (refs. 2 through 4). In view of this, model studies were initiated to develop effective wind shielding with an emphasis on minimizing power losses and structural costs. The first phase of this investigation is reported herein.

MODEL DESCRIPTION

General

The model installed in the Ames 40- by 80-Foot Wind Tunnel is shown in figure 1, and dimensions and geometry are given in figure 2 and table I.

The basic inlet protection consisted of a large area with a flat-oval planform enclosed by a perforated plate with 40-percent porosity and and the solid roof supported by streamlined vertical posts (figures 2(a) and 3(a)). A constant-area section with square-celled flow straighteners (figure 3(b)) was located just upstream of the contraction section (figure 3(c)). Alternate flow straighteners, contraction cone (figure 3(d)) and inlet screens were studied and are listed in table II.

The basic exit shown in figure 2(a) was a vertical-exhaust section equipped with turning vanes. An alternate exit which consisted of a horizontal screened section is shown in figures 1 and 2(a).

Instrumentation

The vertical and transverse locations of the total and static pressure probes and the direction rake in the test section are shown in figure 4. The pressure probes were located in a plane 63.5 mm (2.5 in), or 14.7 percent of the test-section length, downstream of the test-section entrance or about 190.5 mm (7.5 in) downstream of the start of the constant-area section. The static pressure rise across the fans was measured by orifices located 0.3 fan diameters ahead of and behind the fan in each nacelle.

TEST PROCEDURE

The test program was conducted with the model elevated from the 40- by 80-Foot Wind Tunnel test-section floor (out of the boundary layer) on legs as shown in figures 1(b) and 2(b). The centerline of the model was set at selected azimuth angles, measured from the wind axis, to simulate various wind directions.

The model test-section dynamic pressure was set initially at about ten inches of water with the external wind at zero dynamic pressure. The subsequent measurements were made with the wind held steady according to the following schedule.

Approximate test section dynamic pressure Q_o, mm of water	Approximate wind dynamic pressure Q_w, mm (in) of water	Nominal Q_w/Q_o
254.0 (10)	0 (0)	0
254.0 (10)	2.5 (0.1)	0.01
254.0 (10)	6.4 (0.25)	0.025
254.0 (10)	12.7 (0.5)	0.05
254.0 (10)	25.4 (1.0)	0.1
101.6 (4)	25.4 (1.0)	0.25
50.8 (2)	25.4 (1.0)	0.5
50.8 (2)	50.8 (2.0)	1.0
101.6 (4)	50.8 (2.0)	0.5
254.0 (10)	50.8 (2.0)	0.2

Reduction of Data

The pressure data were measured using multiple-tube manometers and recorded photographically. Flow-angularity data, total-pressure loss measurements and test-section dynamic pressure variation values were determined by subtracting the zero-wind values from the wind-on values and hence are the variations due only to the effects of external winds. The local dynamic pressures used to determine $\frac{\Delta Q_*}{Q_o}$ were found by linear interpolation of local pressure coefficient values.

Accuracy of Measurements

The azimuth angles were set with an accuracy of about ± 2 degrees.

The pressure readings which were used to determine the pressure coefficients, pressure ratios and angularities were accurate to about ± 1.27 mm (± 0.05 in) of water. The effect of this on the accuracy of data presented in the figures was determined for the values of Q_o corresponding to the schedule of Q_w/Q_o values shown in the section on TEST PROCEDURE. For convenience, these accuracies are shown as functions of Q_w/Q_o in sketch (a).

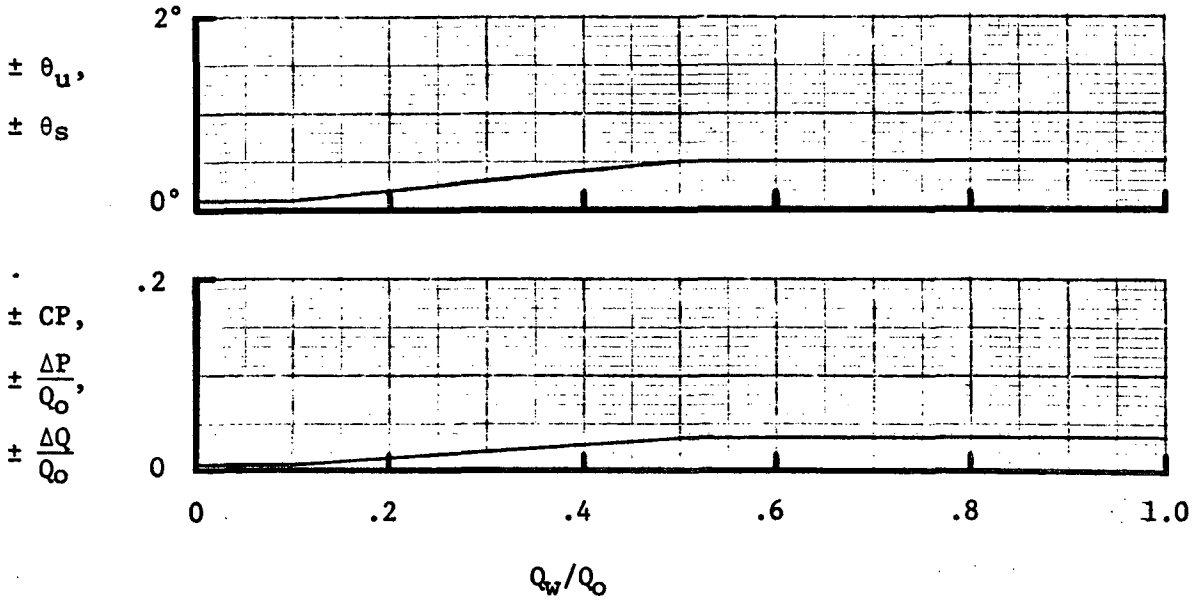

SKETCH (a)

4

RESULTS

The plotted data are indexed in table II by configuration. The basic data are presented in figures 5 through 21. Included are test-section flow angularities as functions of dynamic pressure ratio, pressure coefficients as functions of test-section location, and inlet and total pressure losses as functions of dynamic pressure ratio. The following results are shown in summary plots: the effects of wind direction on the test-section flow for the basic configuration (figure 22), the effects of variation of inlet components (figures 23 through 26), the effect of exit type (figure 27), and the comparison with flow quality criteria (figure 28).

To evaluate the flow quality of the basic configuration the flow quality criteria of reference 5 were used. Figure 28 compares the experimental results with these criteria at several wind conditions. It is evident that for the basic configuration the test section velocity deviation in each of the three directions was generally less than ½ knot (0.26 m/sec) for wind velocities of 15 knots (7.7 m/sec) or less. At more severe wind conditions the test-section flow characteristics exceeded the criteria. Figure 28(b) shows that the flow quality is sensitive to wind direction. The axial velocity component appears to be the most critical aspect of external winds since this criterion is exceeded more often.

It is highly likely that further improvements will be derived from optimization of inlet components. For example, the configuration described in reference 5, which had small modifications made to the inlet, had significantly better flow quality.

REFERENCES

1. Krishnaswamy, T. N.; Ramachandra, S. M.; and Krishnamoorthy, V.: Design and Characteristics of 14- by 9-Foot Open Circuit Wind Tunnel, Proc. of Seminar on Aeronautical Sciences, N.A.L., Bangalore, 1961.

2. Anderson, C. F.; and Carleton, W. E.: Effects of External Winds on a 1/40-Scale Model of the Open-Circuit Configuration of the Proposed AEDC Multipurpose Low-Speed Wind Tunnel. AEDC-TR-69-231, 1970.

3. Kirk, J. A.: Experience With a V/STOL Tunnel. Journal of the Royal Aeronautical Society, Vol. 71, No. 681, September, 1967, pp 606-622.

4. Leef, C. R.; and Hendry, R. G.: Development of a Nonrecirculating Wind Tunnel Configuration Insensitive to External Winds. Journal of Aircraft, Vol. 6, No. 3, May-June 1969, pp 221-227.

5. Mort, Kenneth W., Eckert, William T., and Kelly, Mark W.: The Steady-State Flow Quality of a Model of a Non-Return Wind Tunnel. NASA TM X-62,170, 1972.

TABLE I.- MODEL DIMENSIONS FOR THE BASIC CONFIGURATION

Test section area, sq m (sq in)	0.083	(128.8)
Inlet and exit screens		
Porosity, percent	40	
Hole diameter, mm (in)	3.175	(0.125)
Flow area at start of fan nacelle contraction, sq m (sq in)	0.402	(623.0)
Flow area at fans, sq m (sq in)	0.224	(347.0)
Fan diameter, mm (in)	213.4	(8.4)
Number of fans	8	
Vertical exit		
Area ratio	8:1	
Turning vanes		
shape: 90° circular arcs, constant thickness, and leading and trailing edges rounded		
chord along arc, mm (in)	79.76	(3.14)
gap, mm (in)	19.05	(0.75)
thickness, mm (in)	3.175	(0.125)

TABLE II.- INDEX TO DATA FIGURES

FIGURE NUMBER	COMMENTS	$-\psi$ (DEG)	CONFIGURATION						
			INLET						EXIT TYPE
			SCREEN[1]	CONTRACTION RATIO	CONTRACTION 1c[1]	LIP RADIUS[1]	FLOW STRAIGHTENERS[1]	ROOF POSTS	
BASIC DATA									
5-7	Basic Configuration	0 to -157½	107x254(42x100)	8:1	135(53)	5.1(2)	2.54x2.54(1x1)	In	Vert
8-10	Modified Configuration	0 to 180	↓	↓	↓	↓	↓	Out	↓
11-13	↓	↓	58x203(23x80)	↓	↓	↓	↓	↓	↓
14-16		↓	61x178(24x70)	4.8:1	112(44)	10.2(4)	6.6x9.4(2.6x3.7)	↓	↓
17(a-c)		90	107x254(42x100)	8:1	135(53)	5.1(2)	10.2x10.2(4x4)	↓	↓
18(a-c)		↓	↓	↓	↓	↓	Out	In	↓
19(a-c)		↓	↓	↓	185(73)	↓	2.54x2.54(1x1)	Out	↓
20(a-c)		↓	Off	4.8:1	112(44)	10.2(4)	6.6x9.4(2.6x3.7)	↓	↓
21	↓	0,90,180	107x254(42x100)	8:1	135(53)	5.1(2)	2.54x2.54(1x1)	↓	Horiz
SUMMARY PLOTS									
	Effect of:								
22(a-d)	Azimuth Angle	0 to -157½	107x254(42x100)	8:1	135(53)	5.1(2)	2.54x2.54(1x1)	In	Vert
23(a,b)	Contraction Ratio	0,135	58x203(23x80)	8:1	135(53)	5.1(2)	2.54x2.54(1x1)	Out	Vert
	↓	↓	61x178(24x70)	4.8:1	112(44)	10.2(4)	6.6x9.4(2.6x3.7)		↓
24(a-c)	Flow Straighteners	90	107x254(42x100)	8:1	135(53)	5.1(2)	Out	In	Vert
	↓	↓	↓	↓	↓	↓	2.54x2.54(1x1)	↓	↓
							↓	Out	
							10.2x10.2(4x4)	↓	
25(a,b)	Inlet Screen Size	0,45	107x254(42x100)	8:1	135(53)	5.1(2)	2.54x2.54(1x1)	Out	Vert
	↓	↓	58x203(23x80)	↓	↓	↓	↓	↓	↓
26(a,b)	Roof Support Posts	0,90	107x254(42x100)	8:1	135(53)	5.1(2)	2.54x2.54(1x1)	Out	Vert
	↓	↓	↓	↓	↓	↓	↓	In	↓
27	Exit Type	0,90,180	107x254(42x100)	8:1	135(53)	5.1(2)	2.54x2.54(1x1)	Out	Vert
	↓	↓	↓	↓	↓	↓	↓	↓	Horiz
28(a,b)	Flow Quality Evaluation	0 to -157½	107x254(42x100)	8:1	135(53)	5.1(2)	2.54x2.54(1x1)	In	Vert

[1]Dimensions given in cm (in).

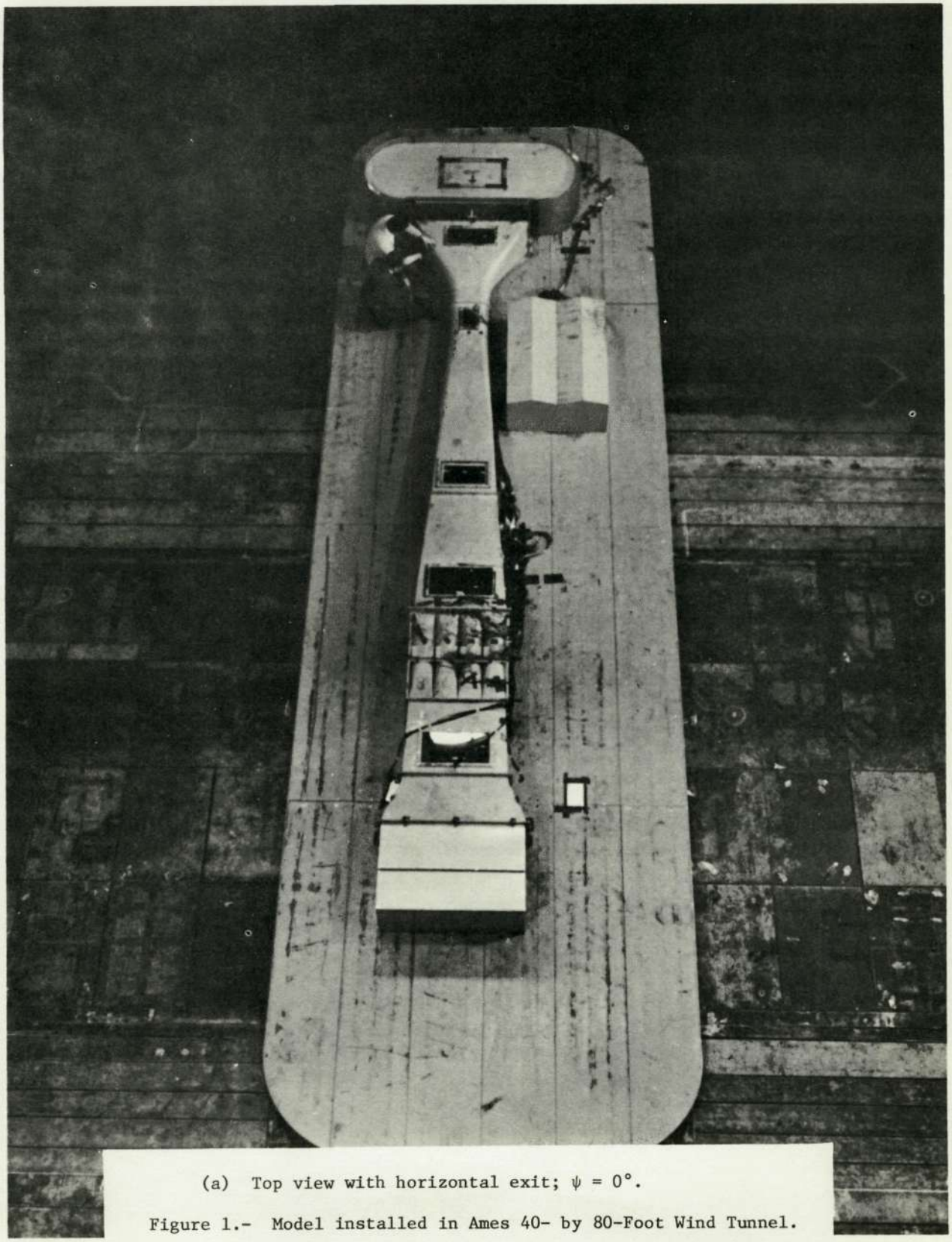

(a) Top view with horizontal exit; $\psi = 0°$.

Figure 1.- Model installed in Ames 40- by 80-Foot Wind Tunnel.

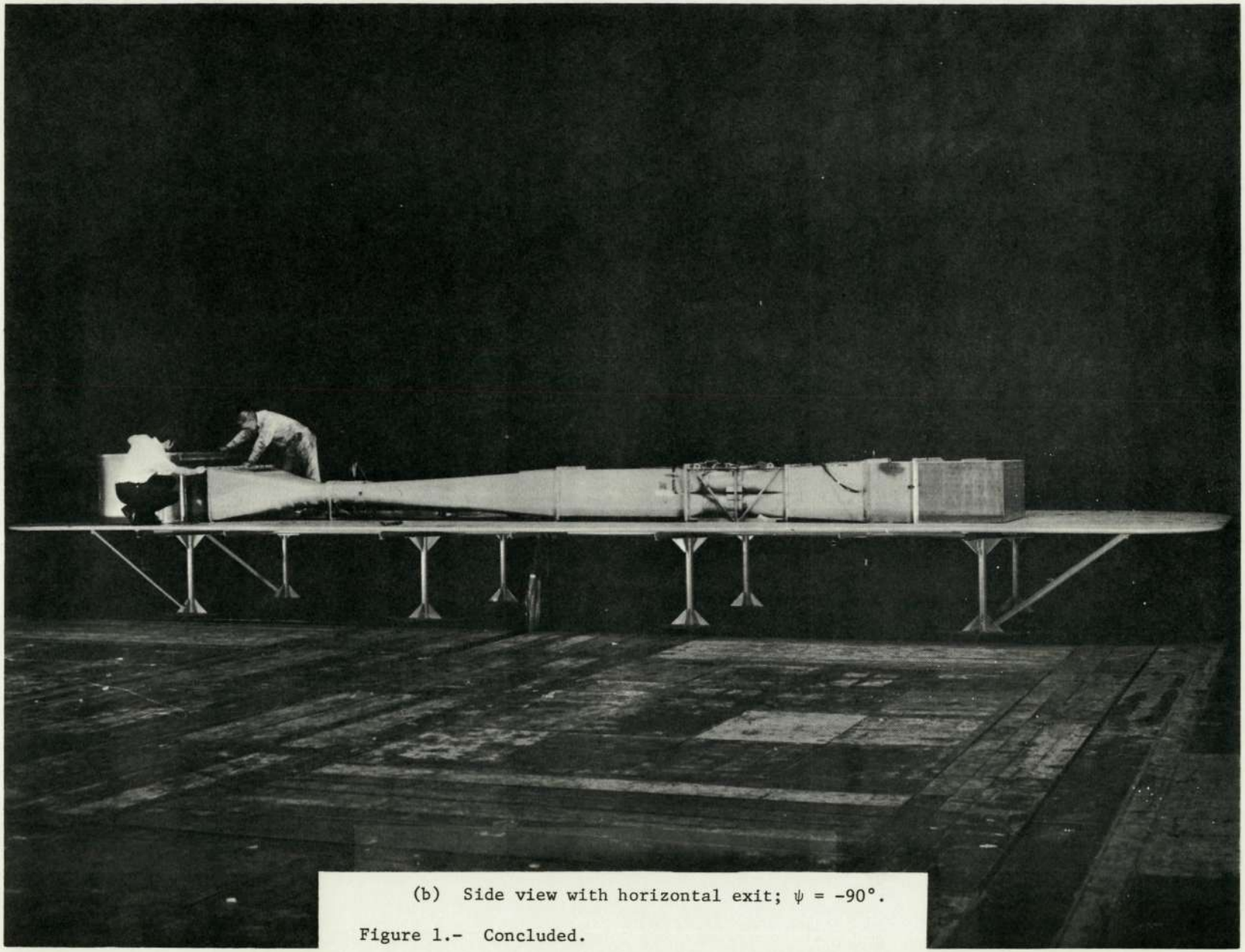

(b) Side view with horizontal exit; $\psi = -90°$.

Figure 1.- Concluded.

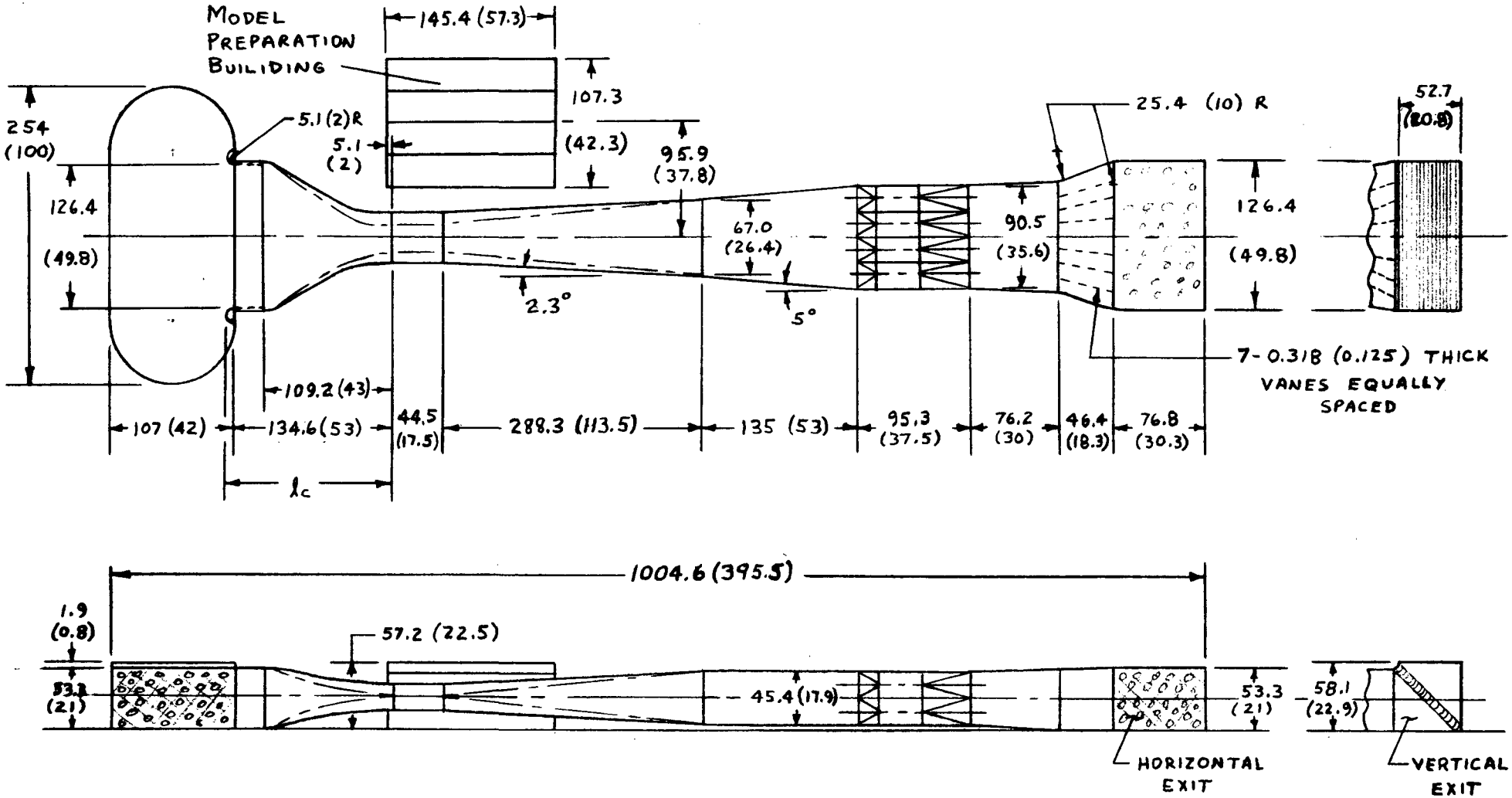

INSIDE DIMENSIONS SHOWN.

DIMENSIONS IN CM (IN).

(a) Model geometry.

Figure 2.- Dimensions for basic configuration.

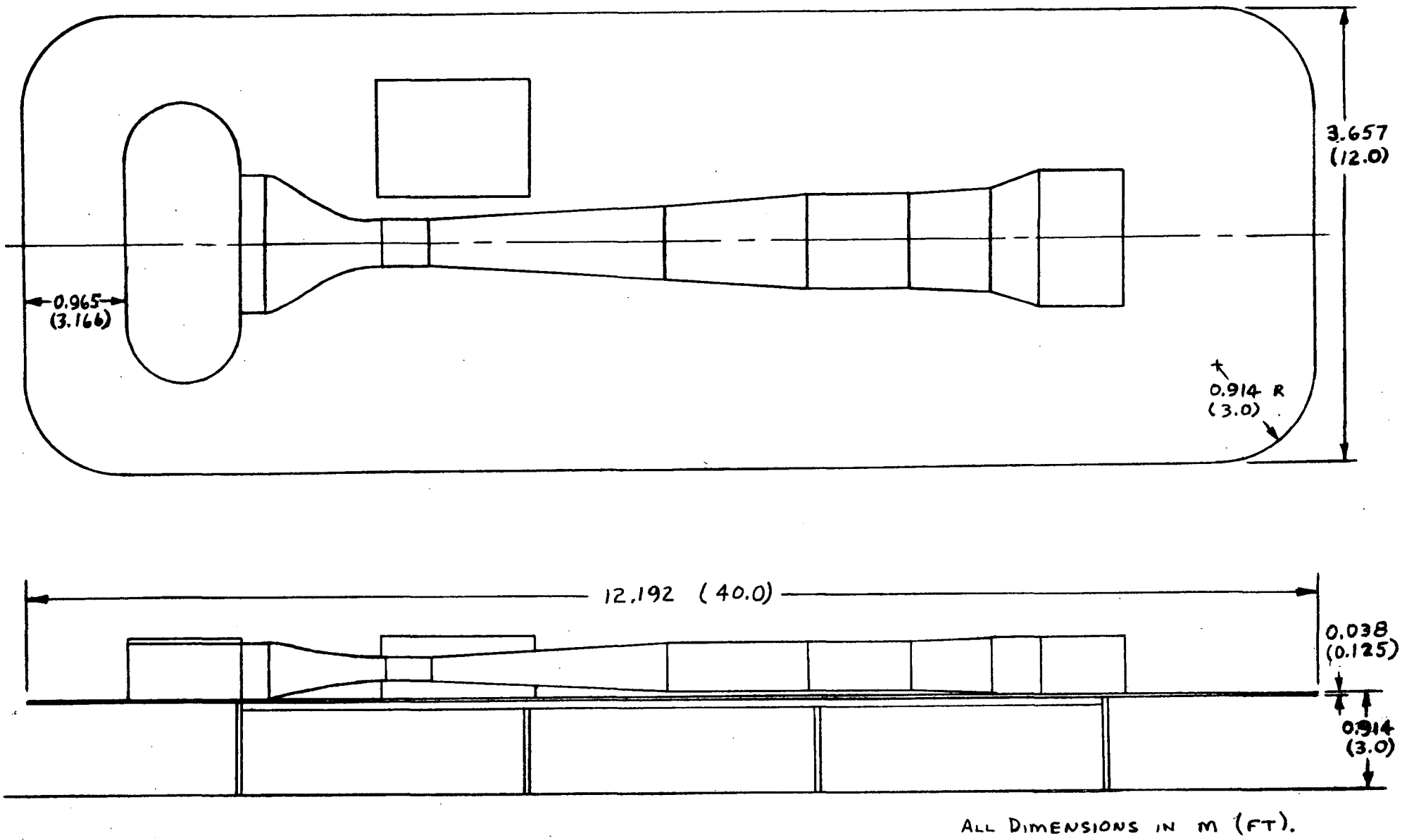

(b) Orientation on groundboard.

Figure 2.- Concluded.

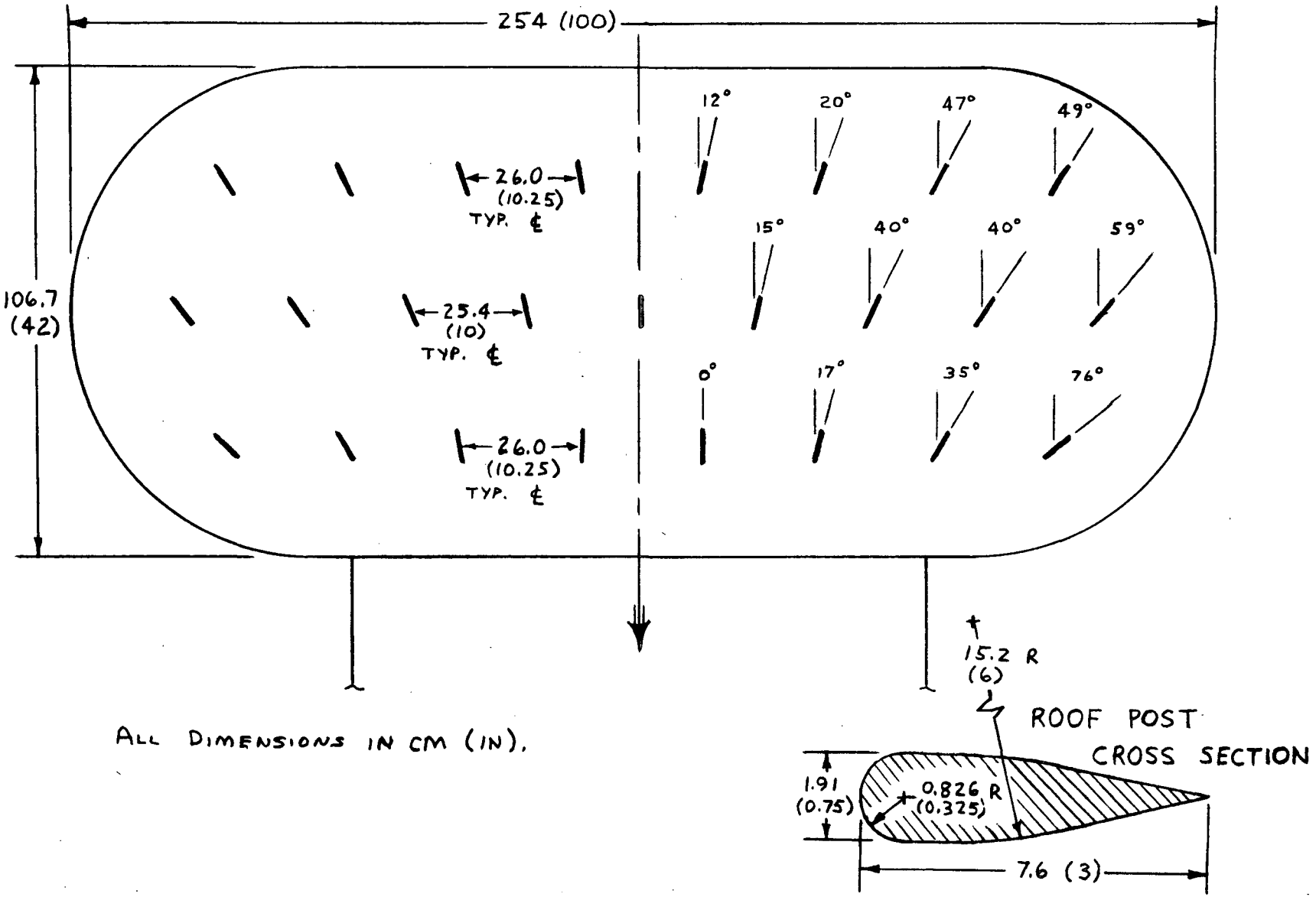

(a) Inlet screen and roof posts.

Figure 3.- Inlet component dimensions.

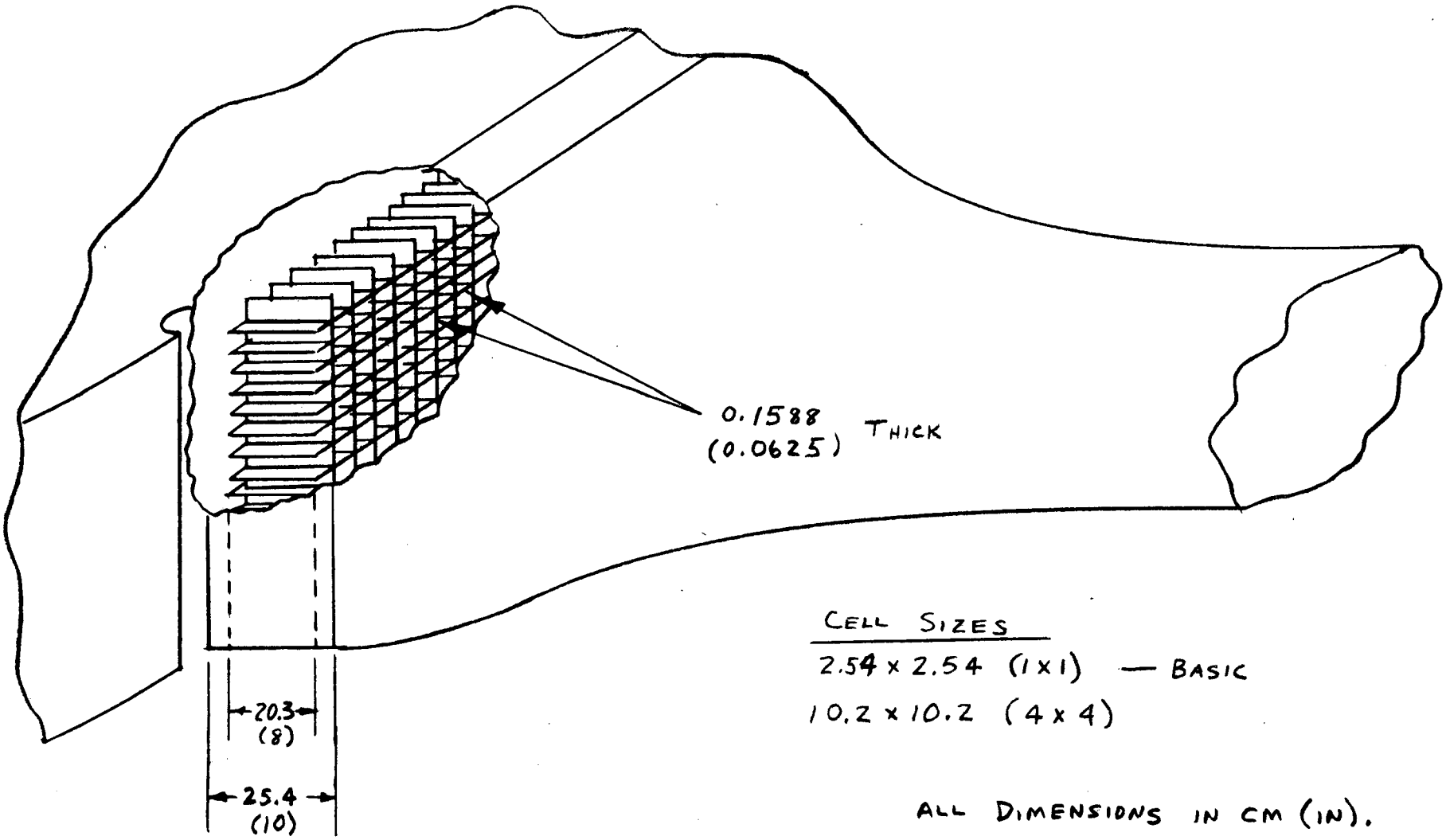

(b) Flow straighteners in 8:1 contraction.

Figure 3.- Continued.

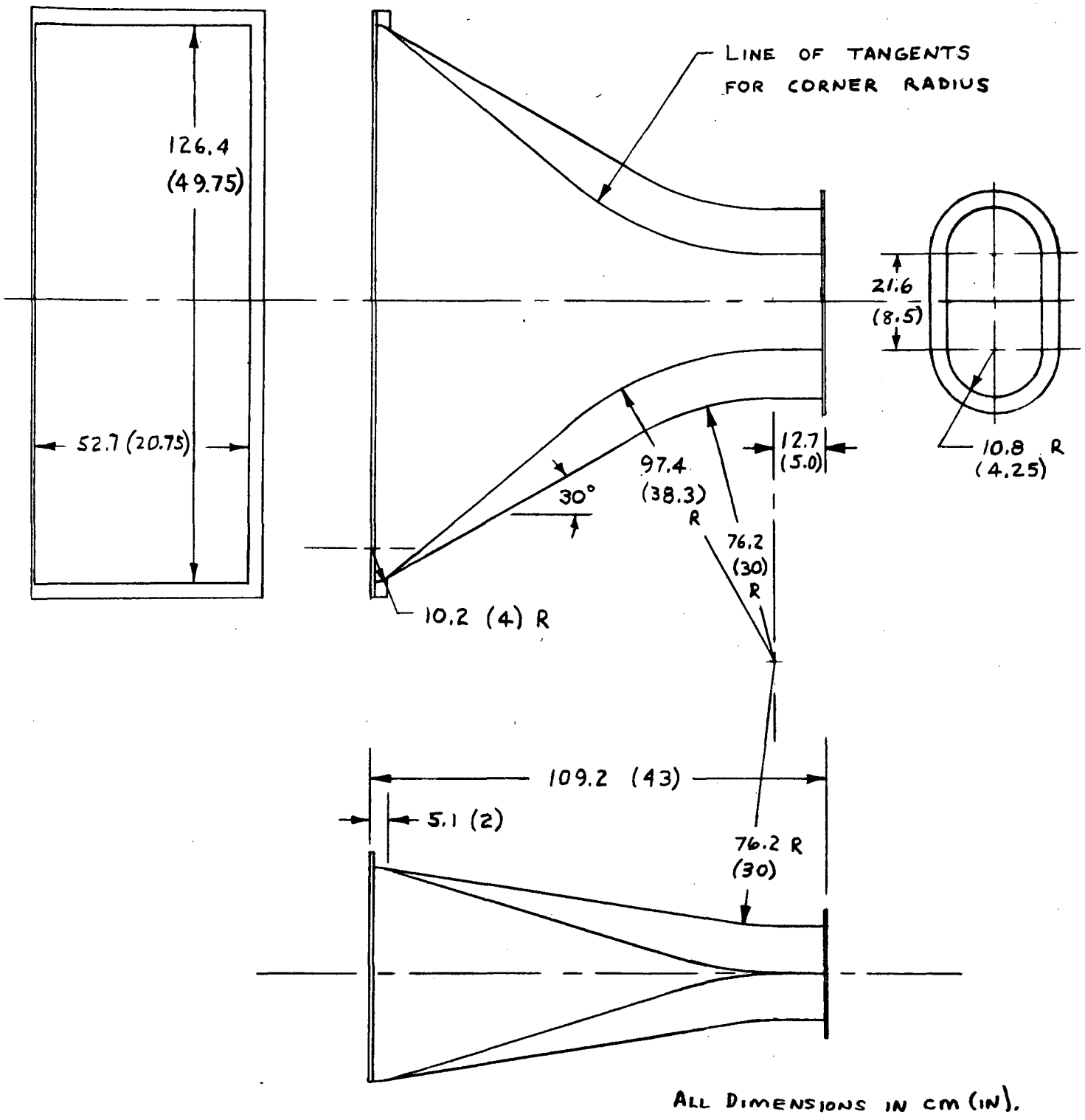

(c) 8:1 contraction.

Figure 3.- Continued.

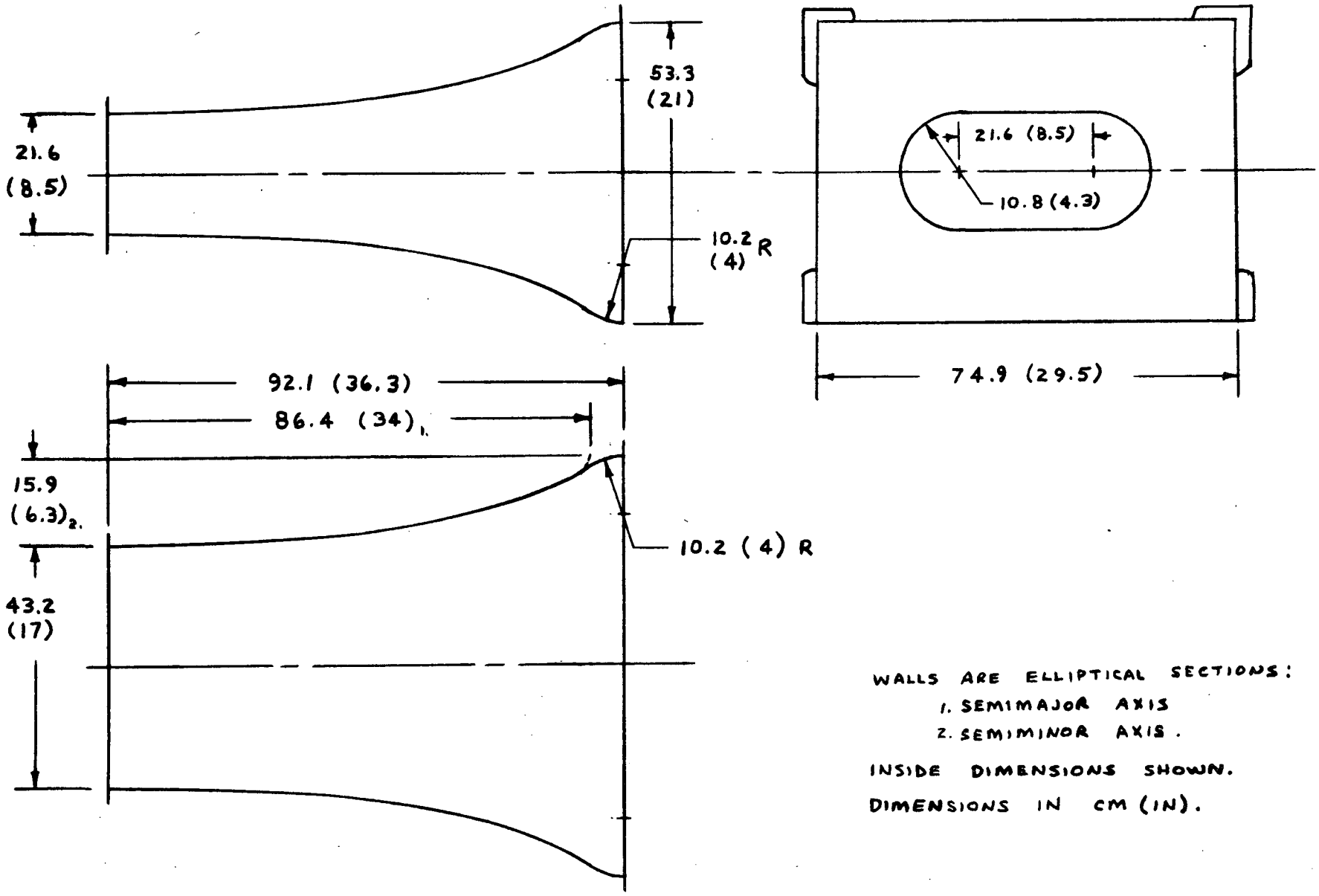

(d) 4.8:1 contraction.

Figure 3.- Concluded.

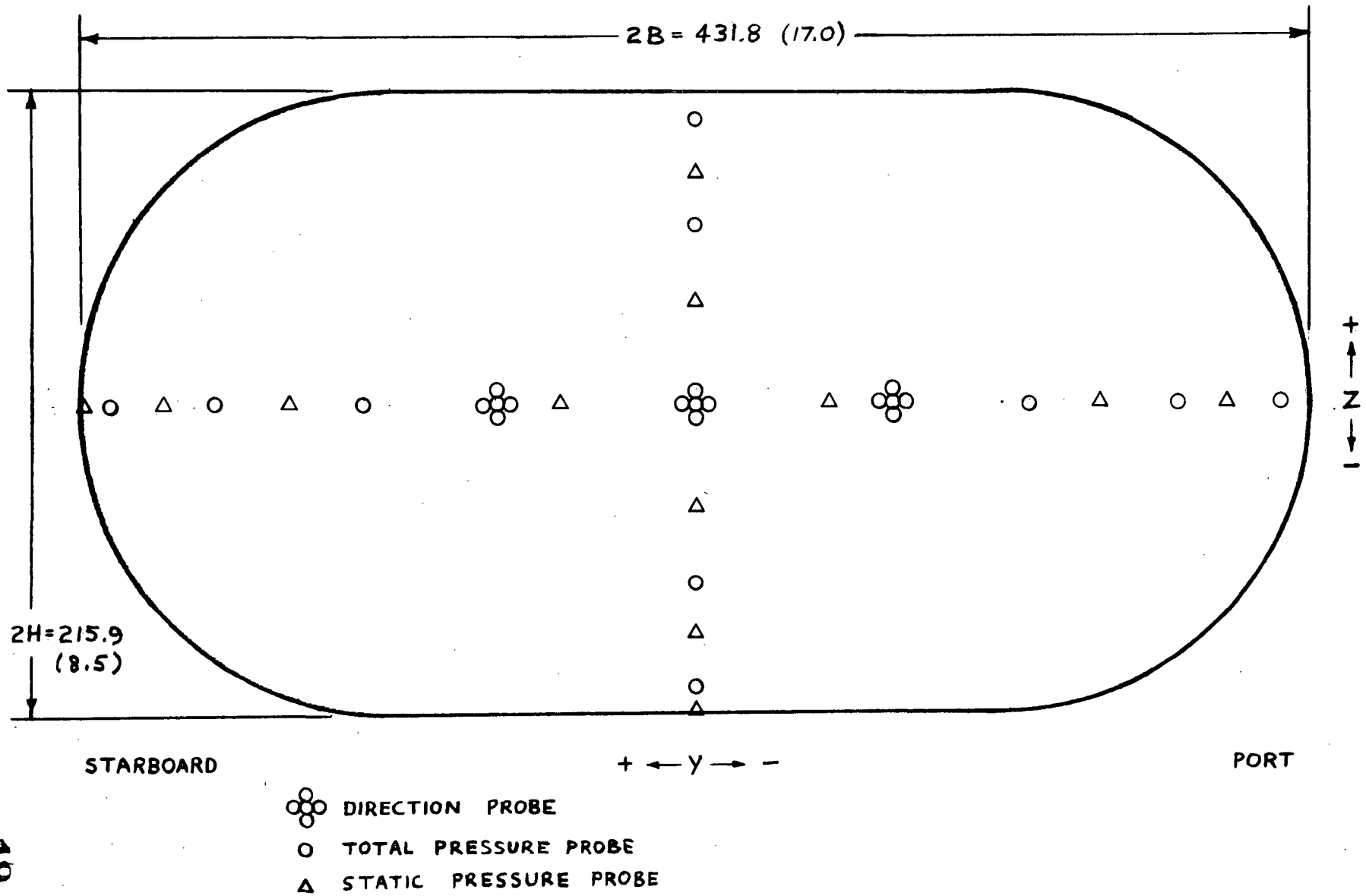

Figure 4.- Test section instrumentation.

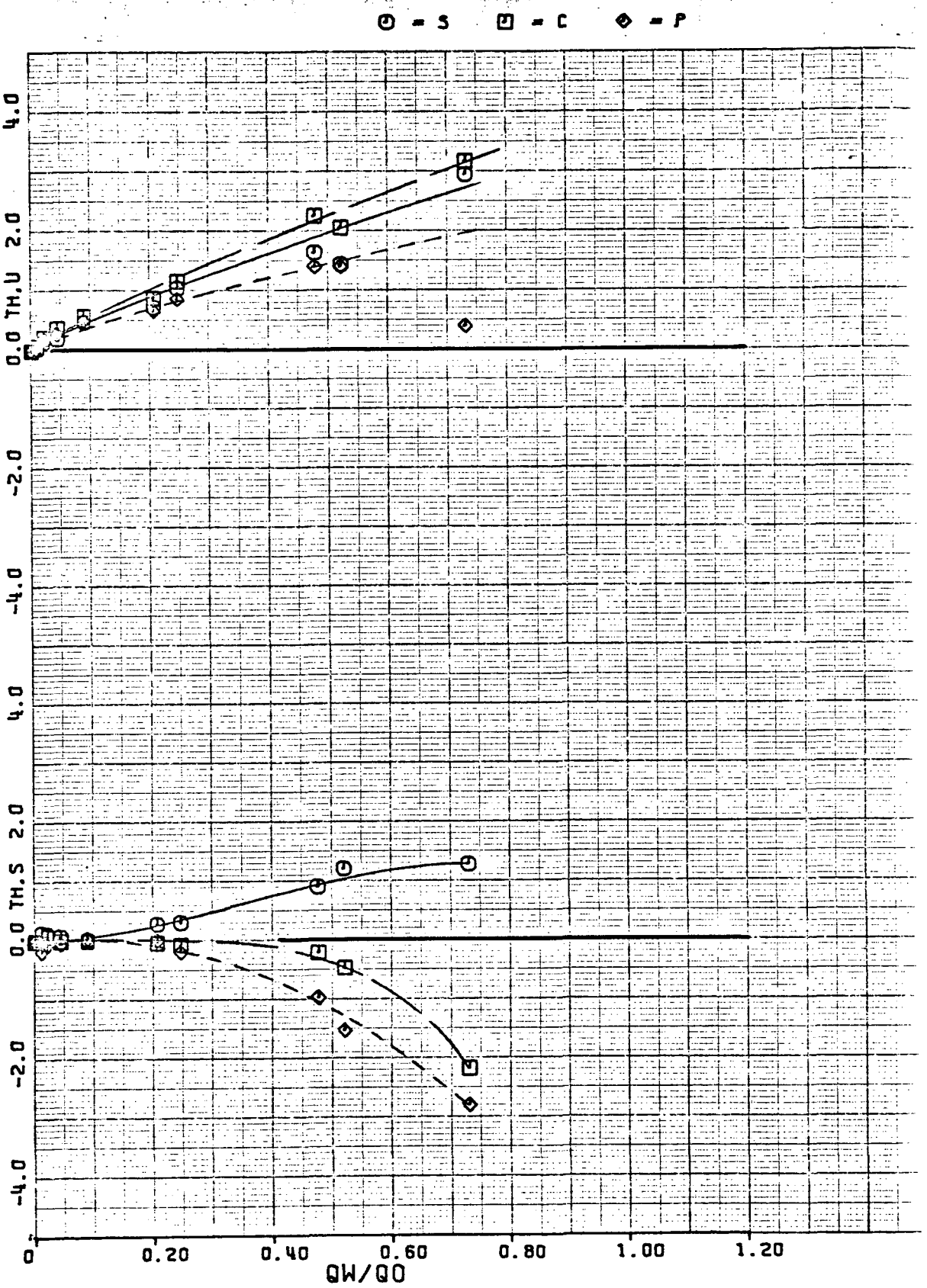

(a) $\psi = 0°$.

Figure 5.- Flow angularity for basic configuration.

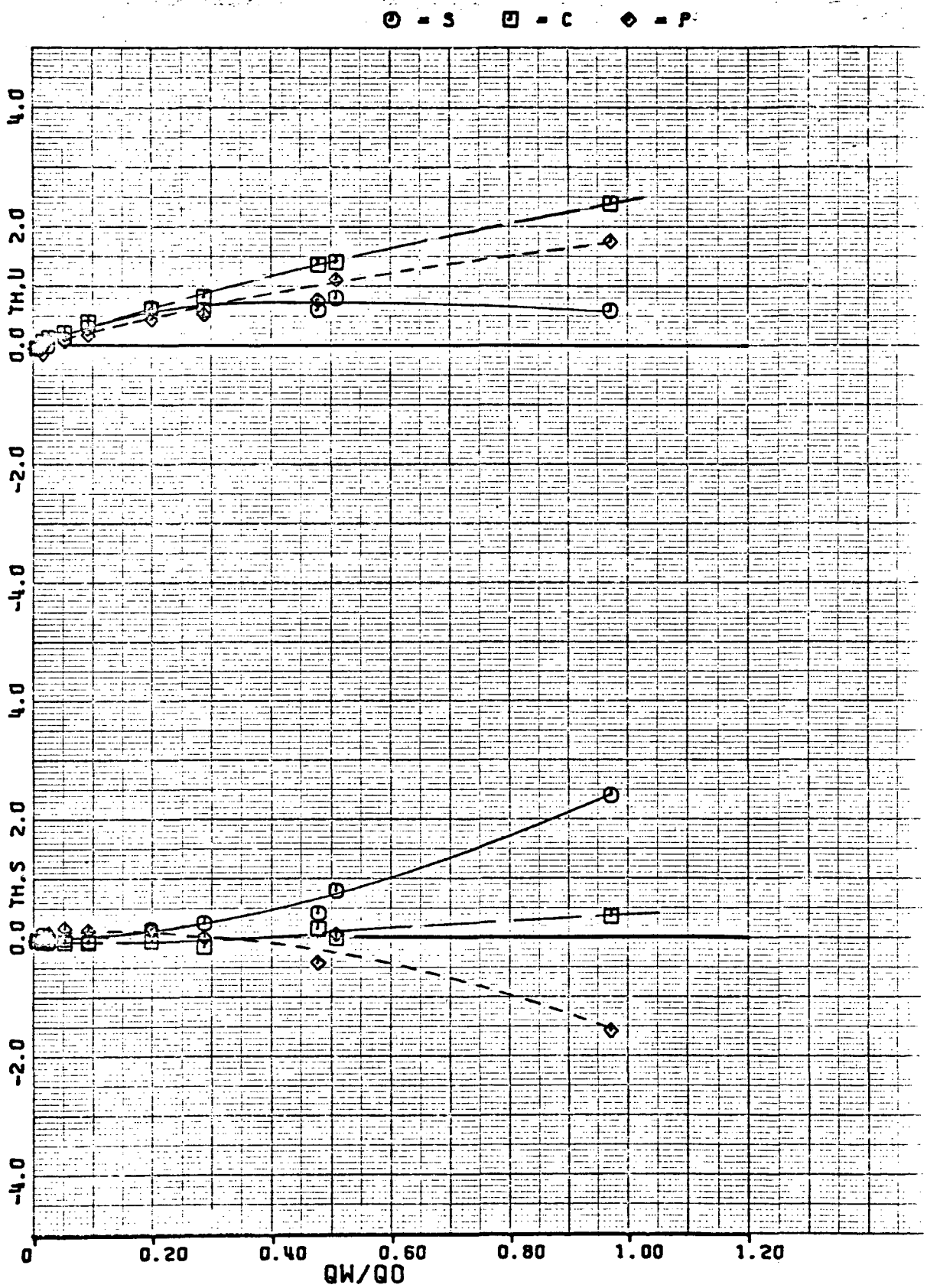

(b) ψ = -22 1/2°.

Figure 5.- Continued.

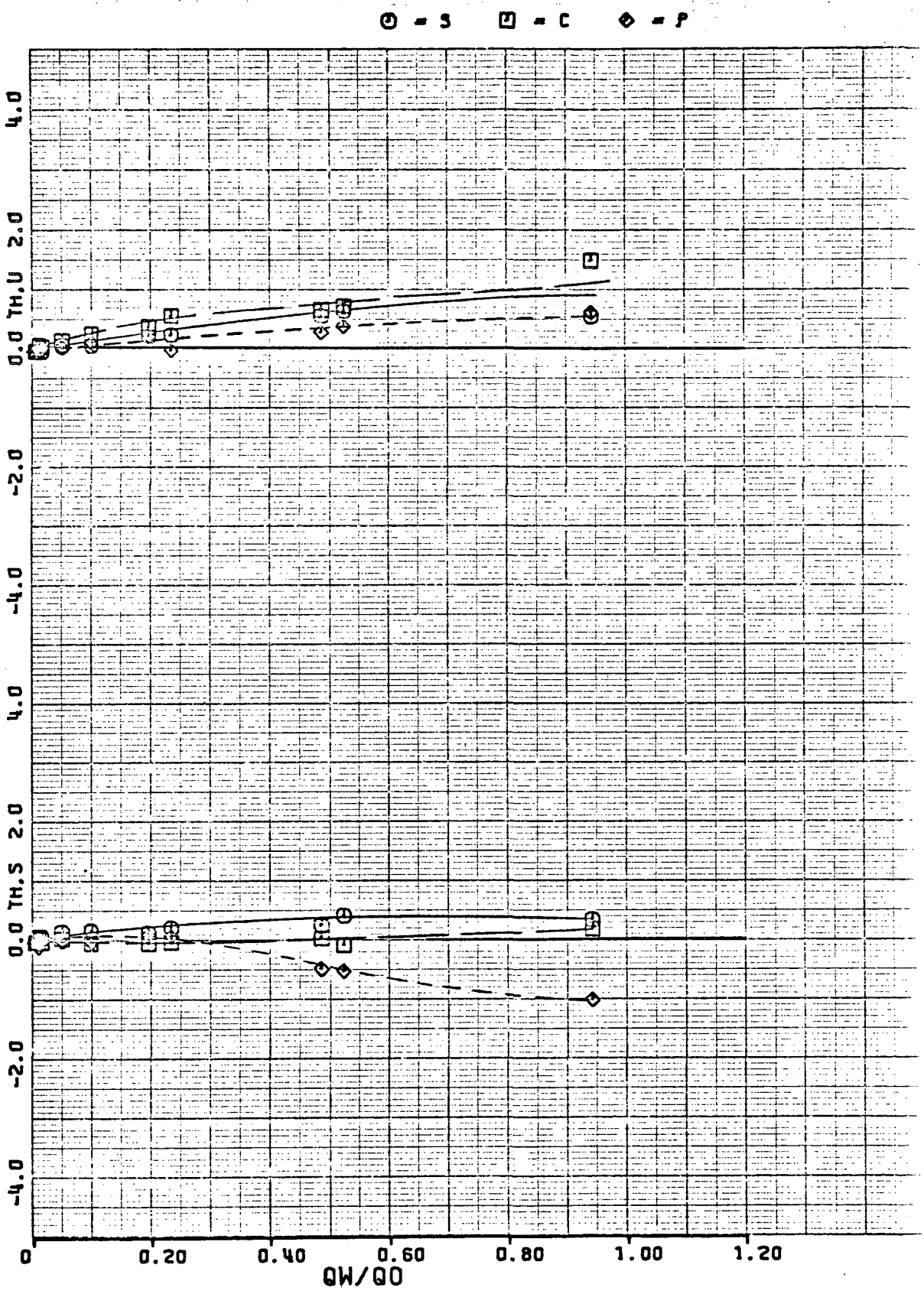

(c) $\psi = -45°$.

Figure 5.- Continued.

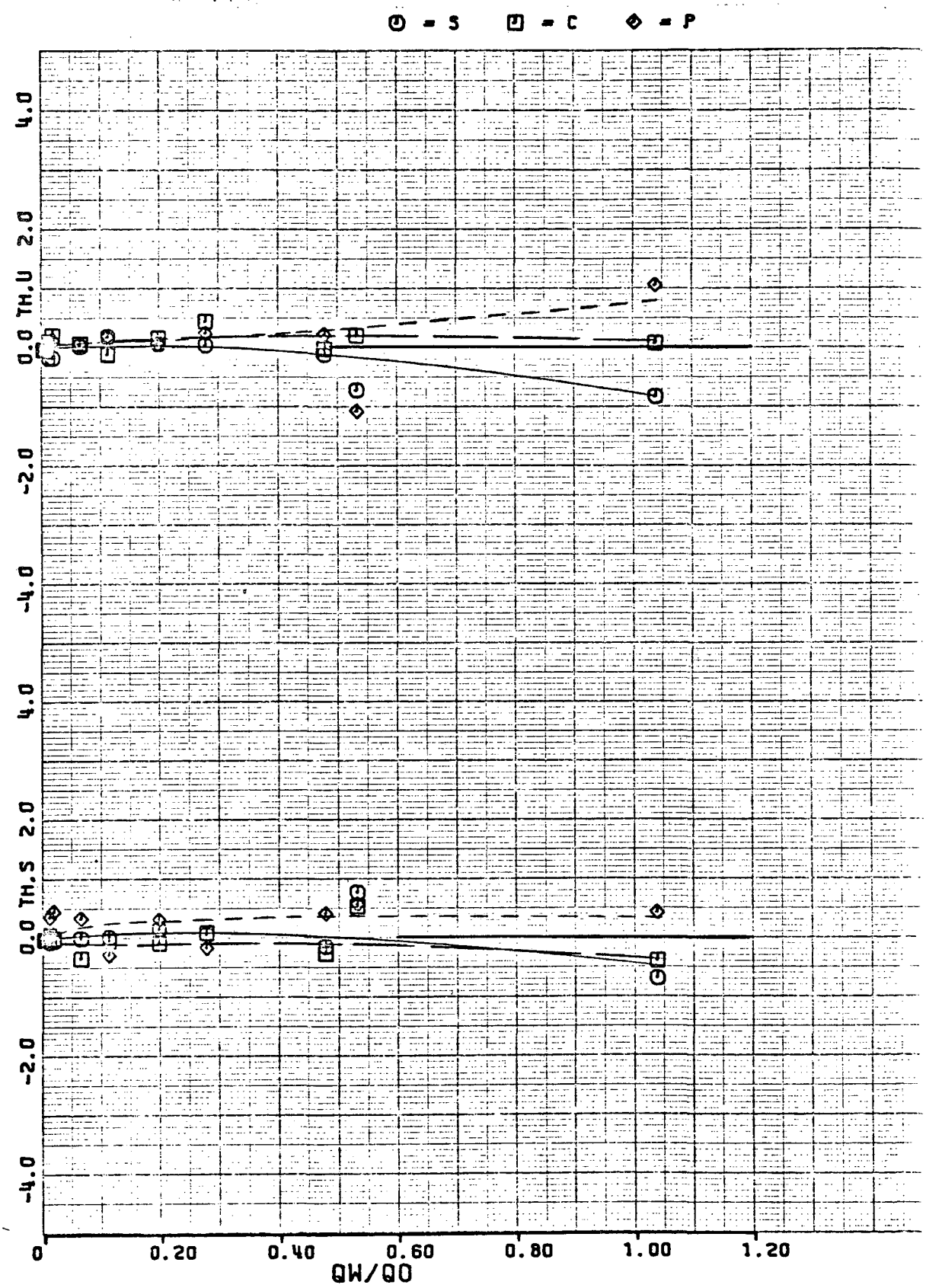

(d) ψ = -67 1/2°.

Figure 5.- Continued.

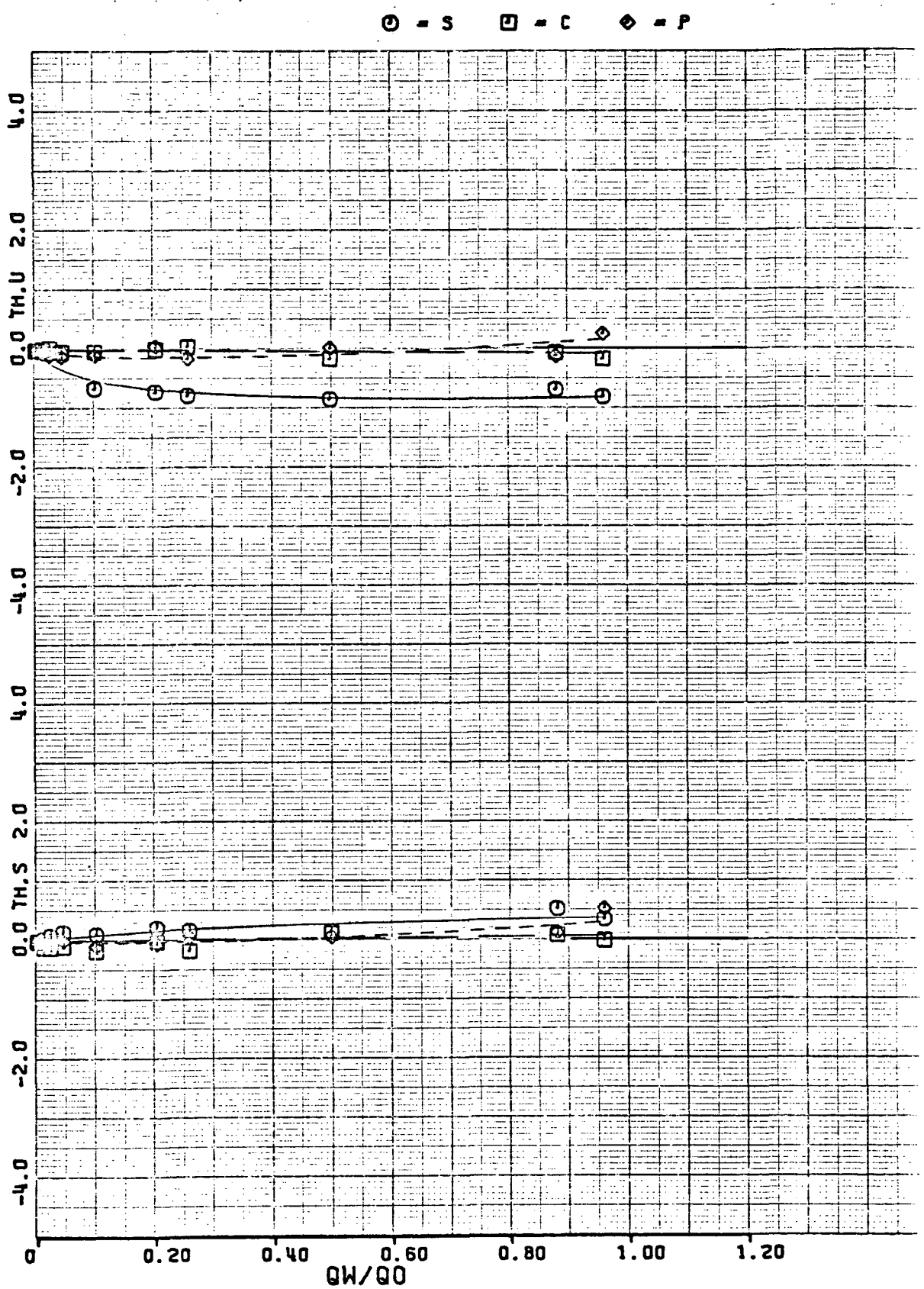

(e) $\psi = -90°$.

Figure 5.- Continued.

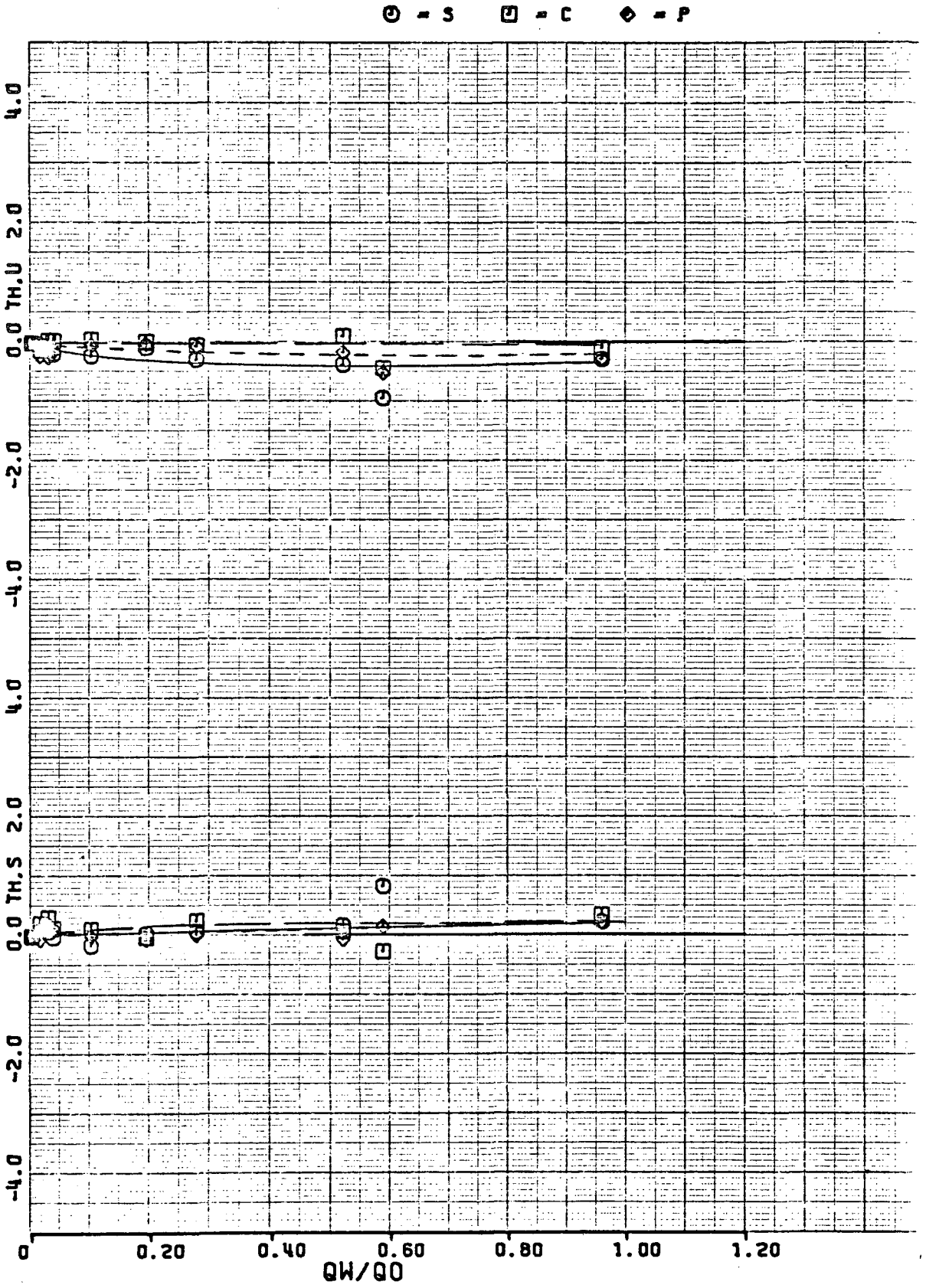

(f) ψ = -112 1/2°.

Figure 5.- Continued.

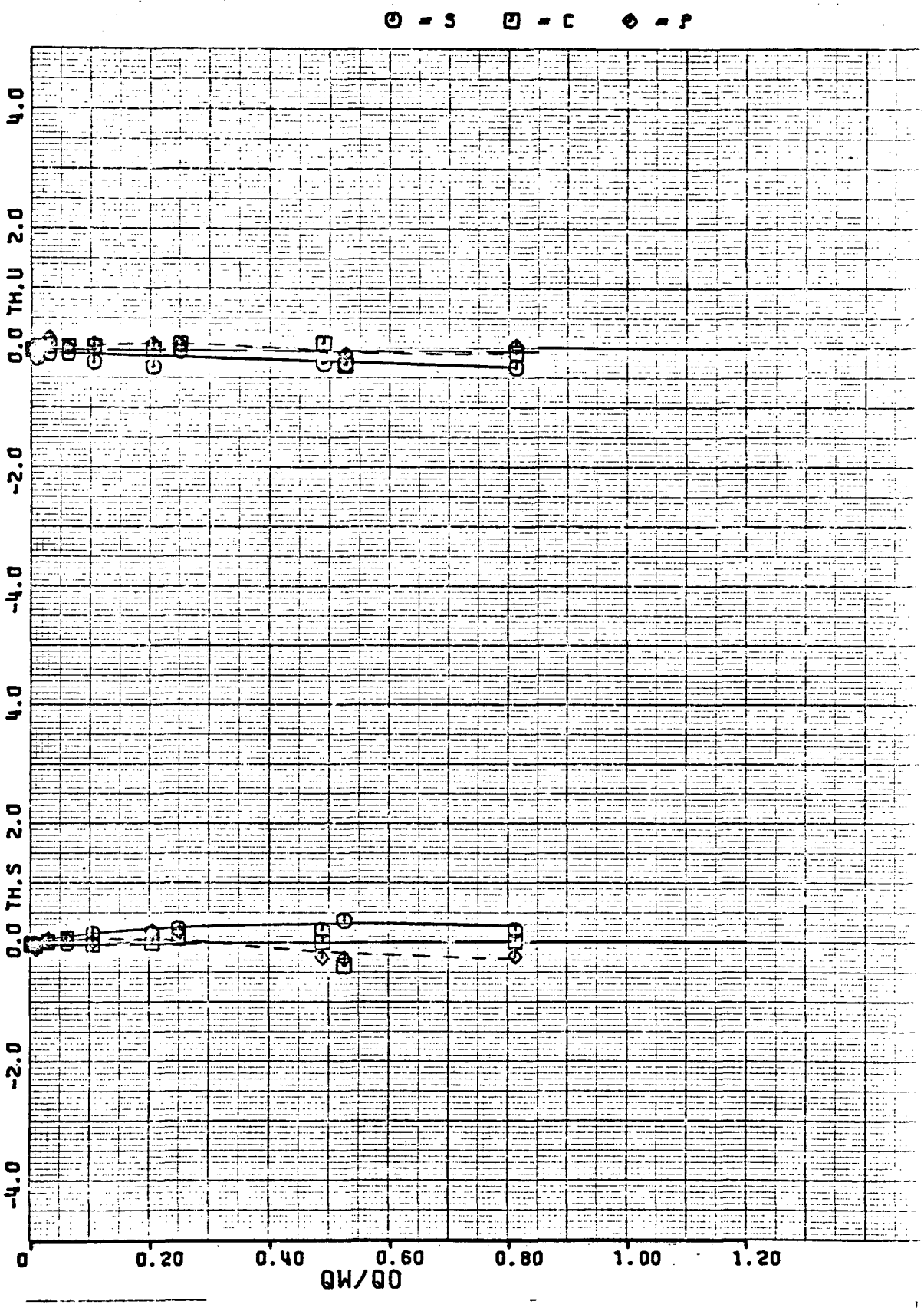

(g) $\psi = -135°$.

Figure 5.- Continued.

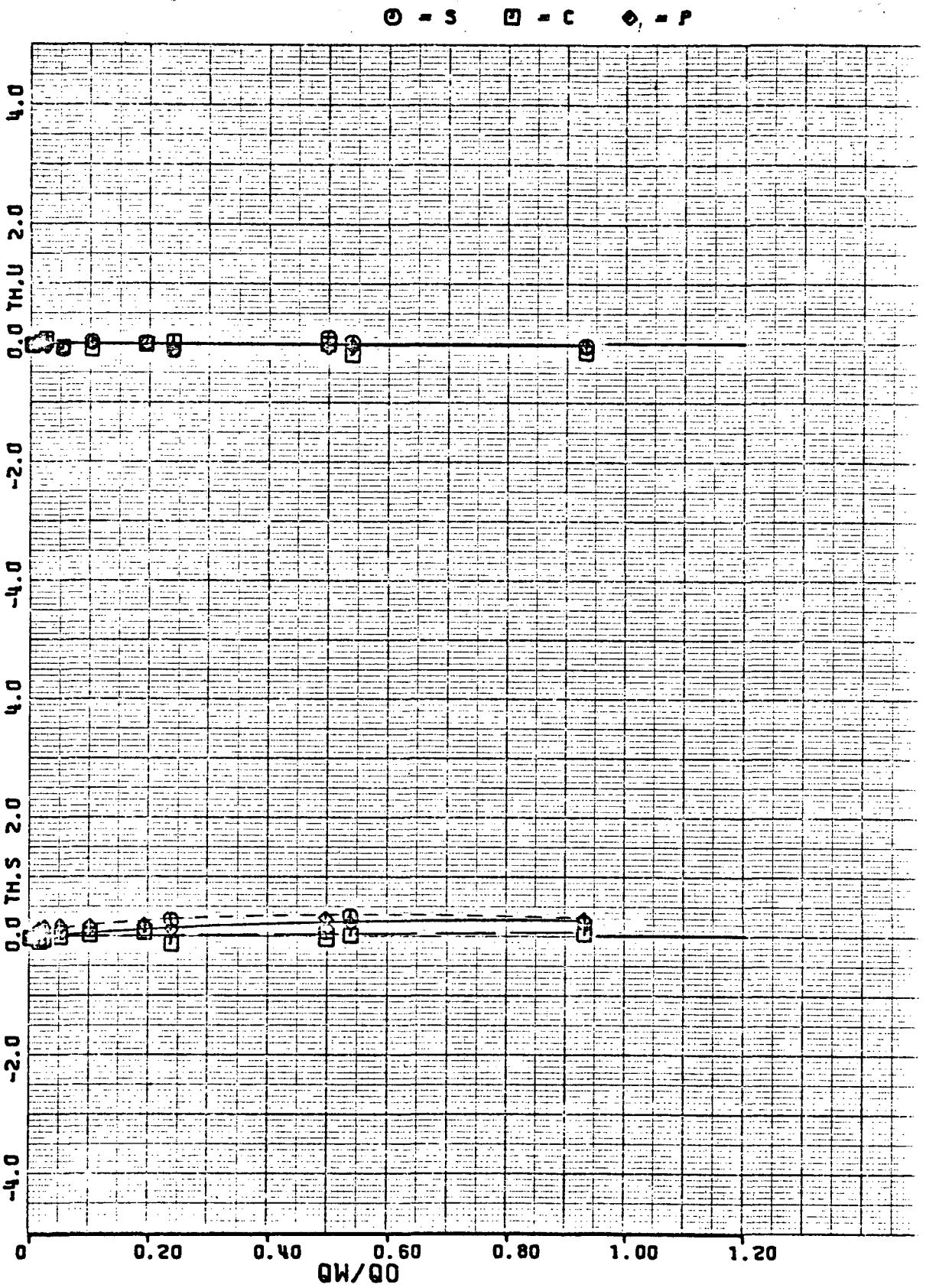

(h) $\psi = -157\ 1/2°$.

Figure 5.- Continued.

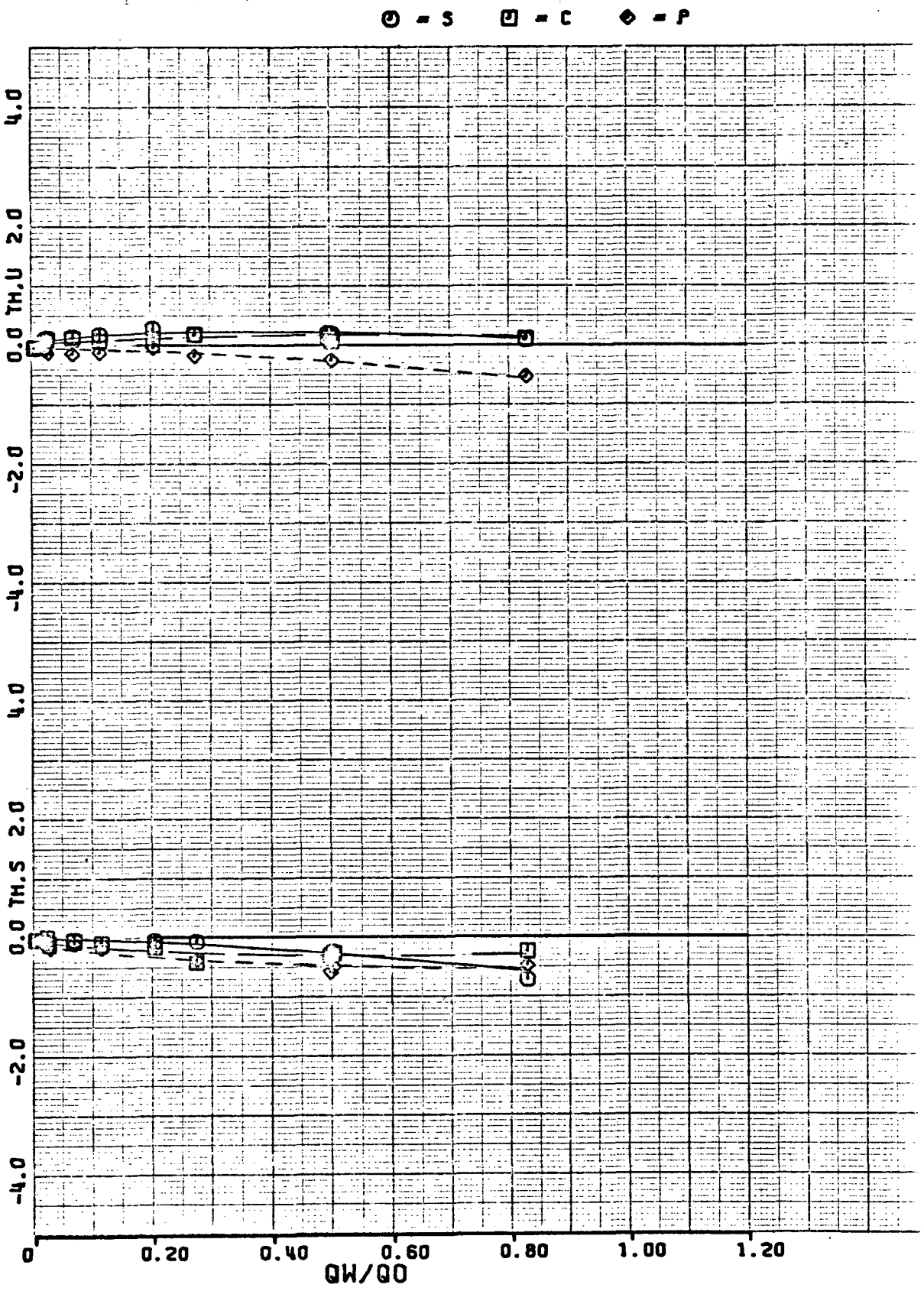

(i) $\psi = 180°$.

Figure 5.- Continued.

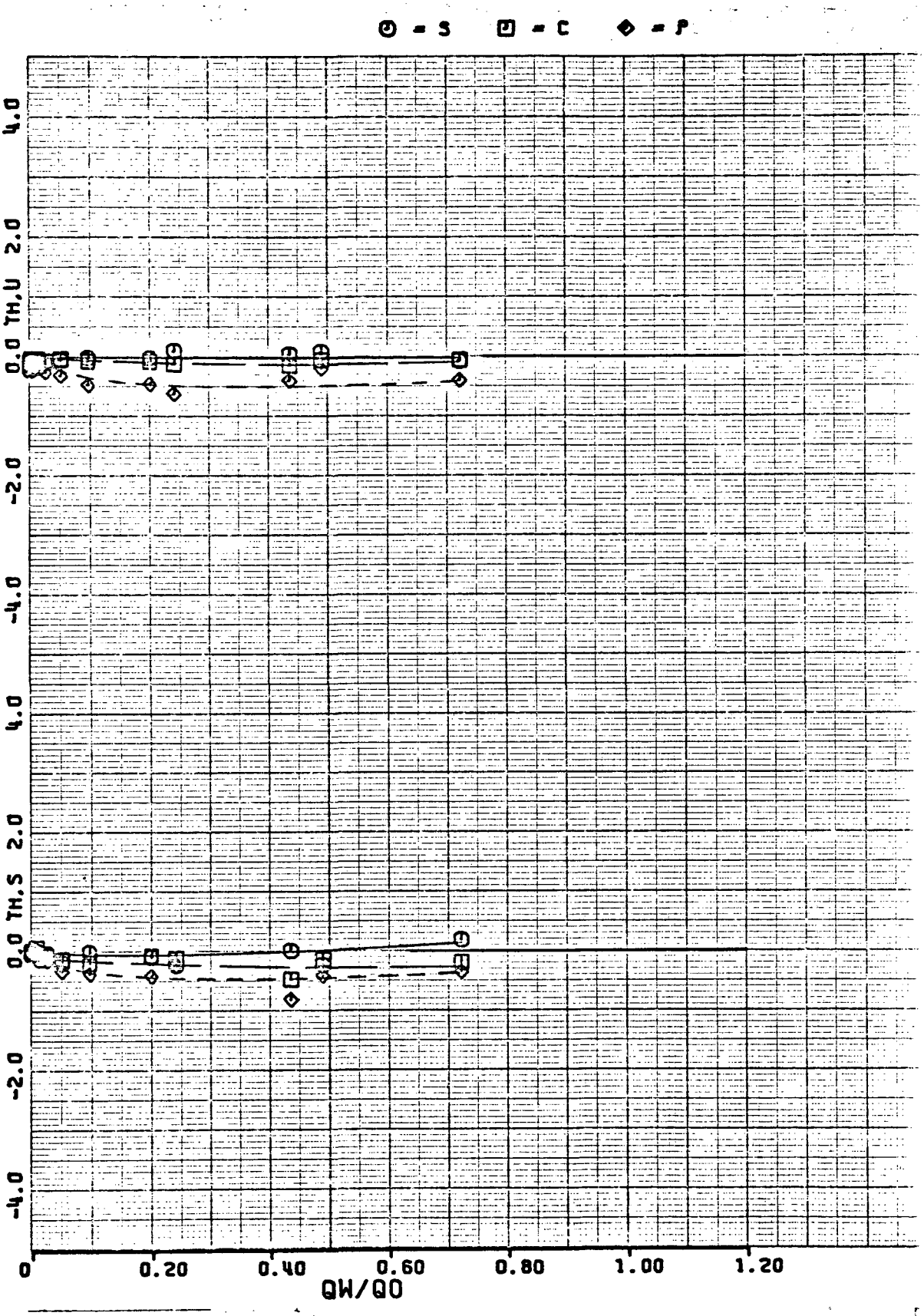

(j) ψ = 157 1/2°.

Figure 5.- Concluded.

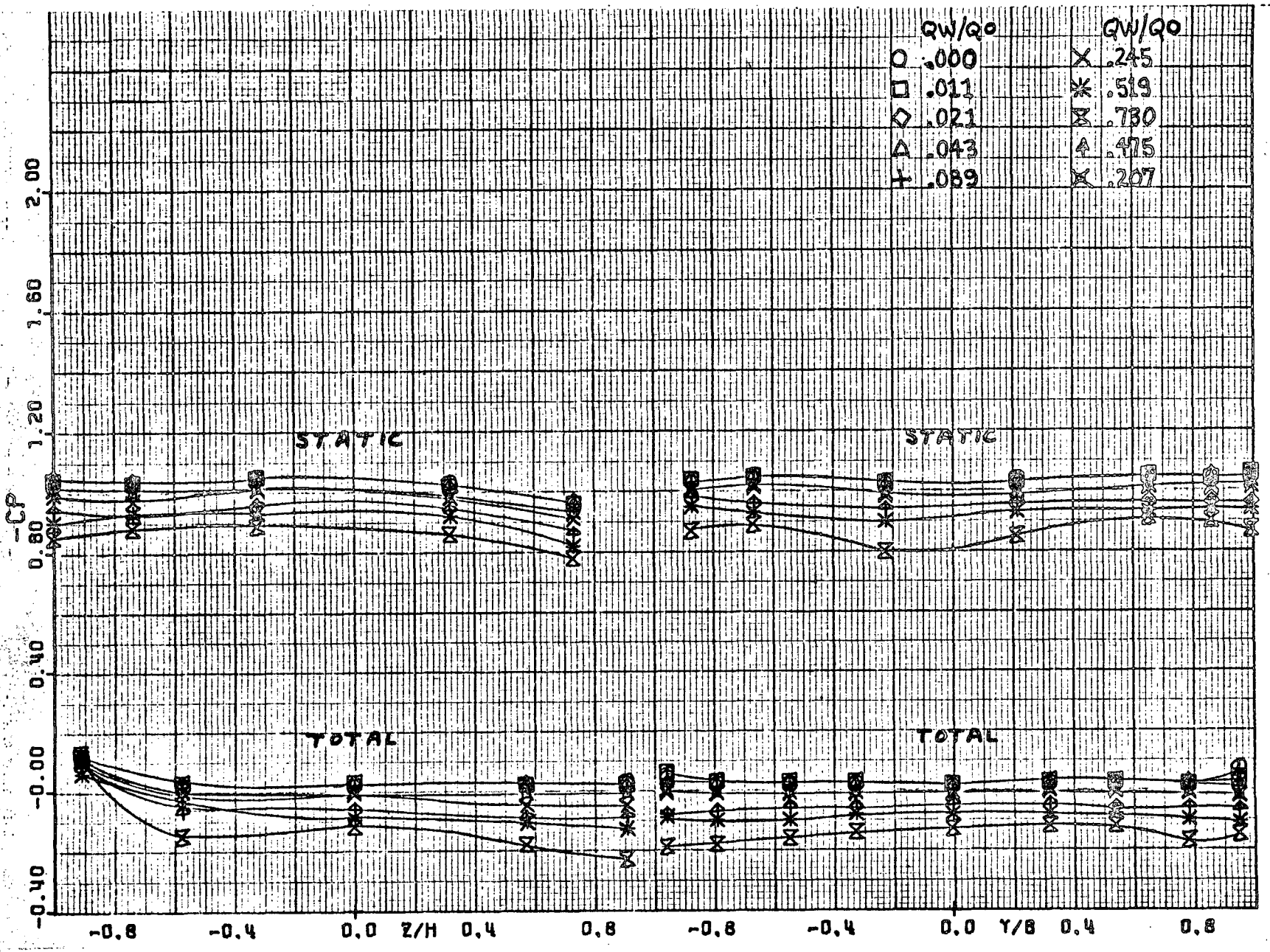

(a) $\psi = 0°$.

Figure 6.- Pressure coefficients for basic configuration.

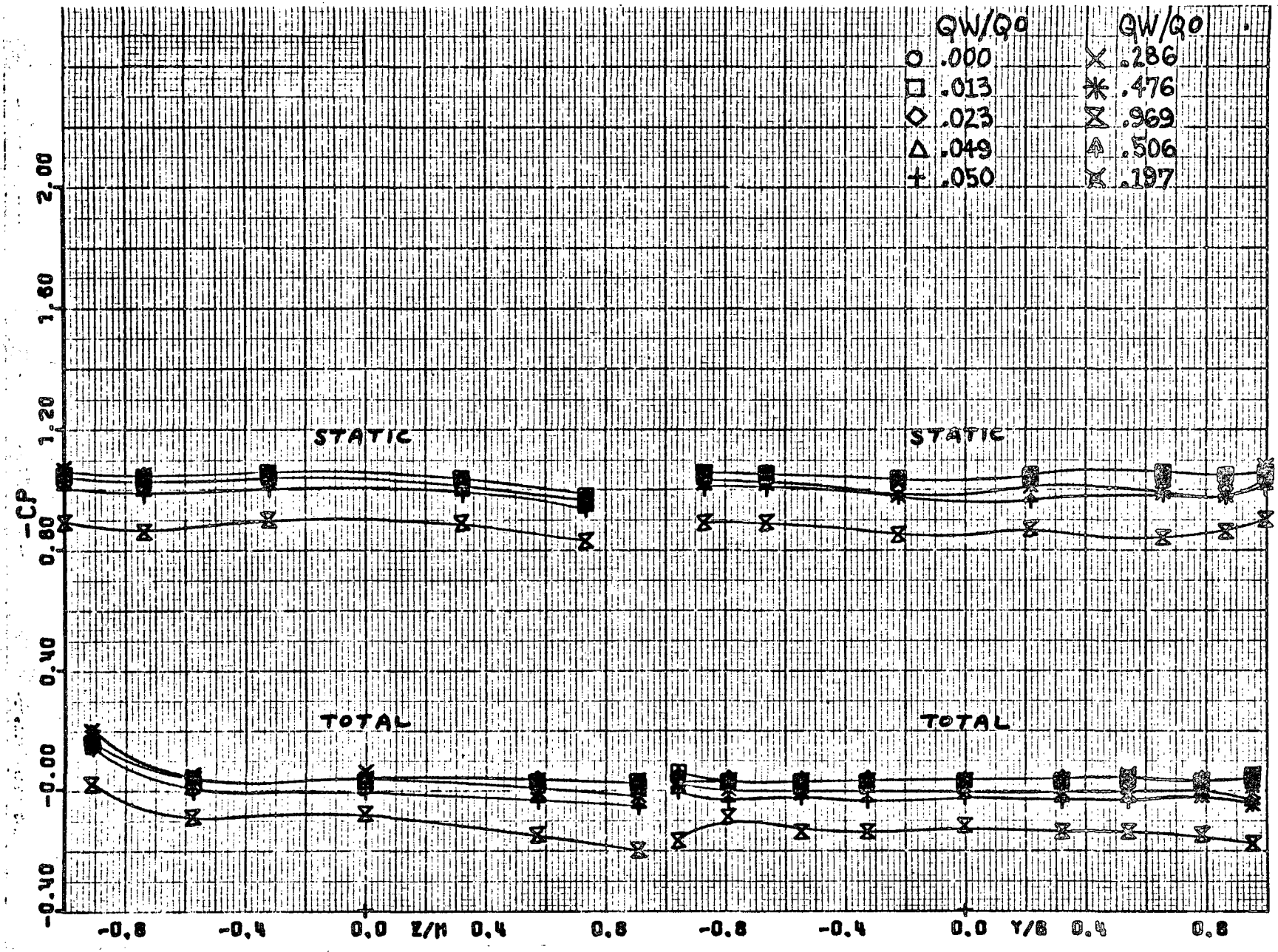

(b) $\psi = -22\ 1/2°$.

Figure 6.- Continued.

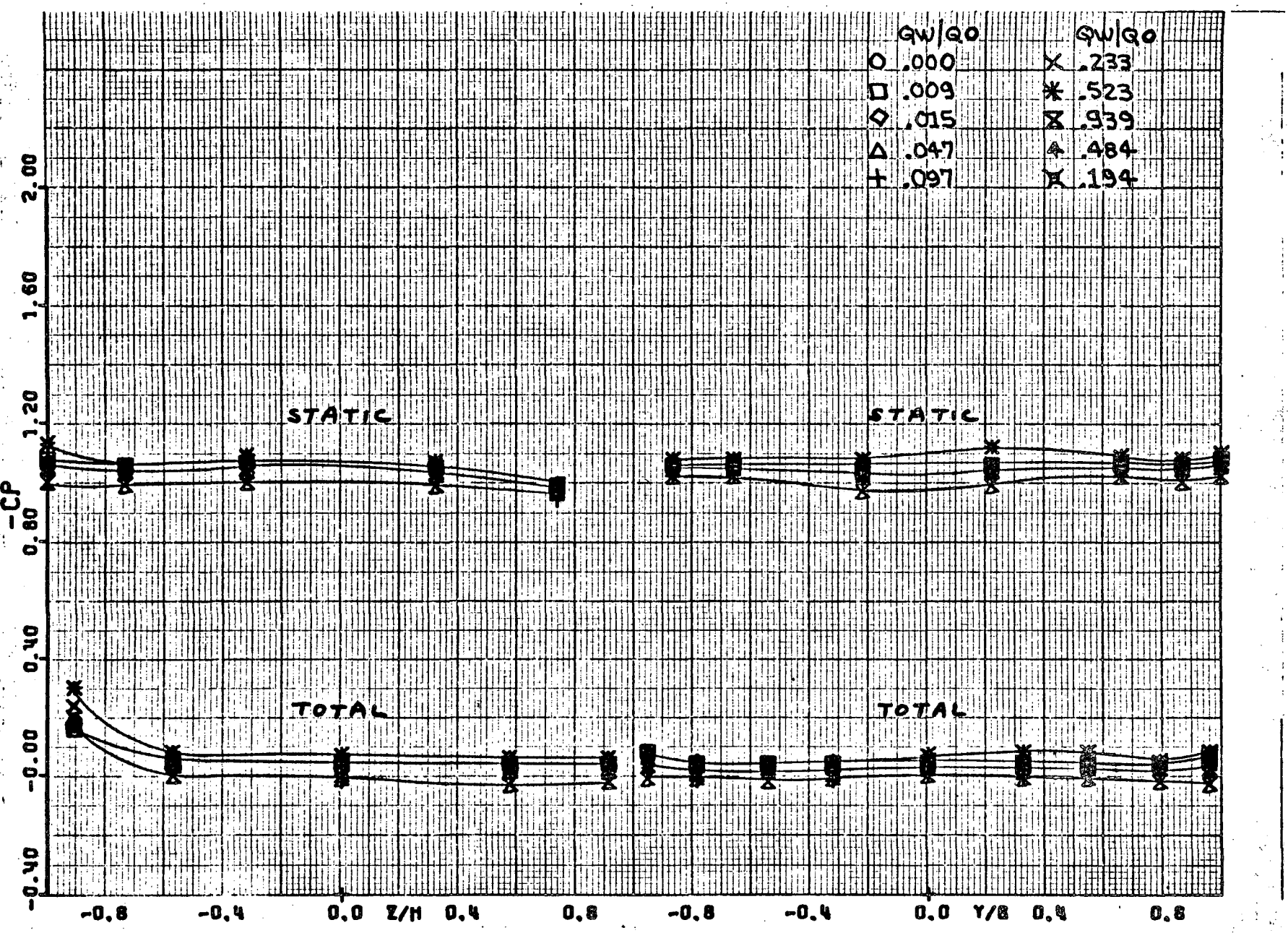

(c) $\psi = -45°$.

Figure 6.- Continued.

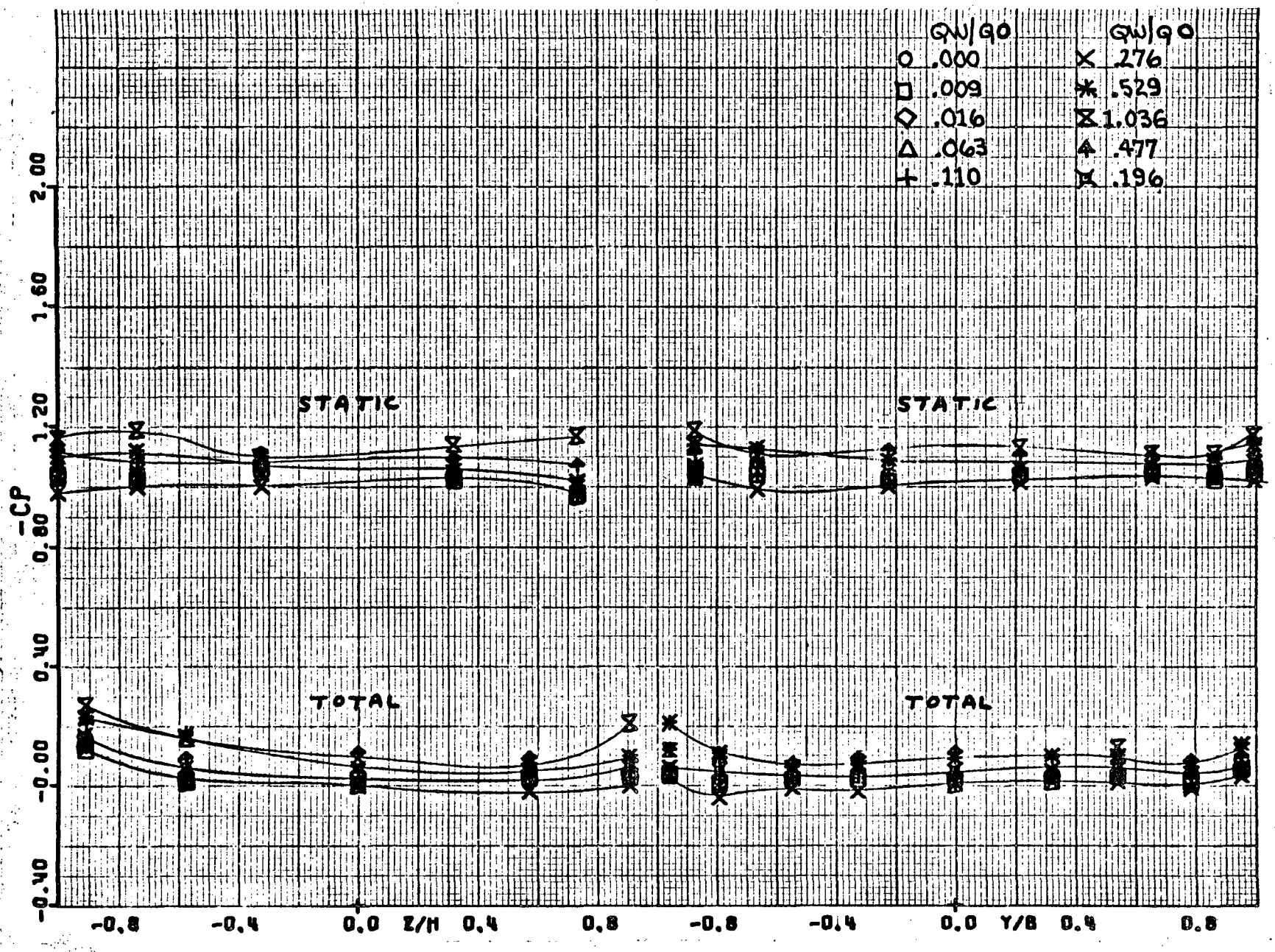

(d) $\Psi = -67\ 1/2°$.

Figure 6.- Continued

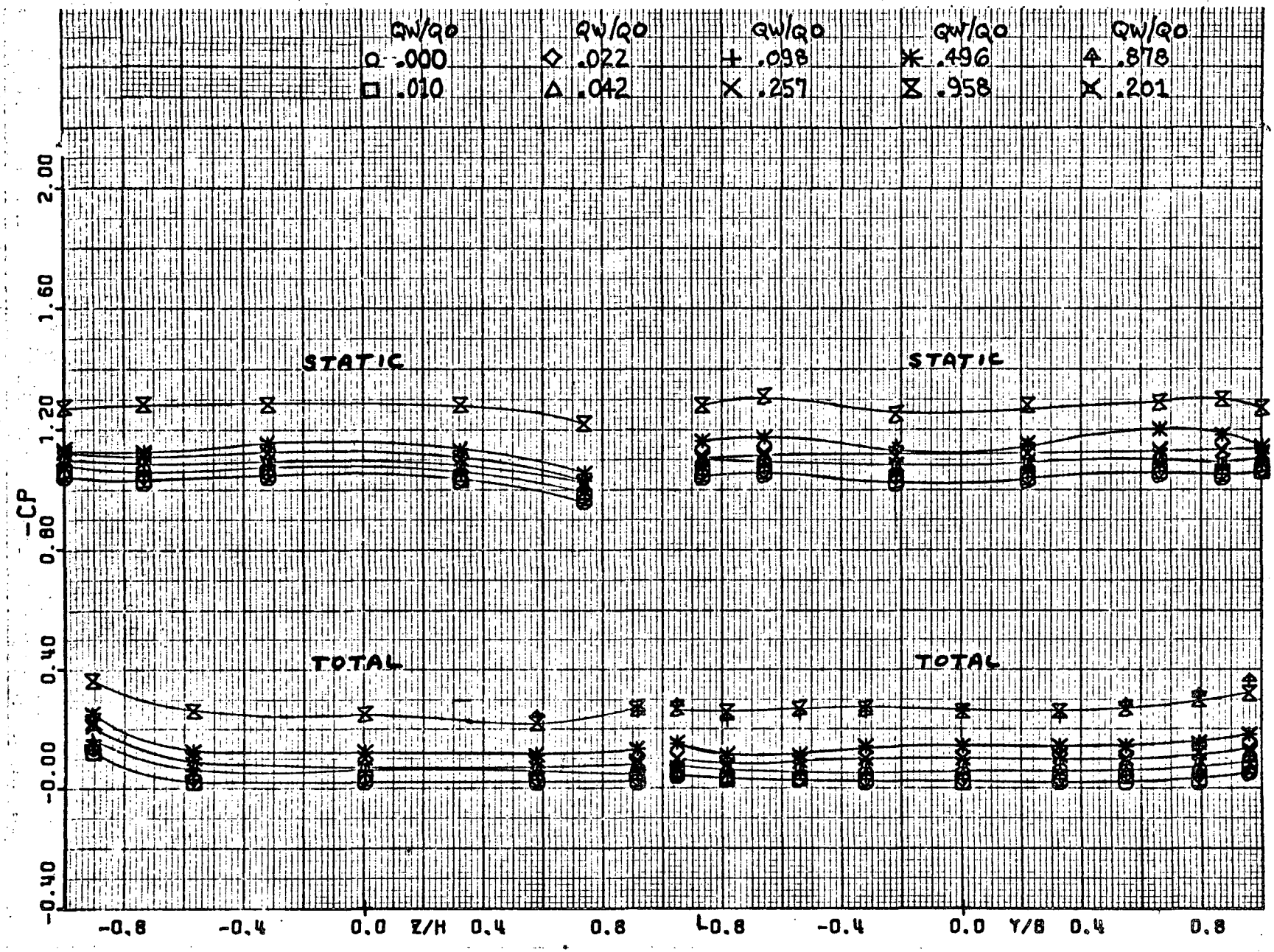

(e) $\psi = -90°$.

Figure 6.- Continued.

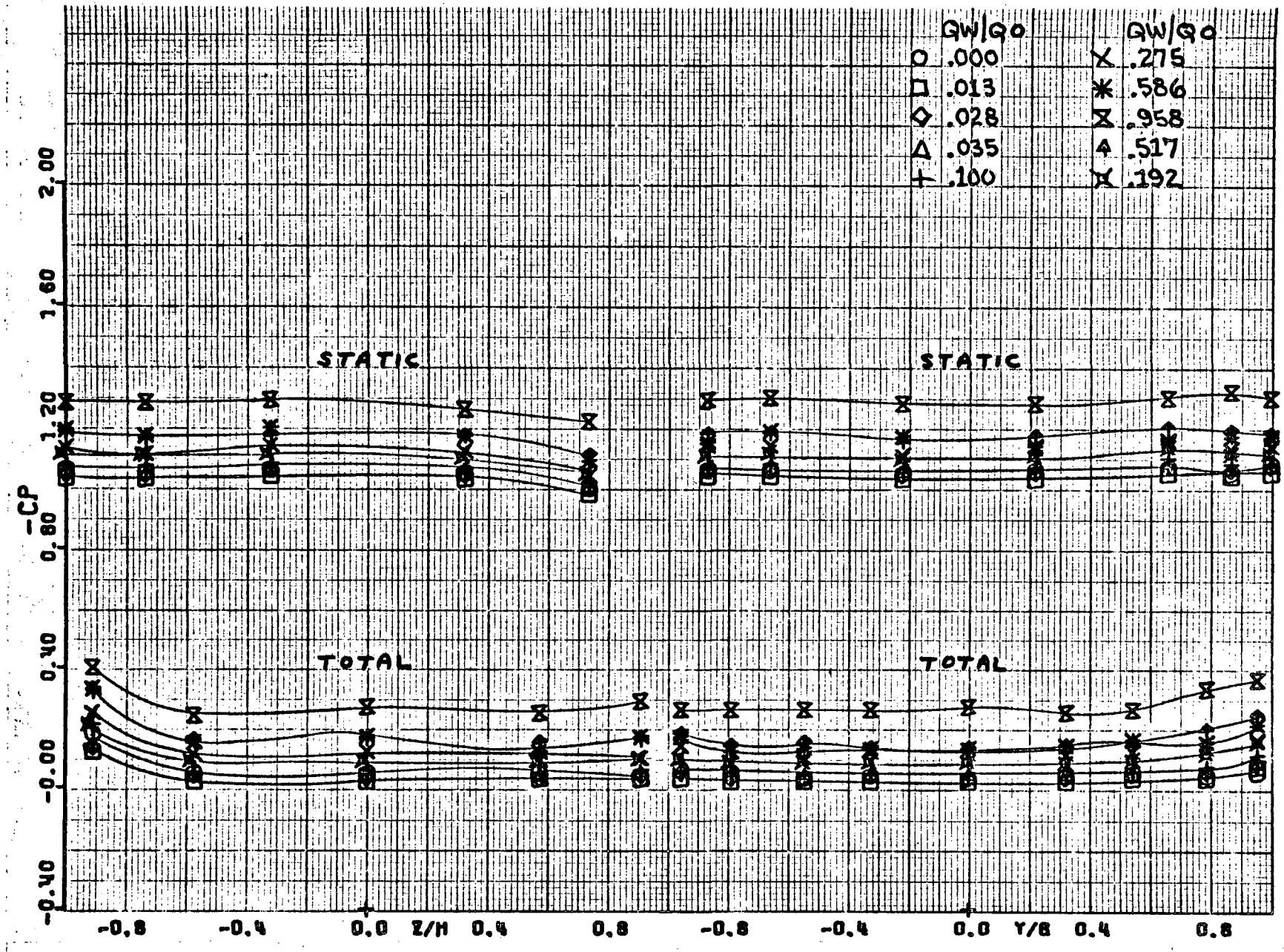

(f) $\psi = -112\ 1/2°$.

Figure 6.- Continued.

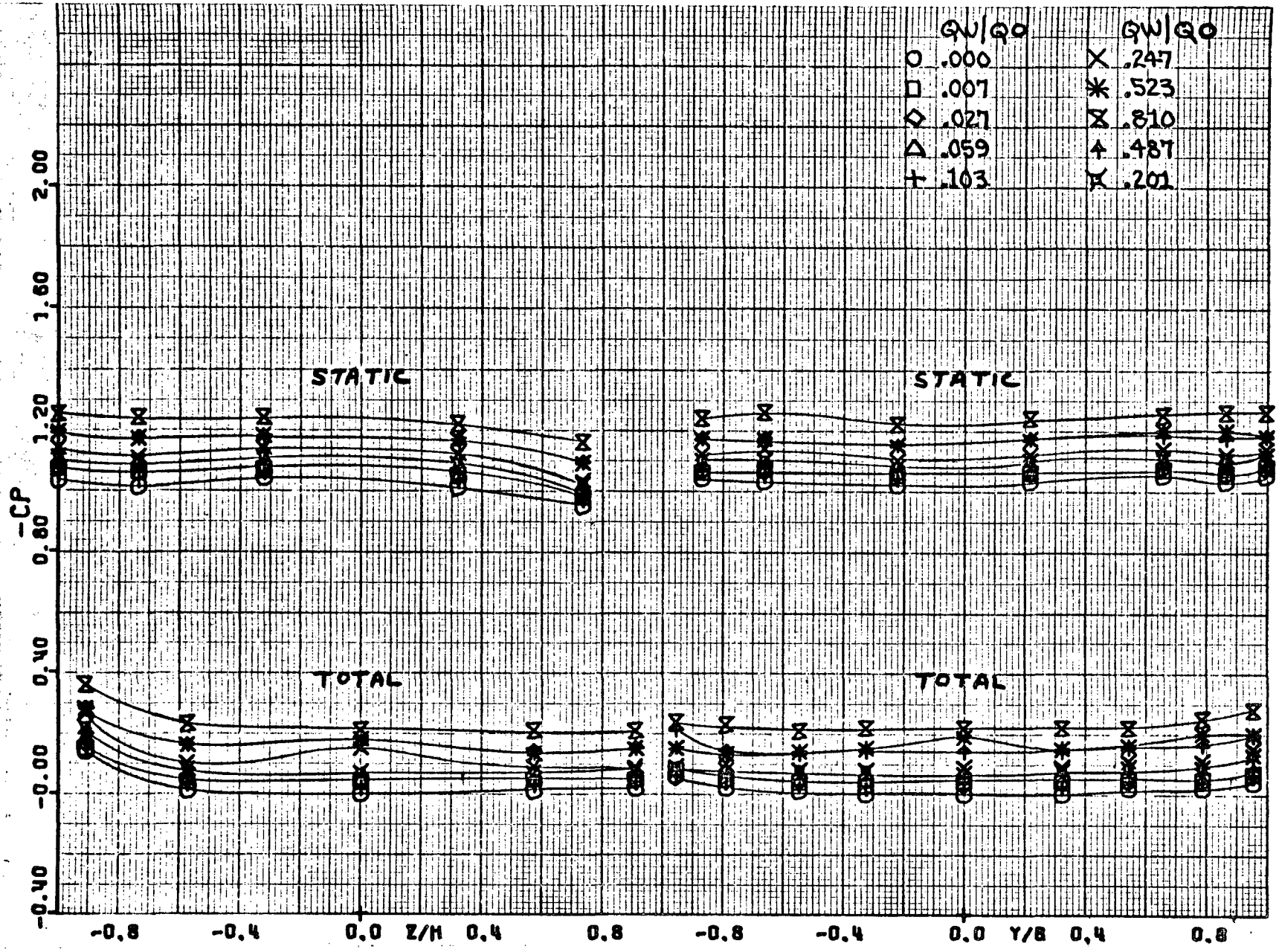

(g). $\psi = -135°$.

Figure 6.- Continued.

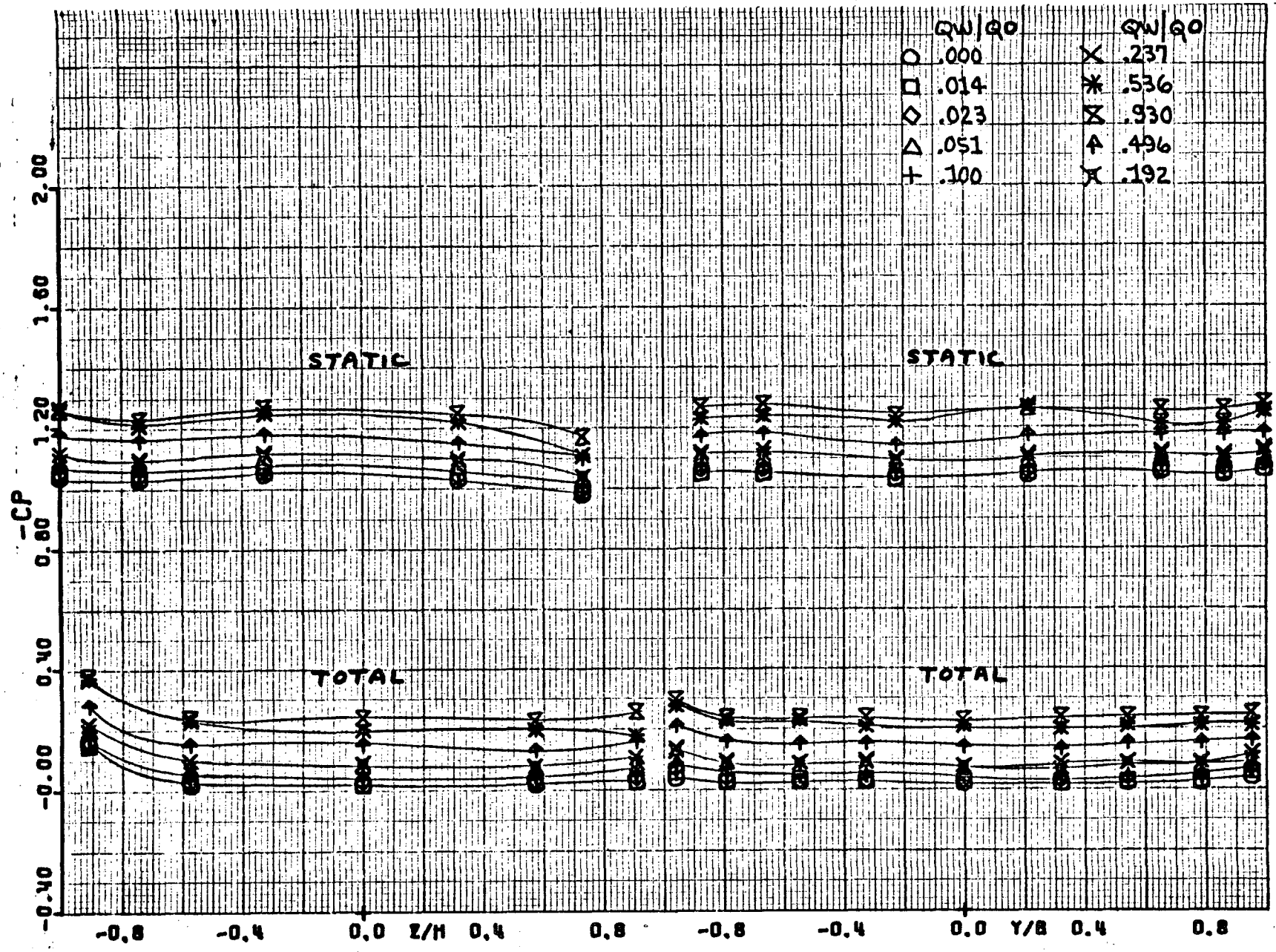

(h) $\psi = -157\ 1/2°$.

Figure 6.- Continued.

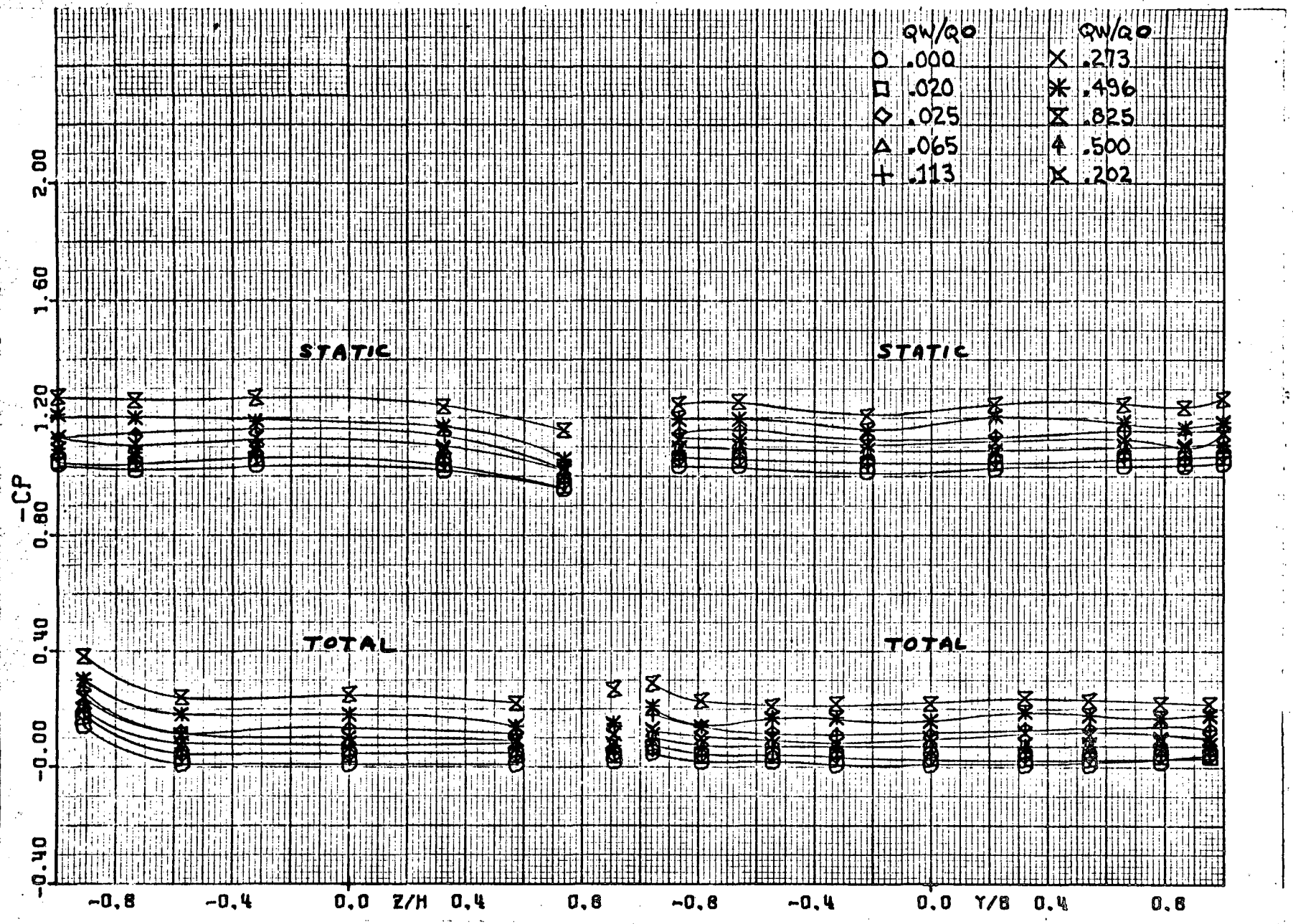

(i) $\psi = 180°$.

Figure 6.- Continued.

(j) $\psi = 157\frac{1}{2}°$.

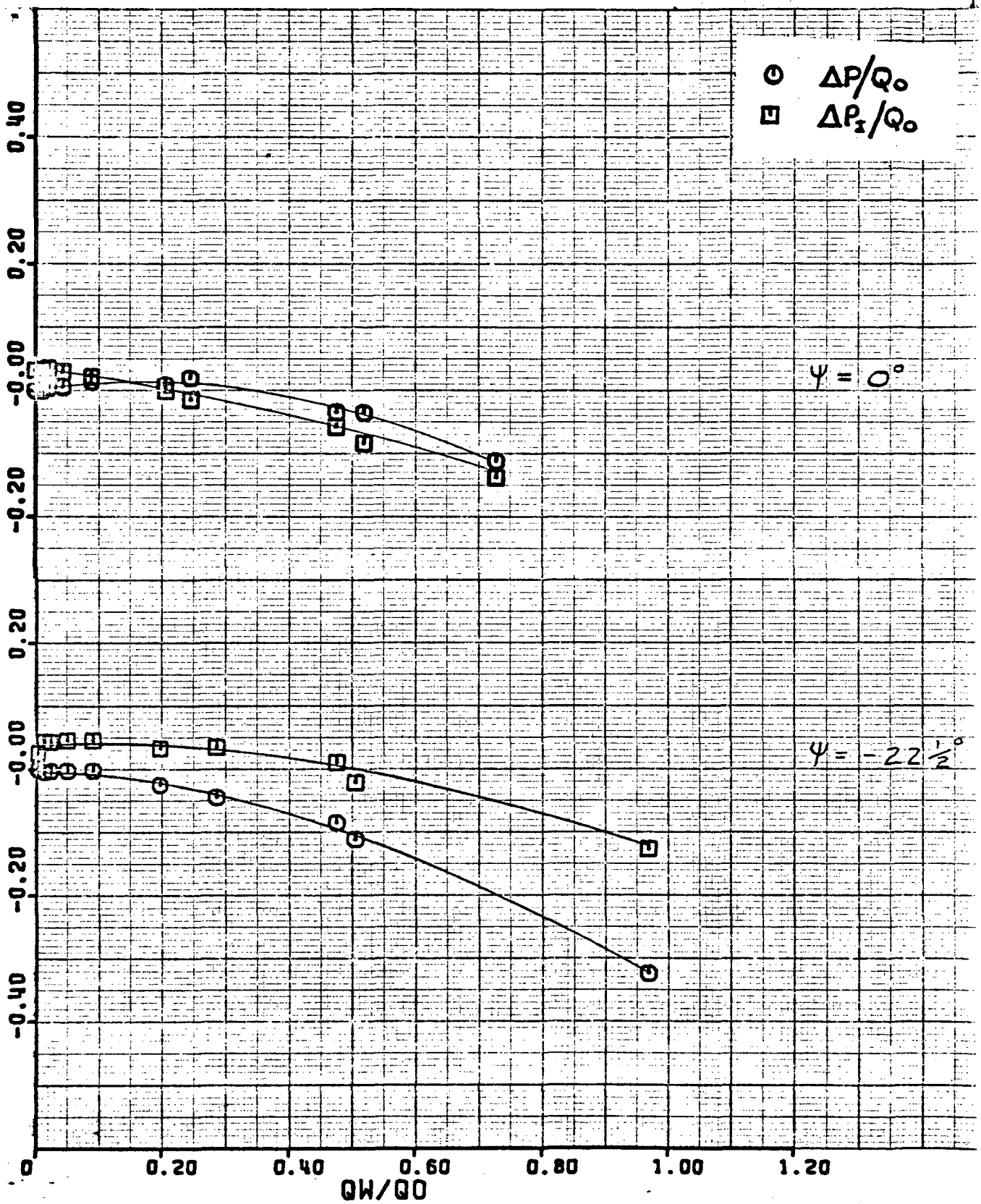

(a) $\psi = 0°$ and $-22\ 1/2°$.

Figure 7.- Pressure losses for basic configuration.

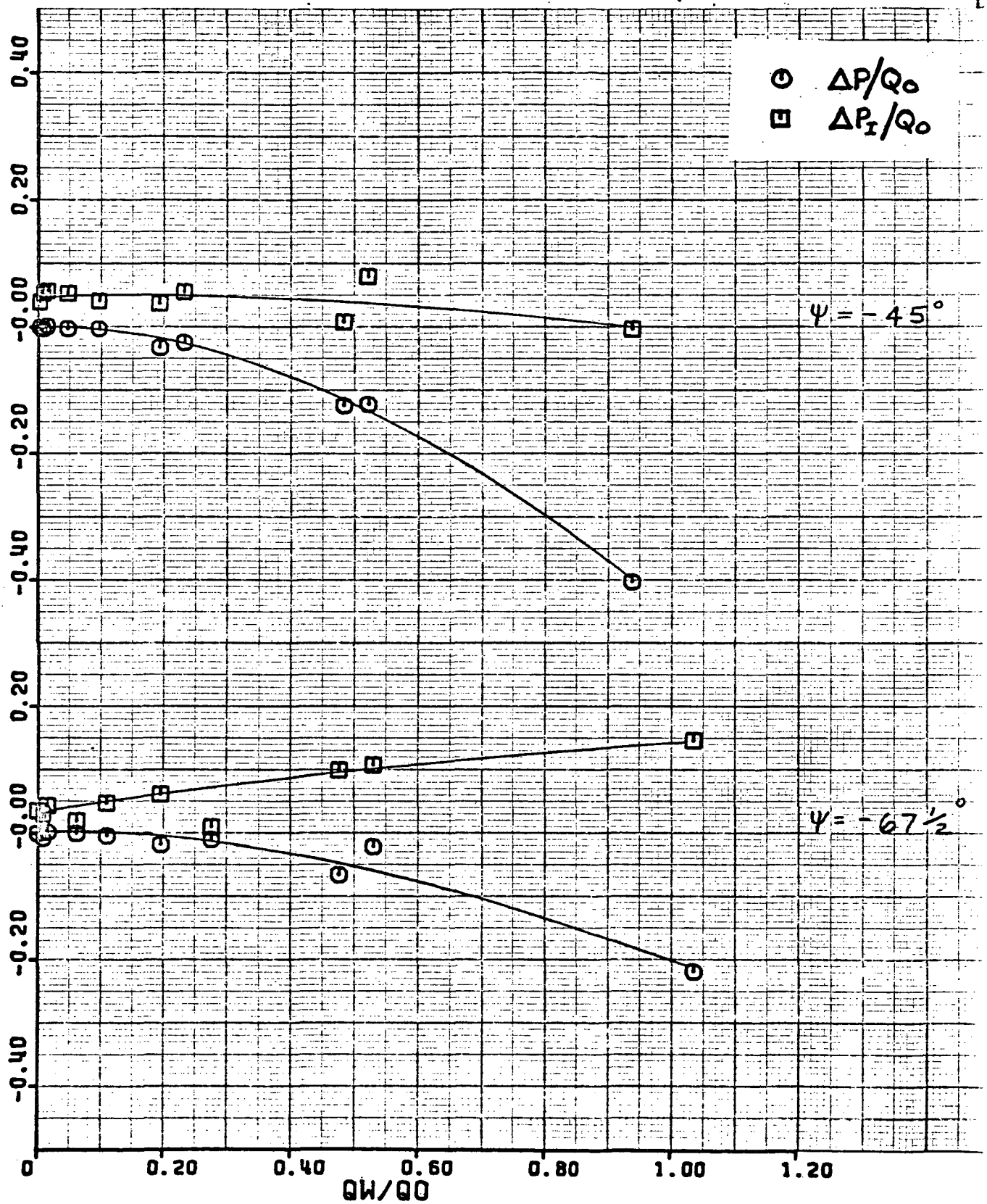

(b) ψ = -45° and -67 1/2°.

Figure 7.- Continued.

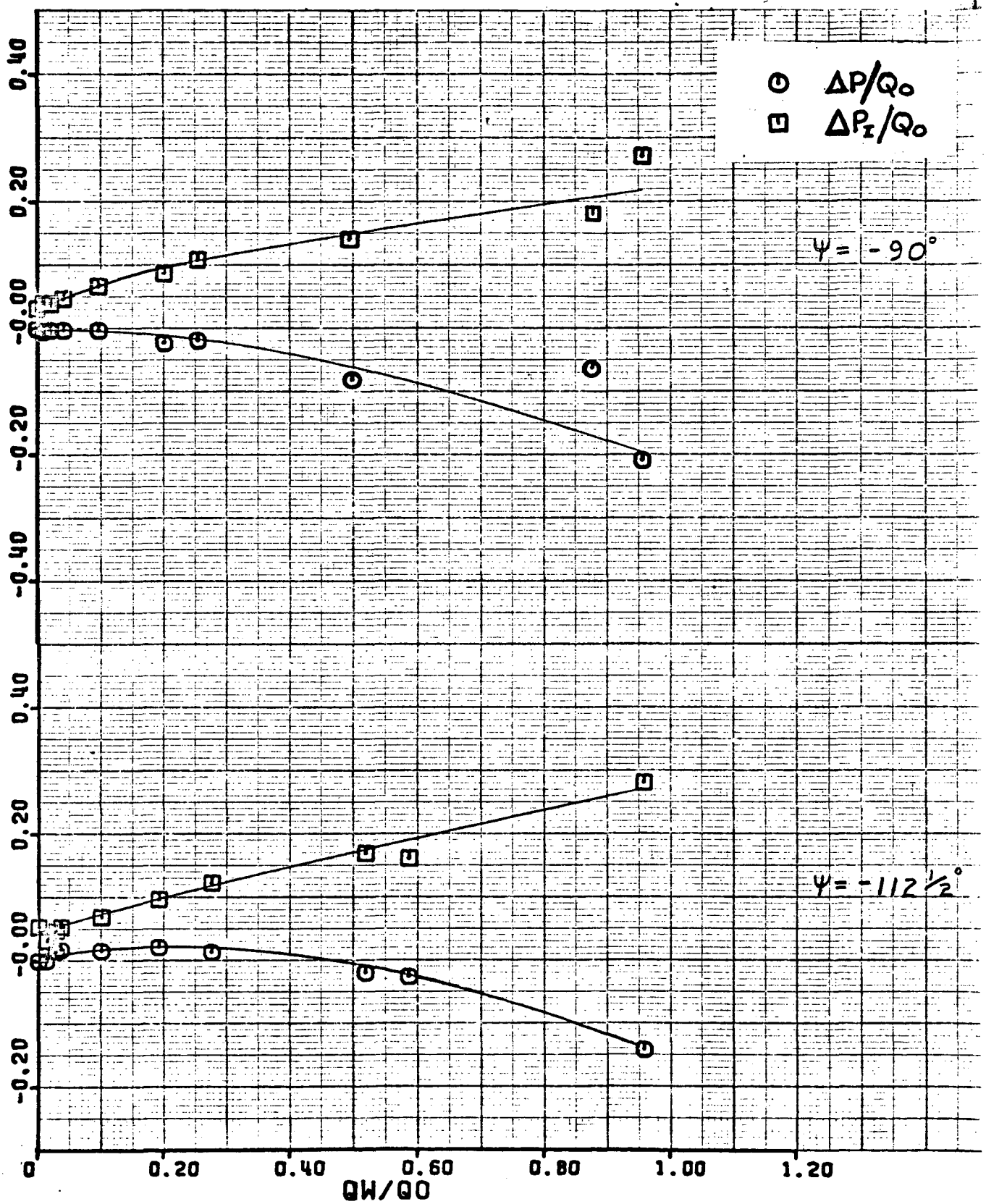

(c) ψ = -90° and -112 1/2°.

Figure 7.- Continued.

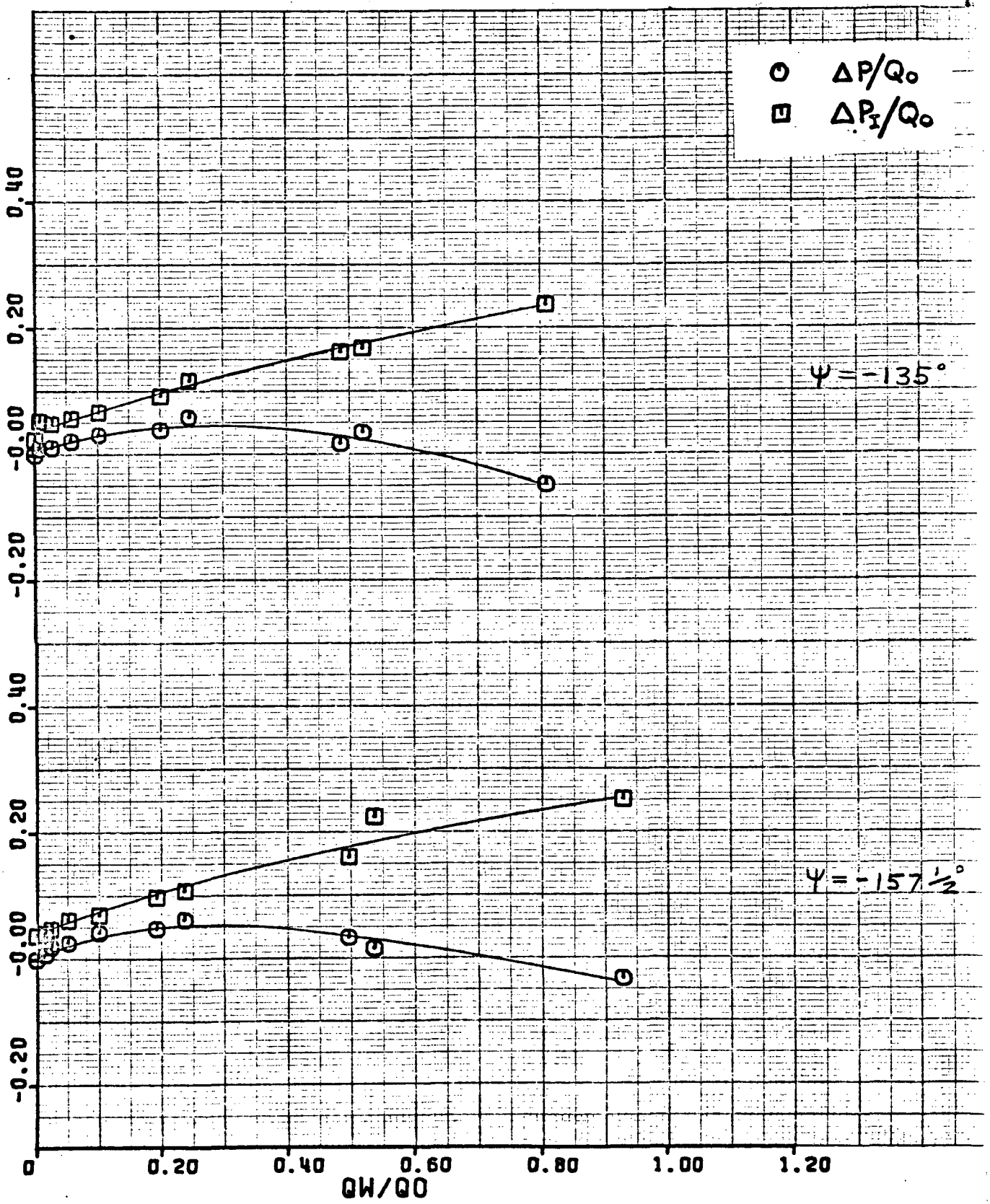

(d) ψ = -135° and -157 1/2°.

Figure 7.- Continued.

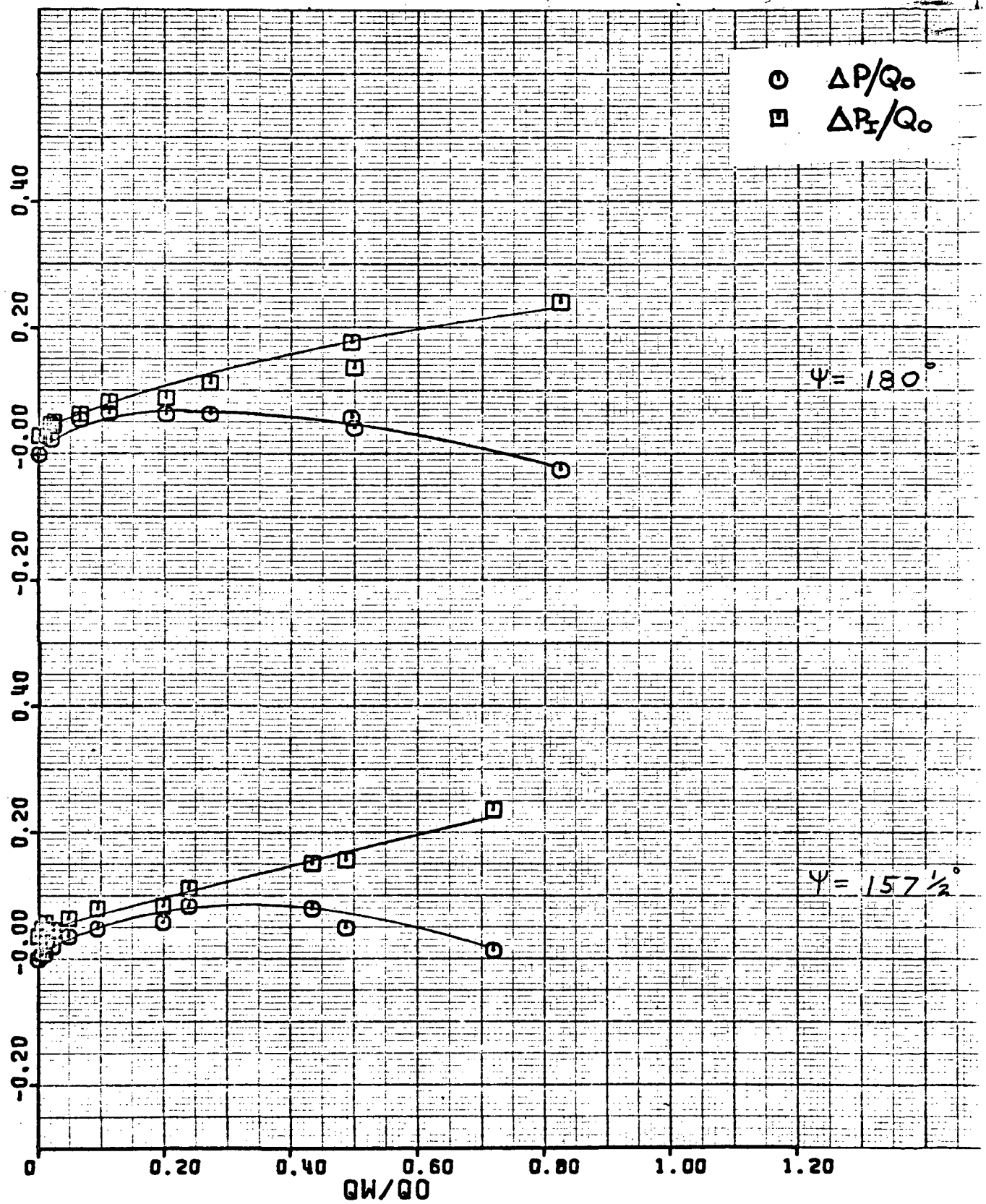

(e) ψ = 180° and 157 1/2°.

Figure 7.- Concluded.

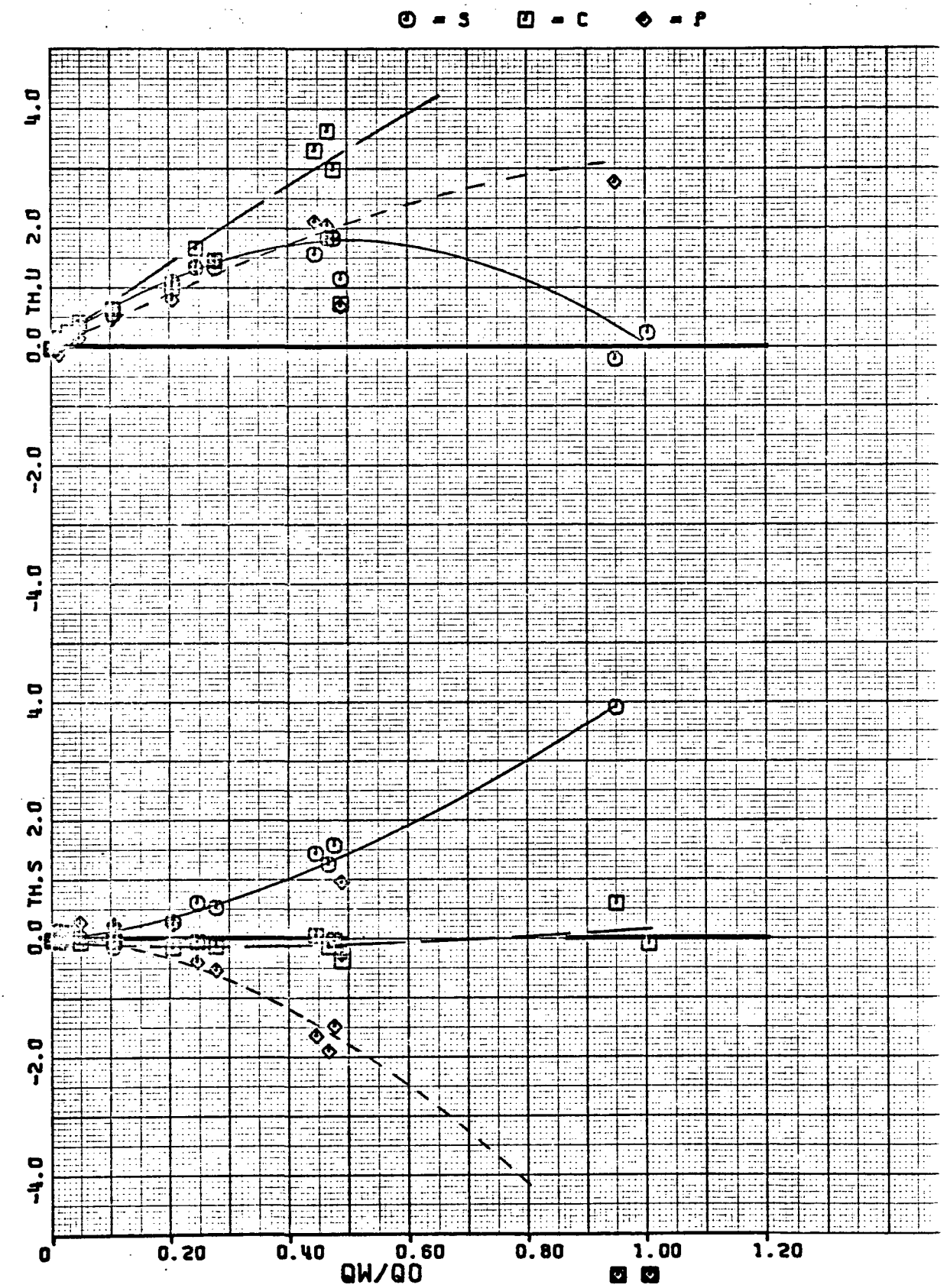

(a) $\psi = 0°$.

Figure 8.- Flow angularity for model without roof posts.

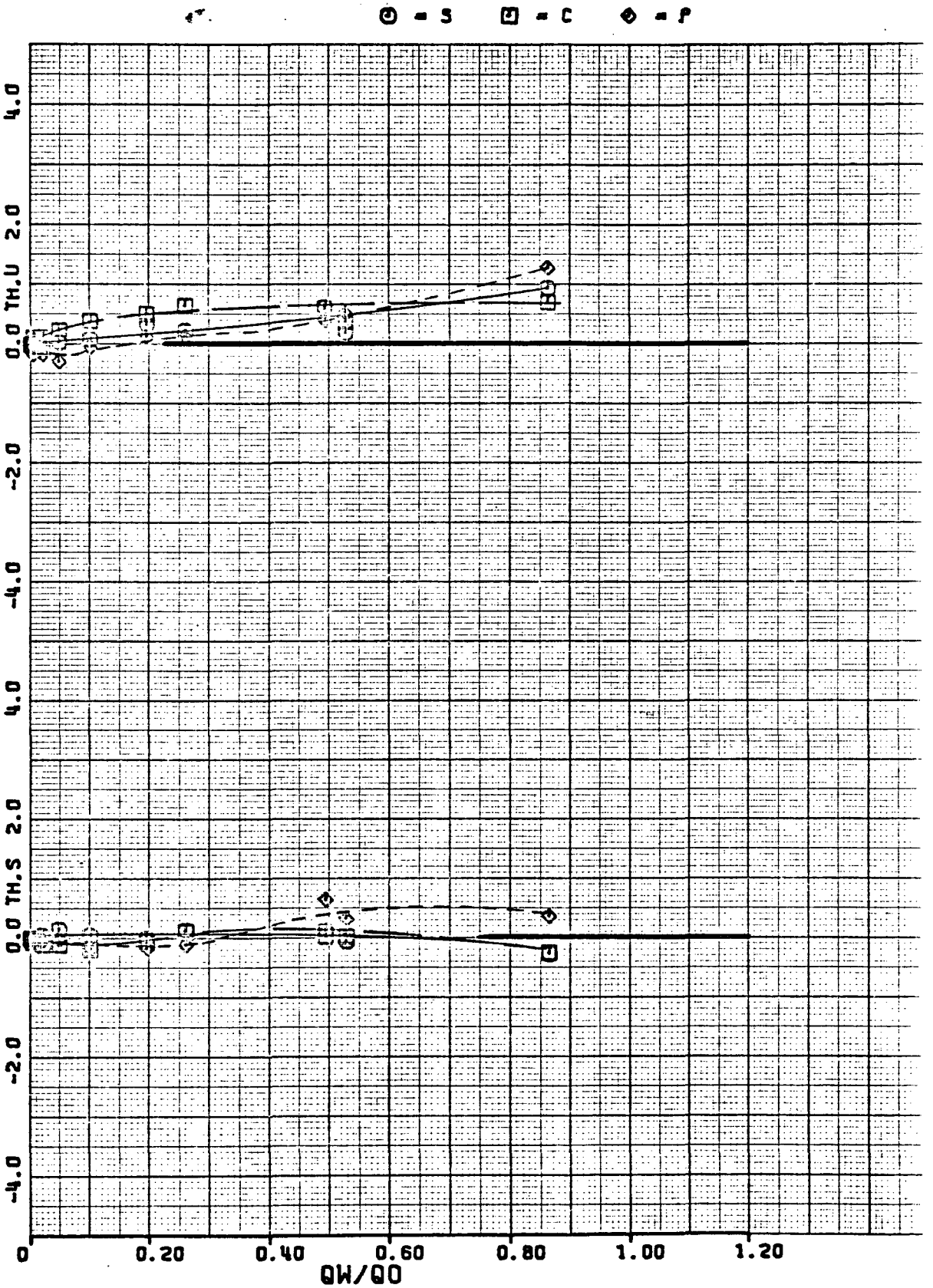

(b) $\psi = -45°$.

Figure 8.- Continued.

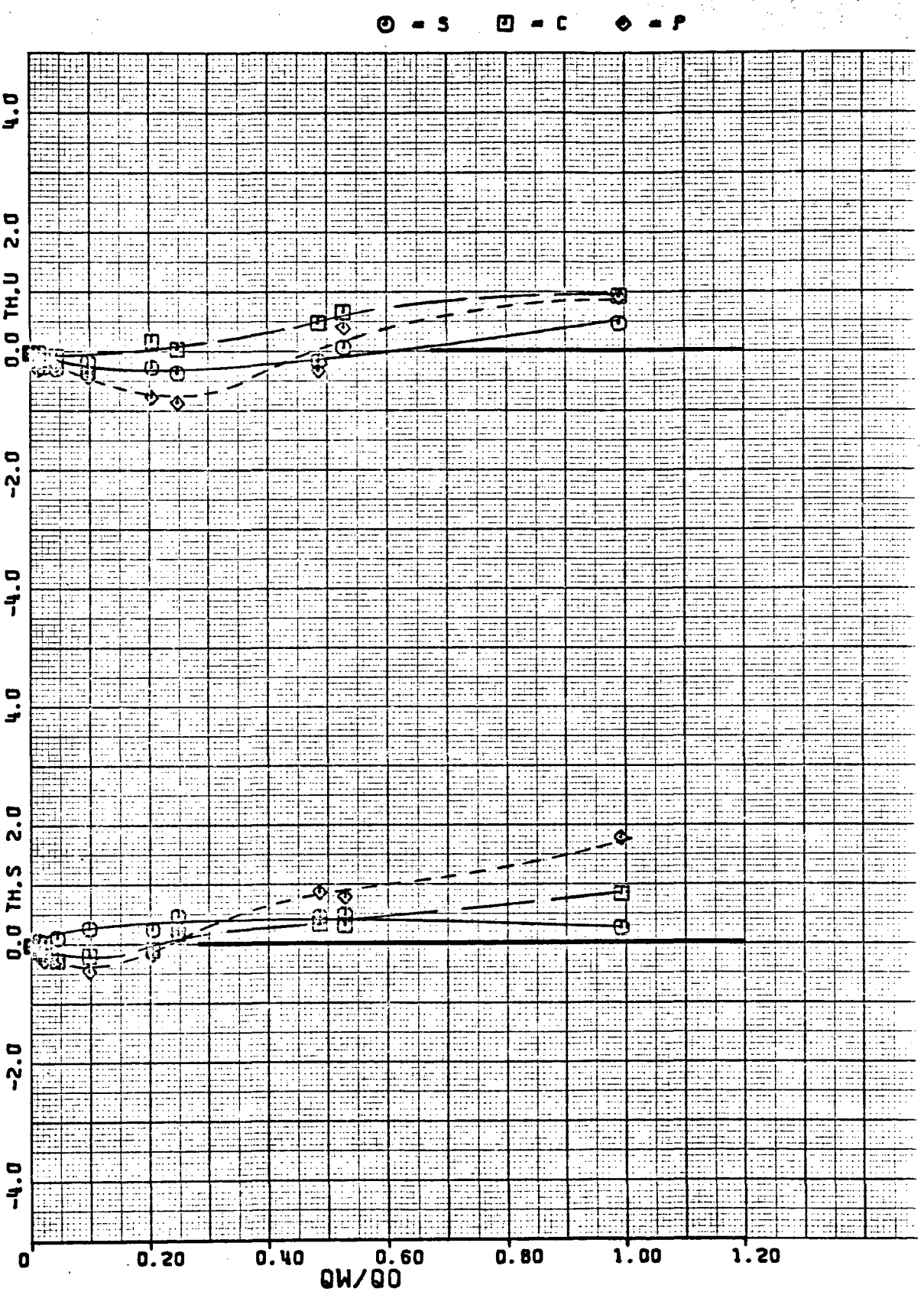

(c) $\psi = -90°$.

Figure 8.- Continued.

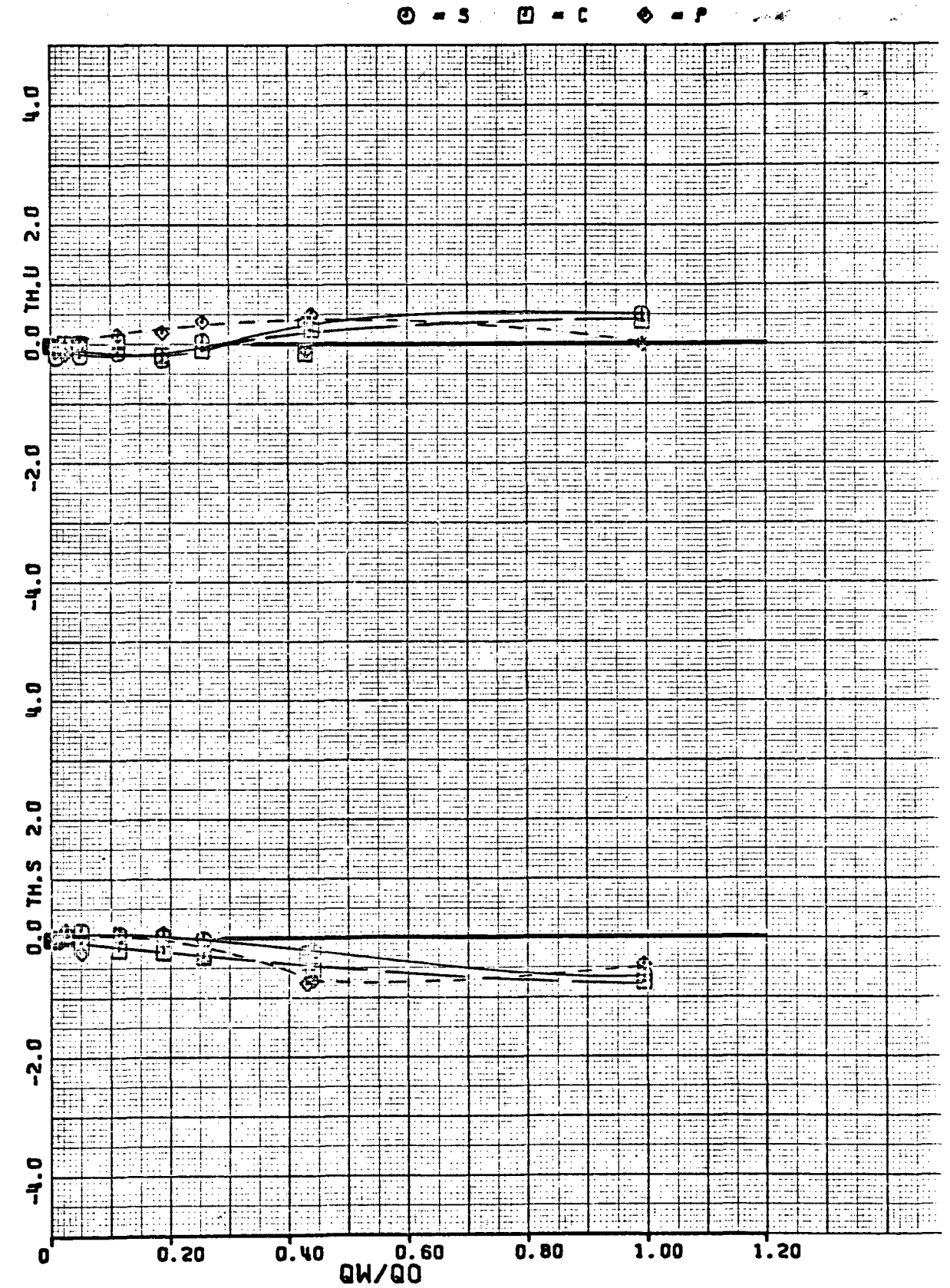

(d) $\psi = -135°$.

Figure 8.- Continued.

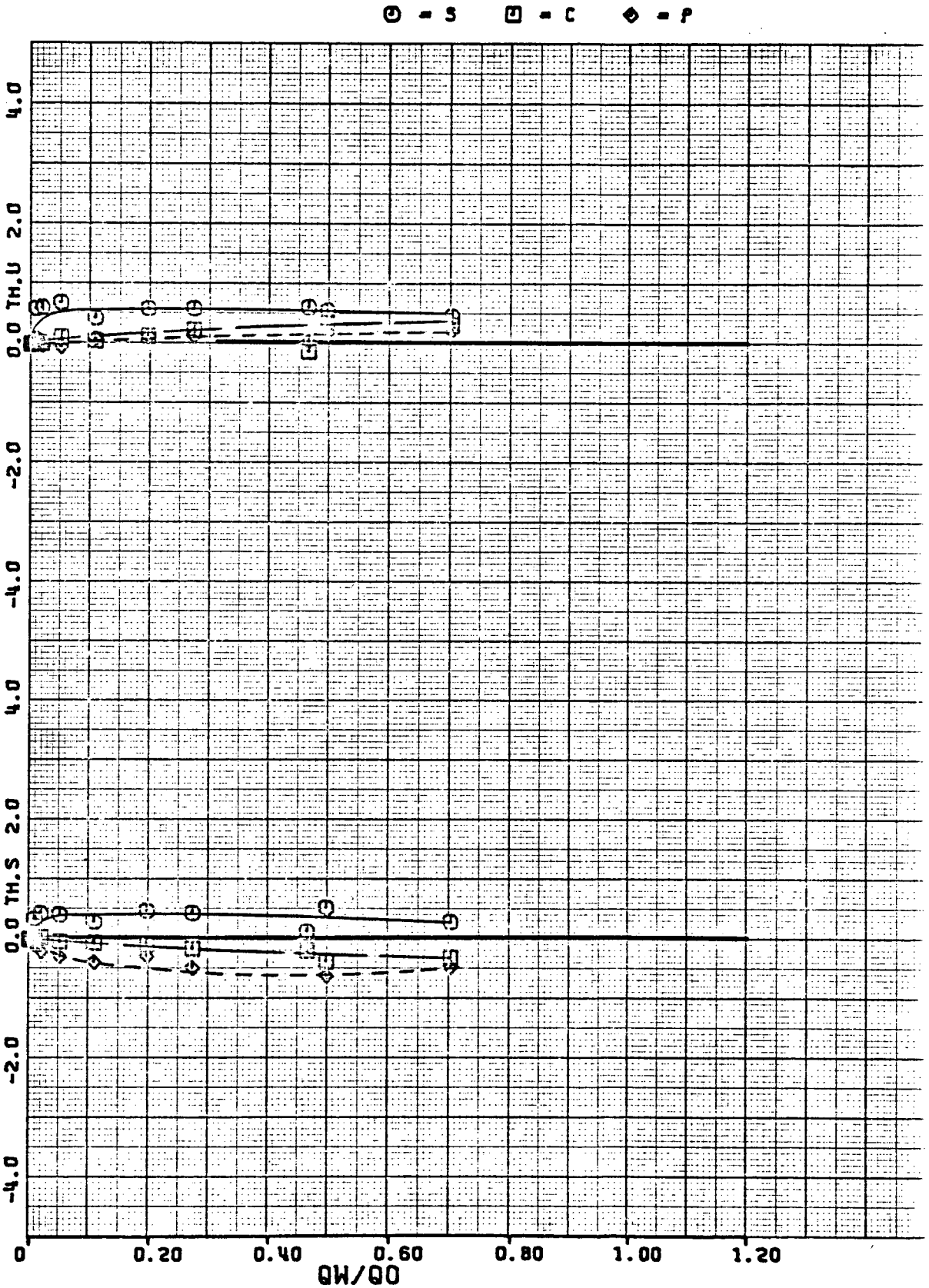

(d) $\psi = 180°$.

Figure 8.- Concluded.

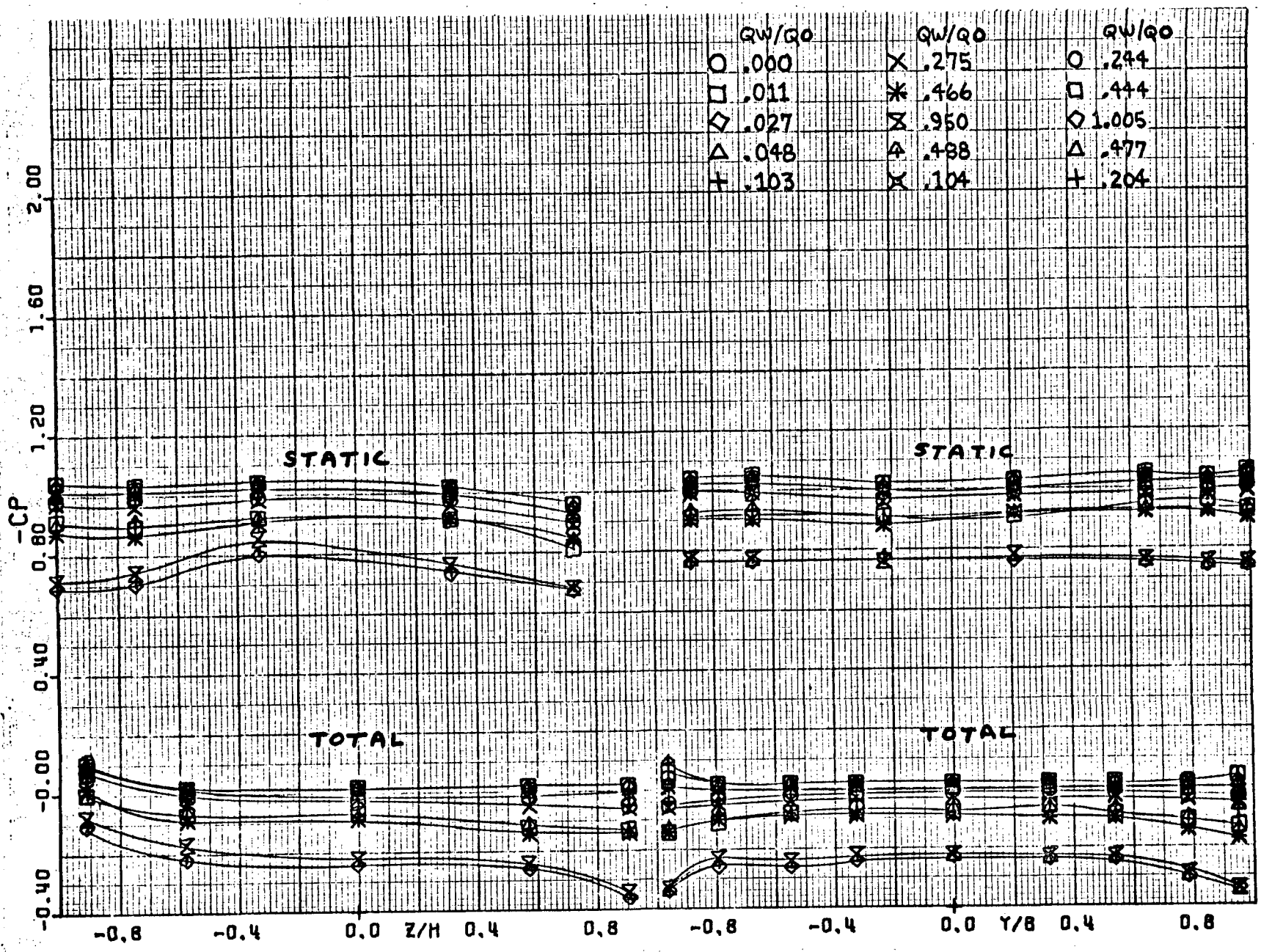

(a) $\psi = 0°$.

Figure 9.- Pressure coefficients for model without roof posts.

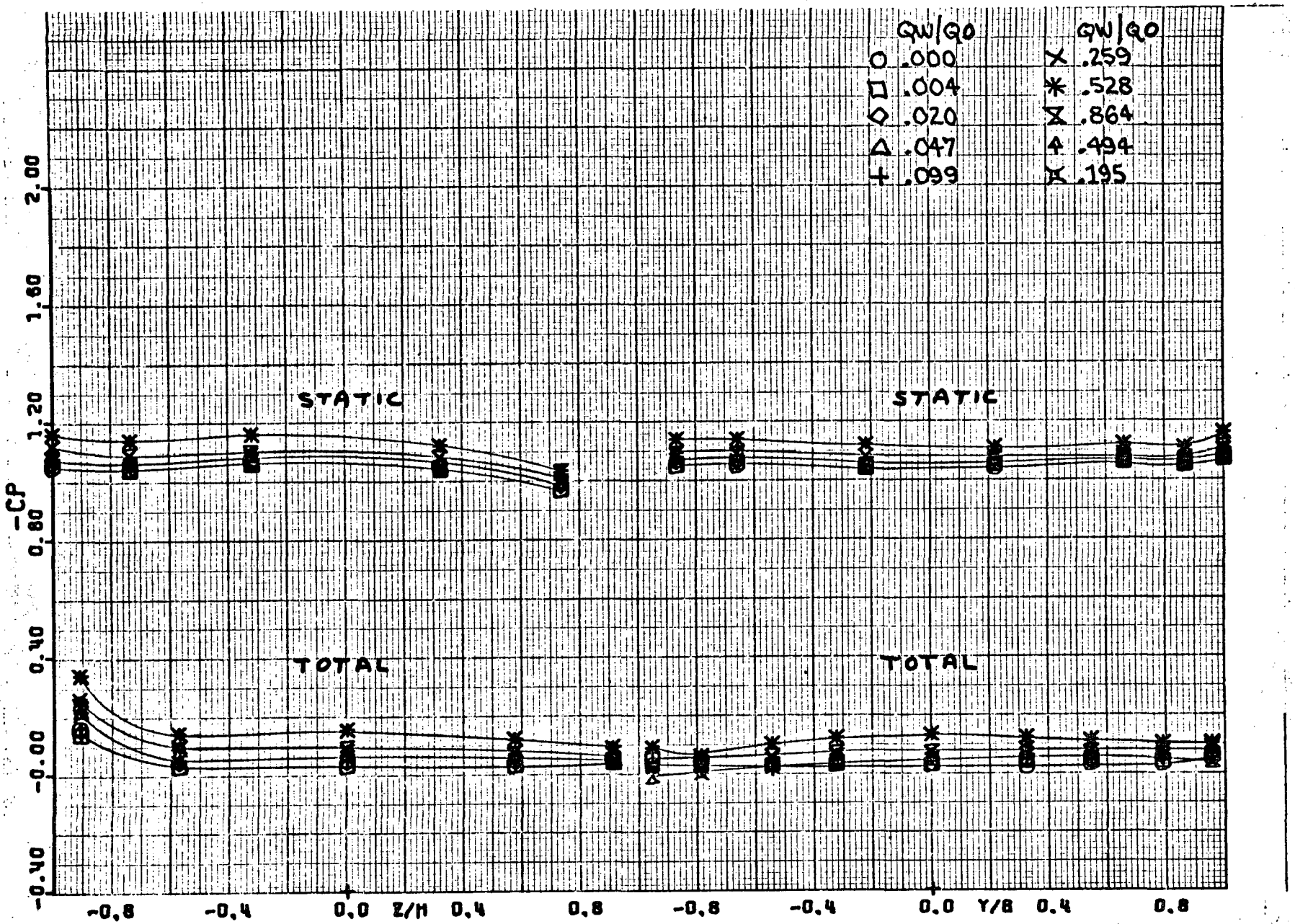

(b) $\psi = -45°$.

Figure 9.- Continued.

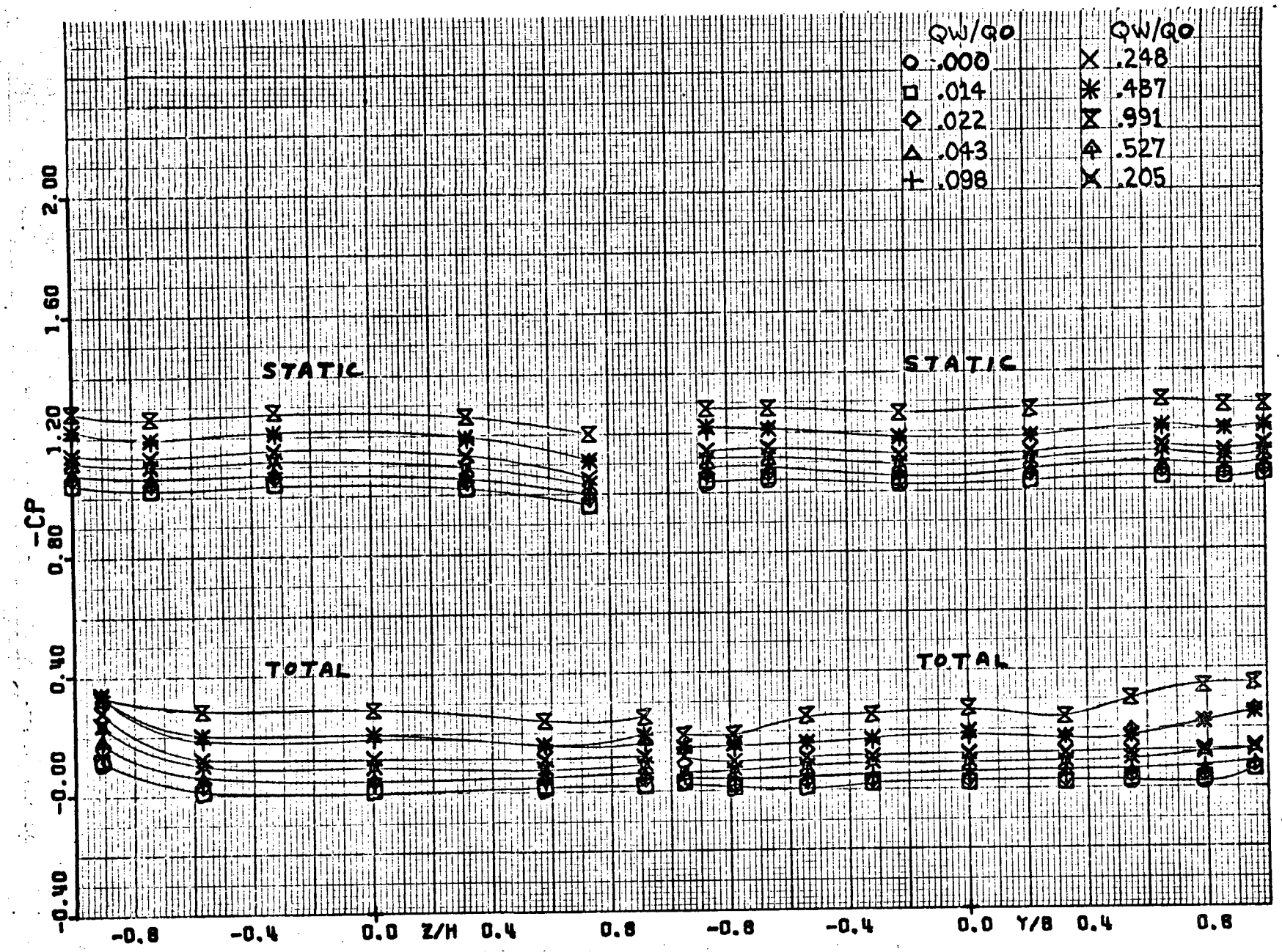

(c) $\psi = -90°$.

Figure 9.- Continued.

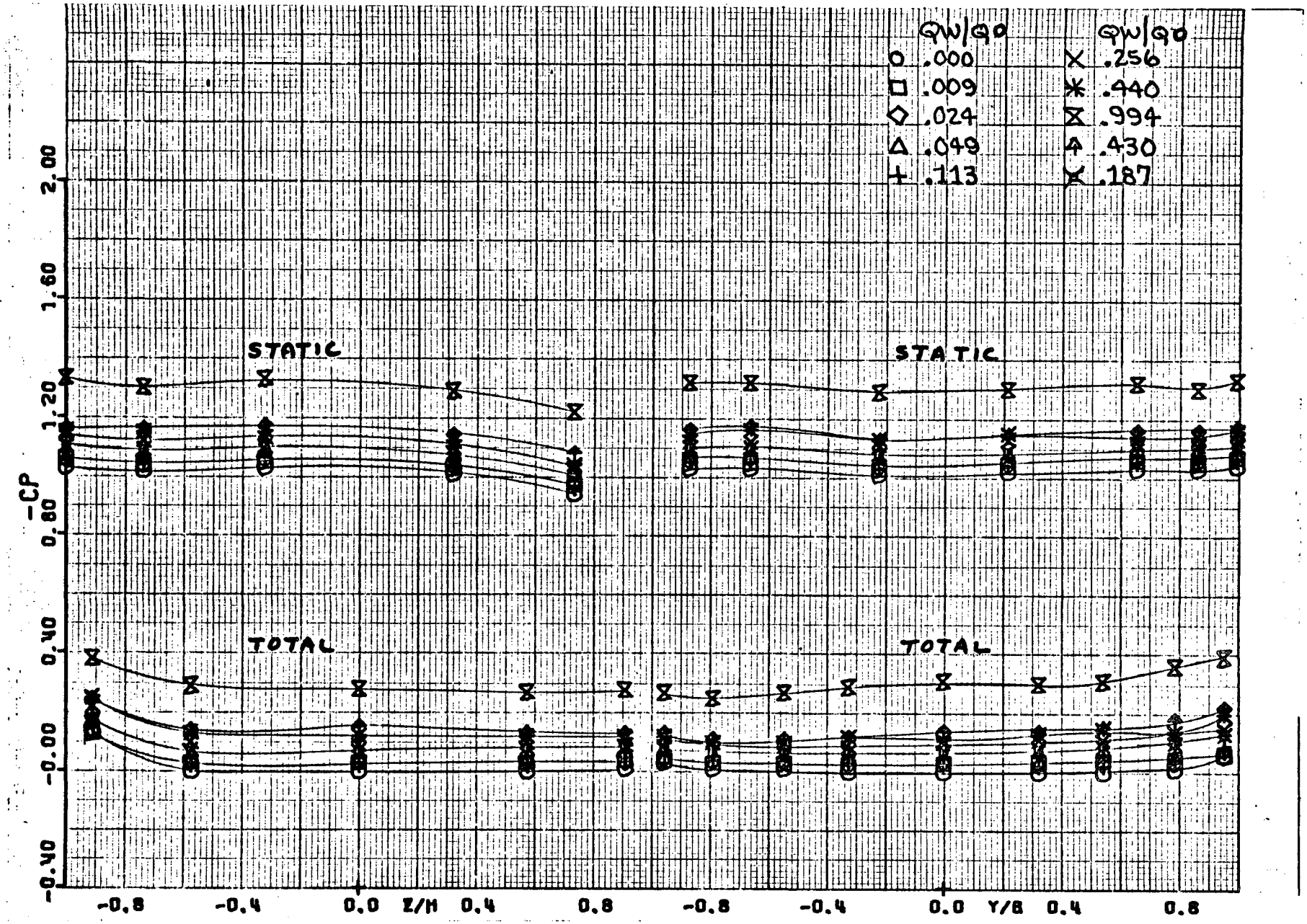

(d) $\psi = -135°$.

Figure 9.- Continued.

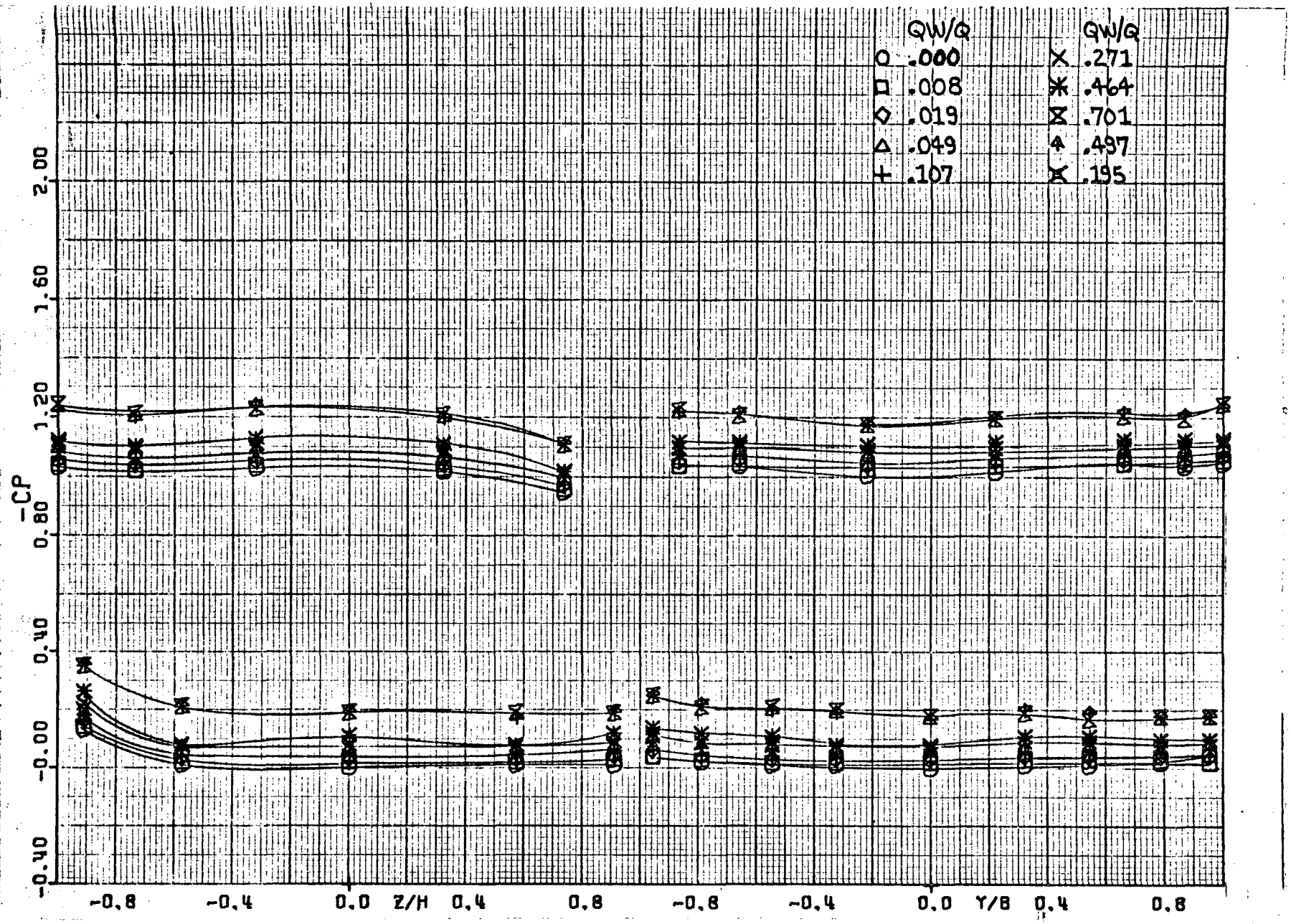

(e) $\psi = 180°$.

Figure 9.- Concluded.

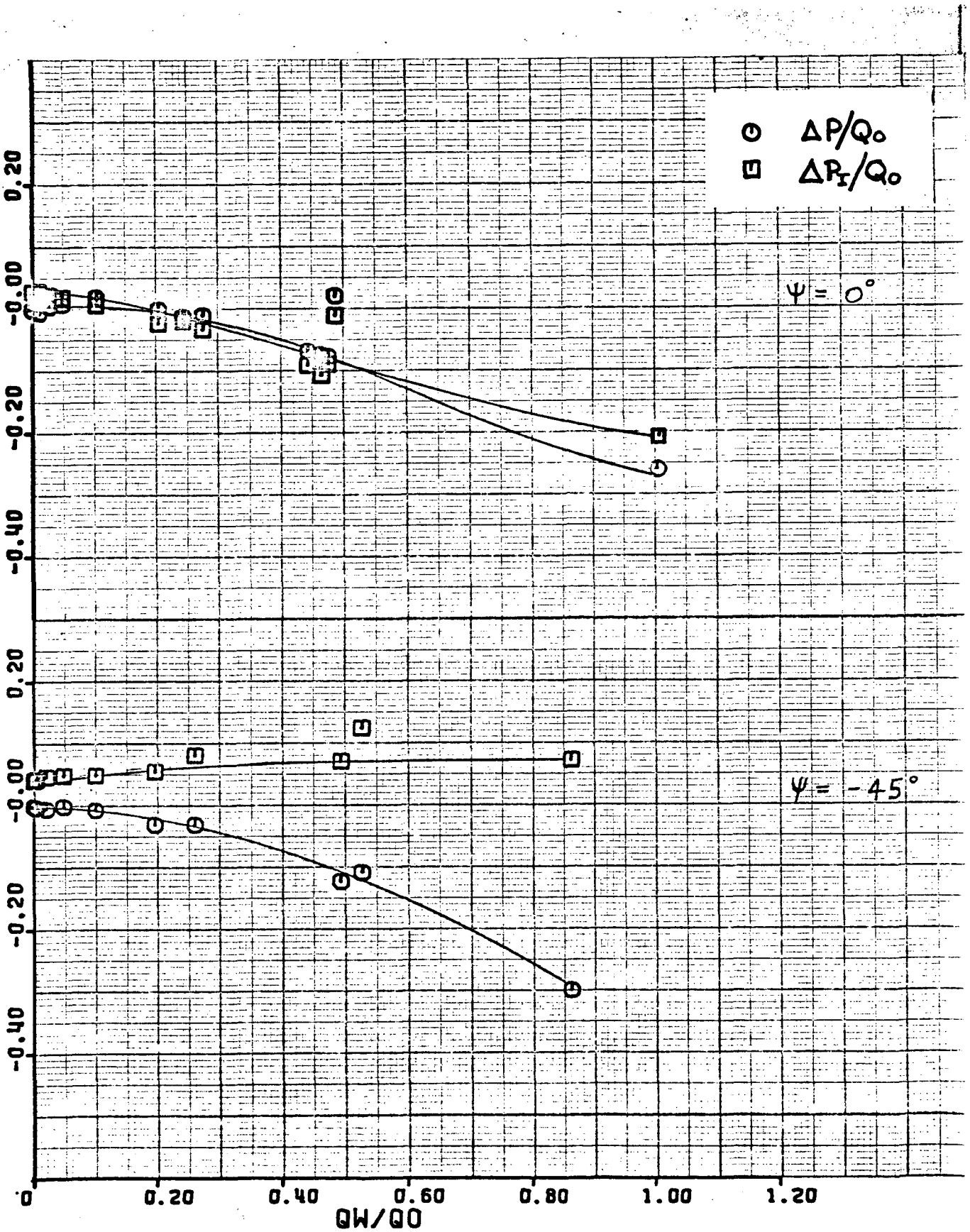

(a) $\psi = 0°$ and $-45°$.

Figure 10.- Pressure losses for model without roof posts.

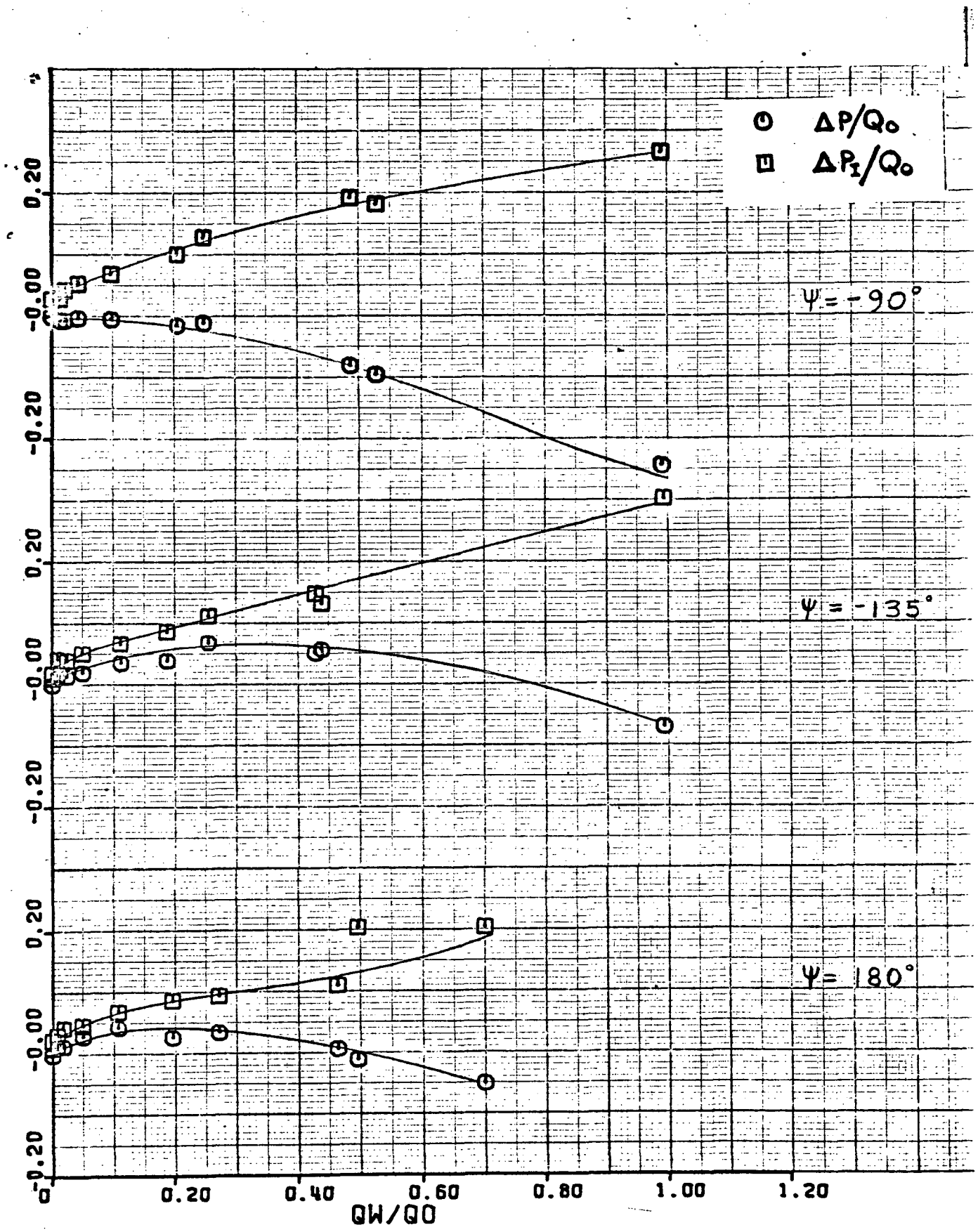

(b) ψ = -90°, -135° and 180°.

Figure 10.- Concluded.

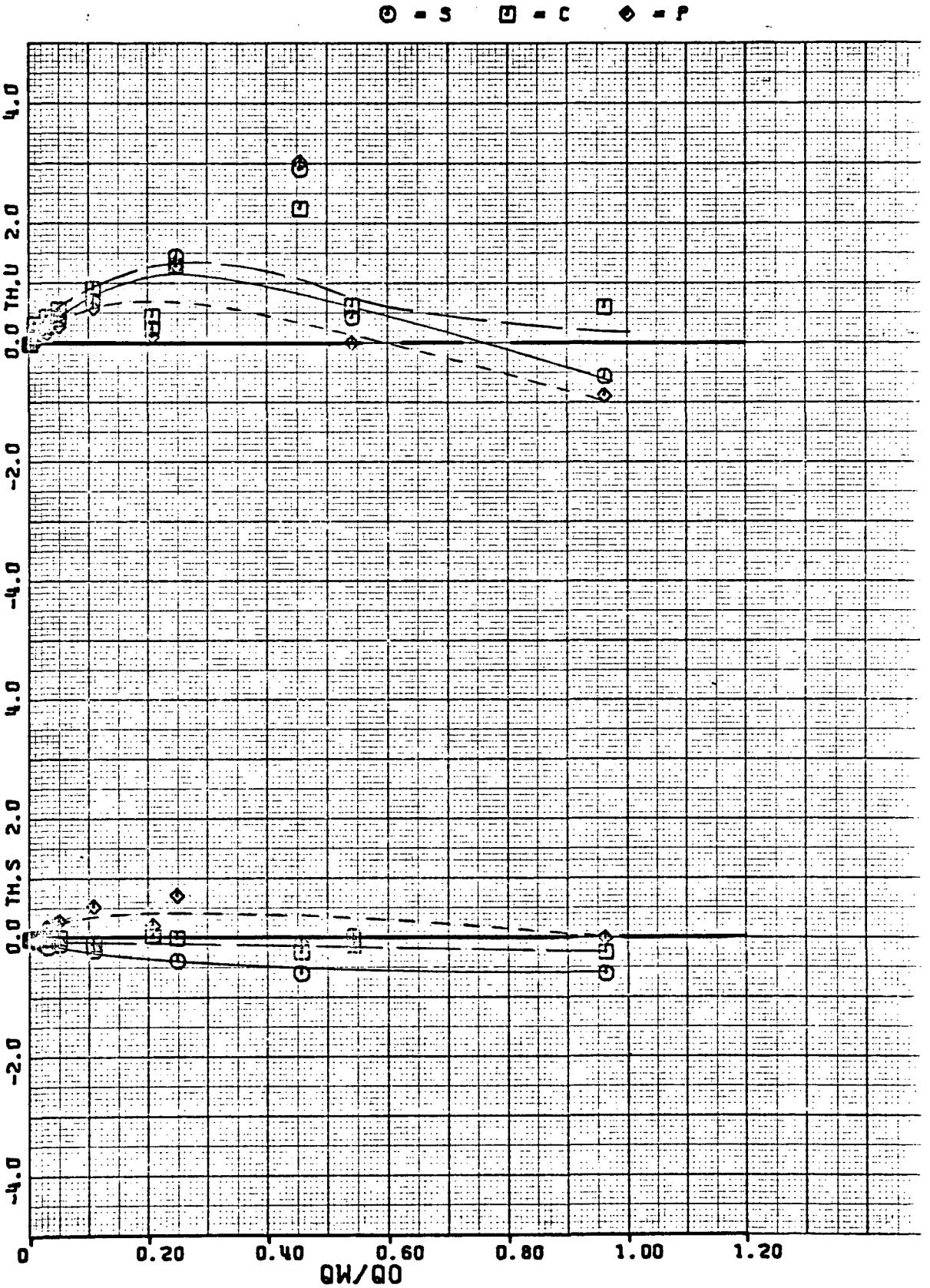

(a) $\psi = 0°$.

Figure 11.- Flow angularity for model with small inlet screen.

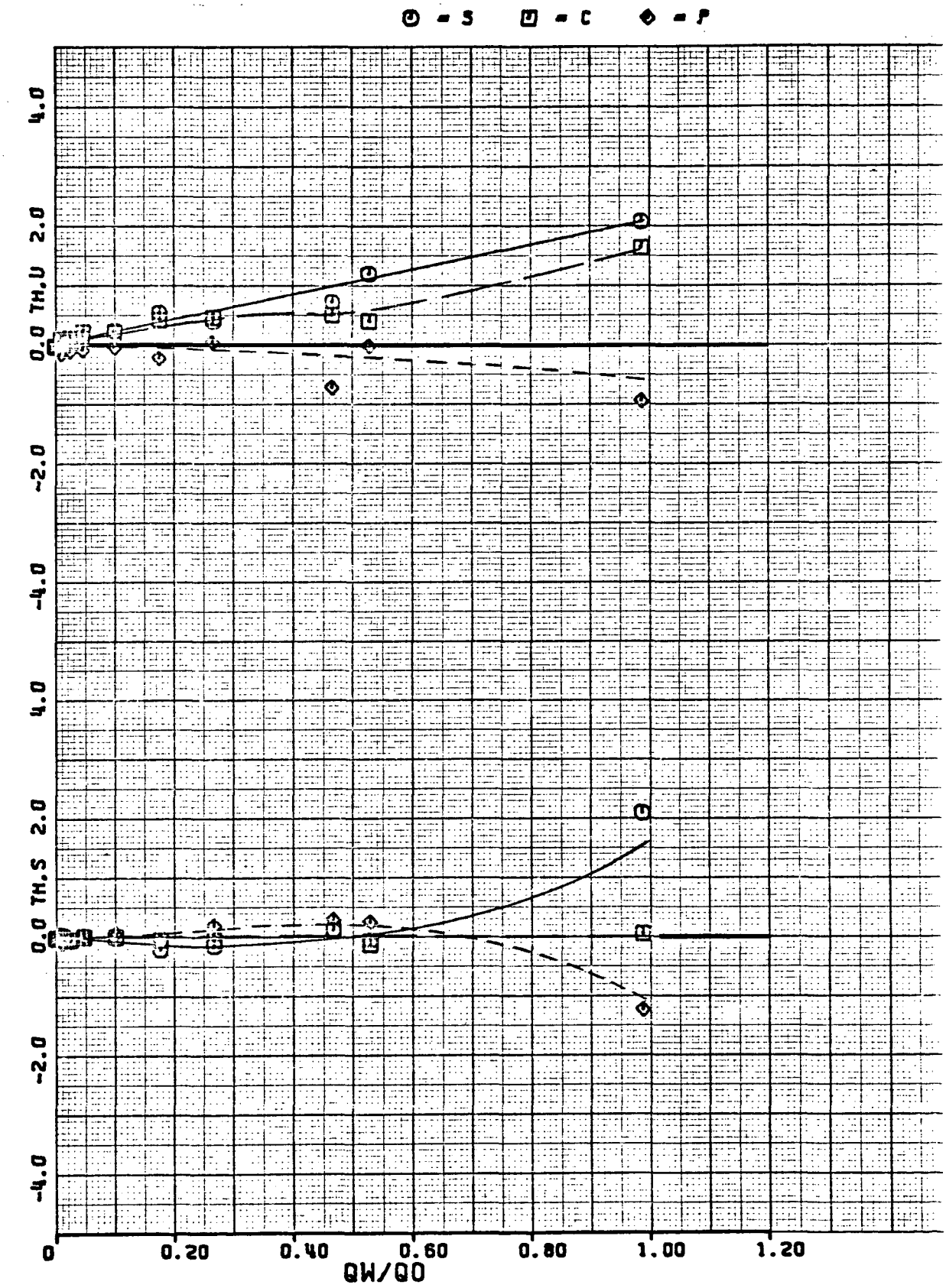

(b) $\psi = -45°$.

Figure 11.- Continued.

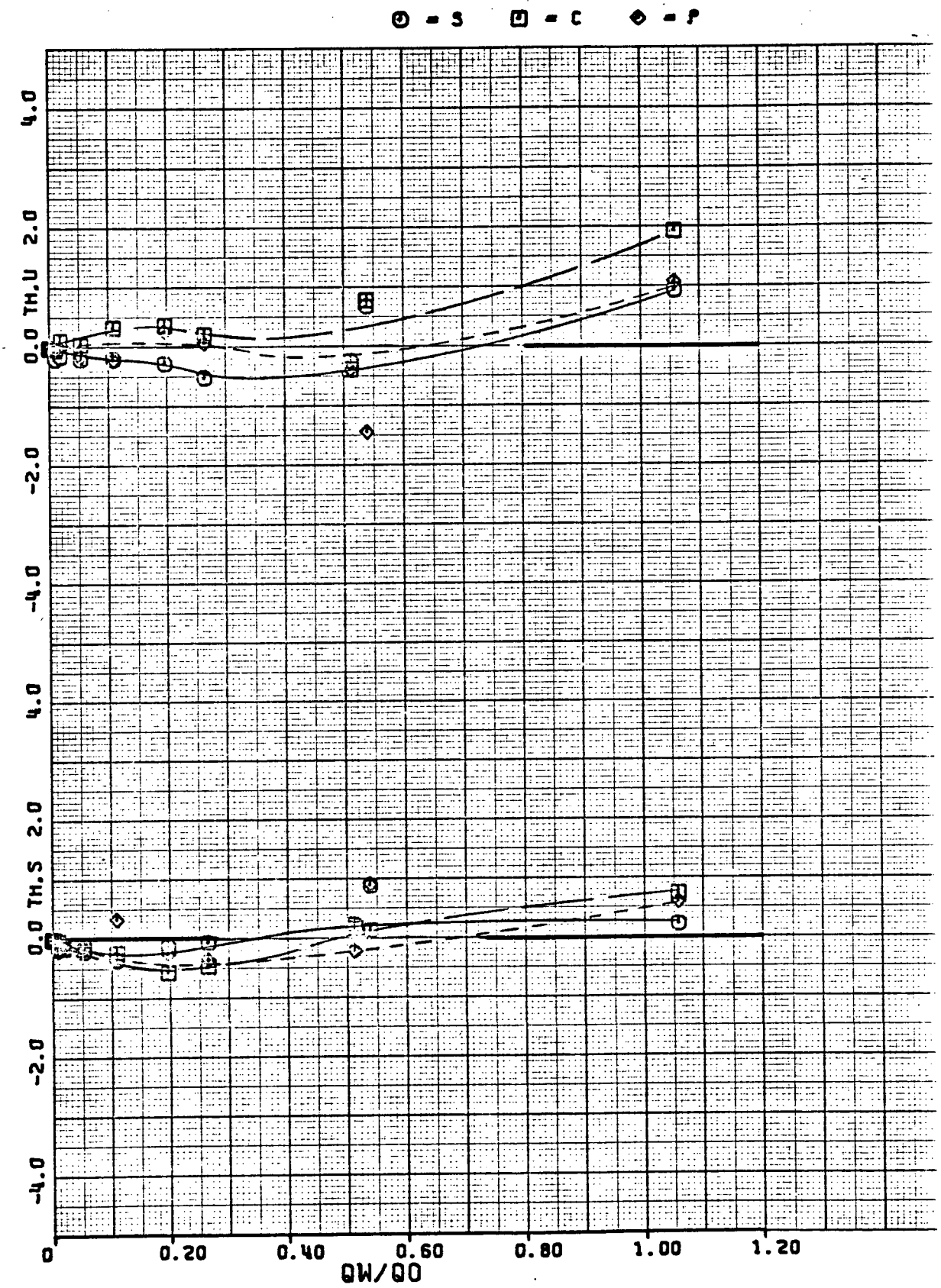

(c) $\psi = -90°$.

Figure 11.- Continued.

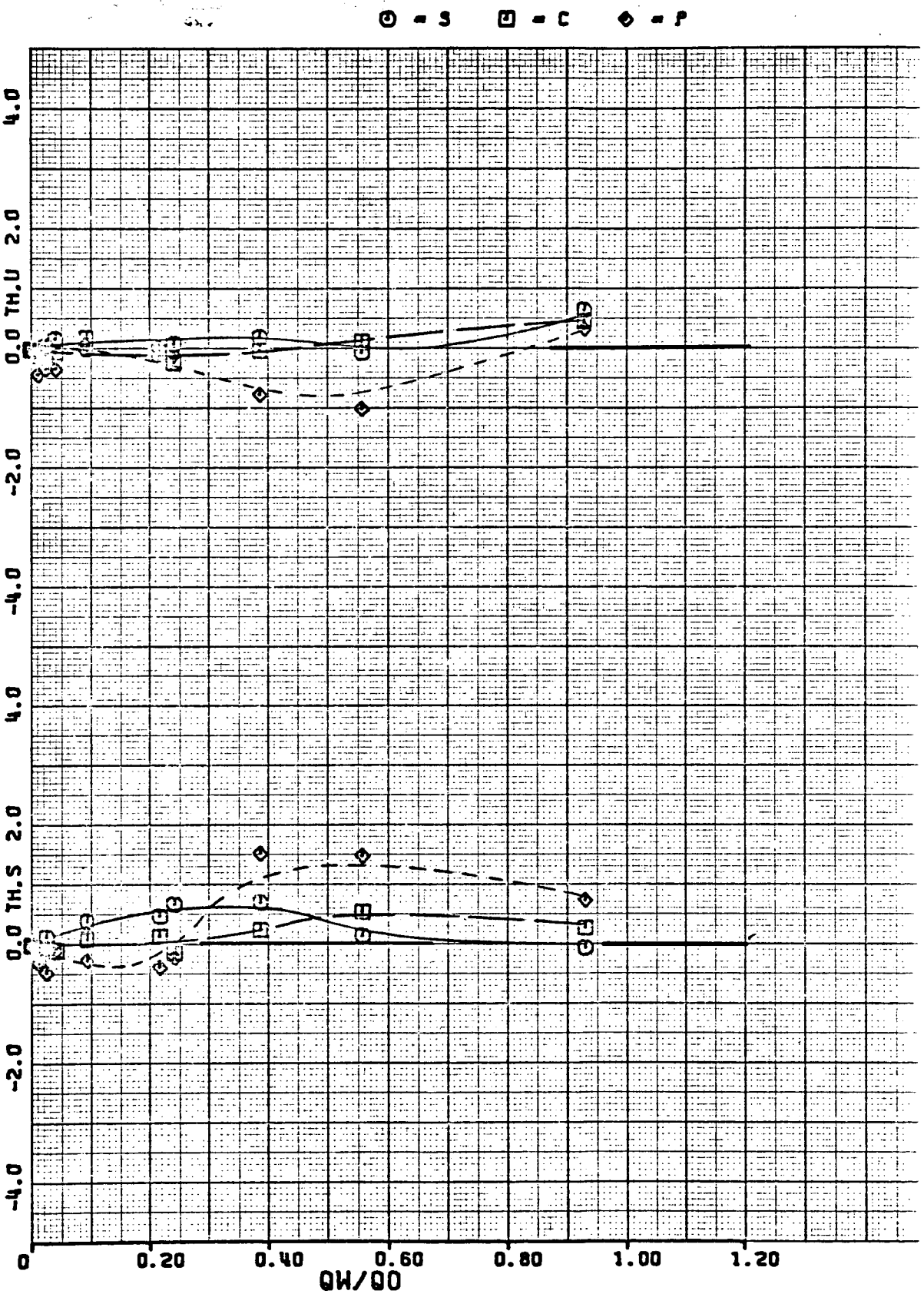

(d) $\psi = -135°$.

Figure 11.- Continued.

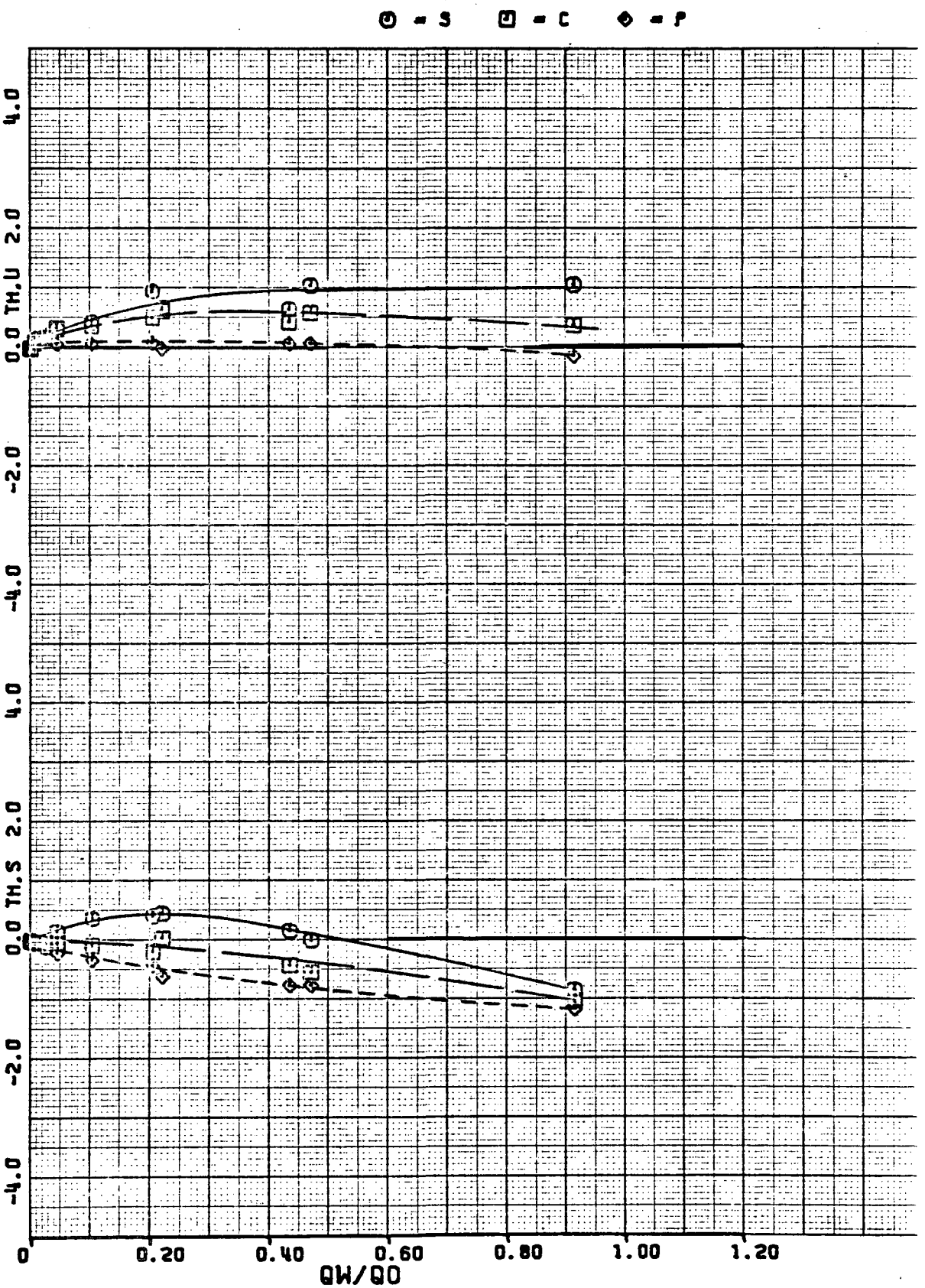

(e) $\psi = 180°$.

Figure 11.- Concluded.

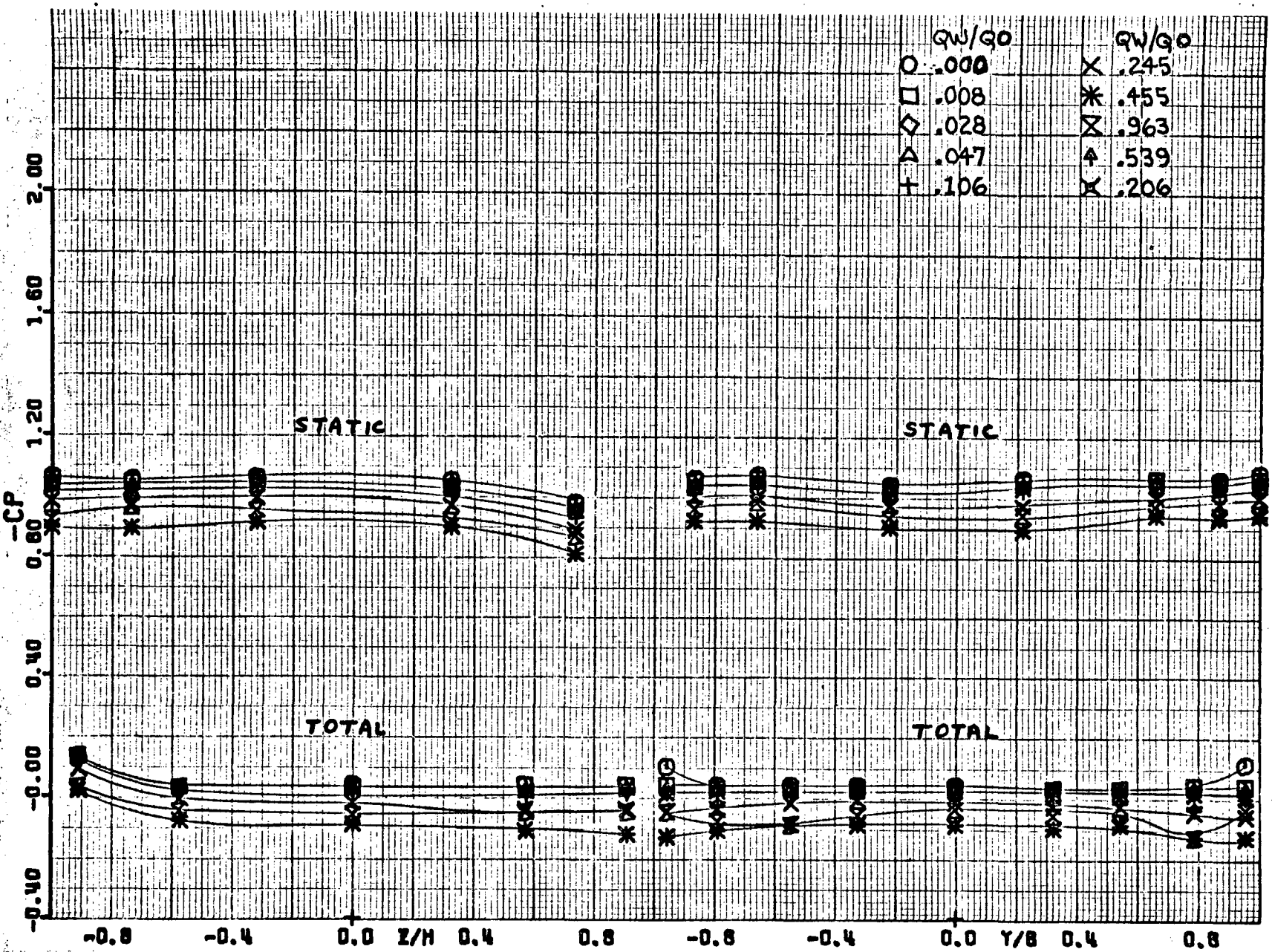

(a) $\psi = 0°$.

Figure 12.- Pressure coefficients for model with small inlet screen.

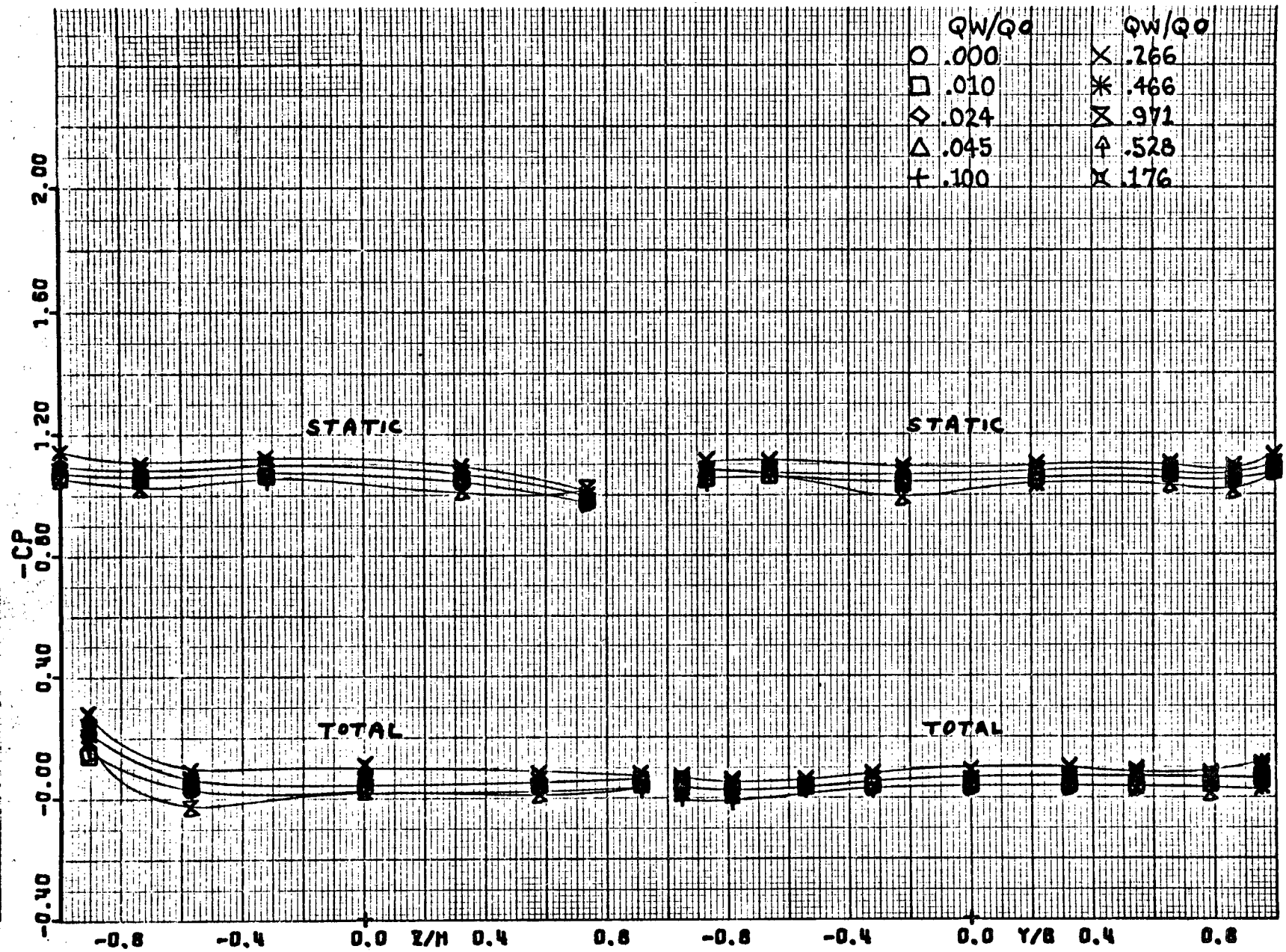

(b). $\psi = -45°$.

Figure 12.- Continued.

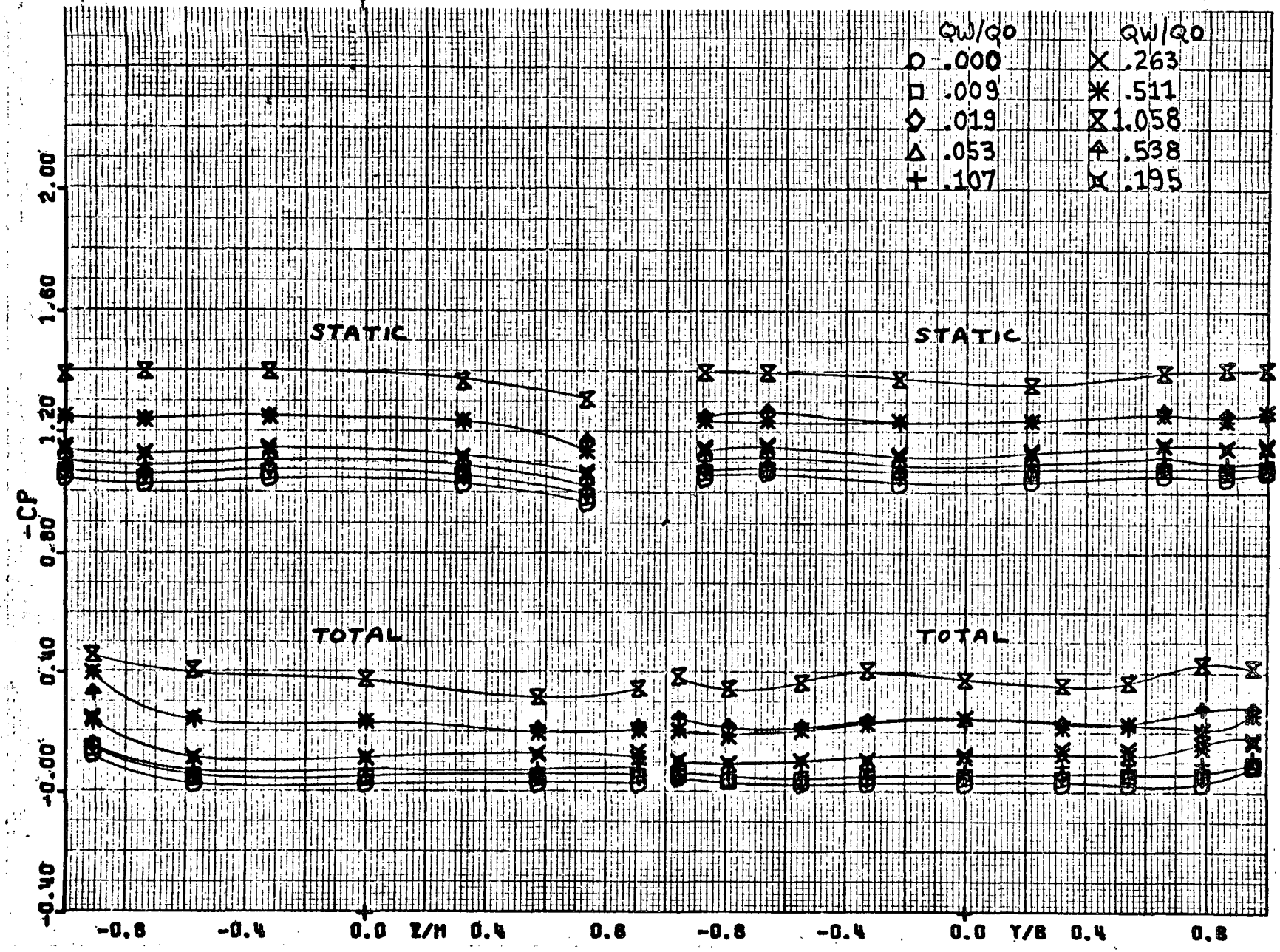

(c). $\psi = -90°$.

Figure 12.- Continued.

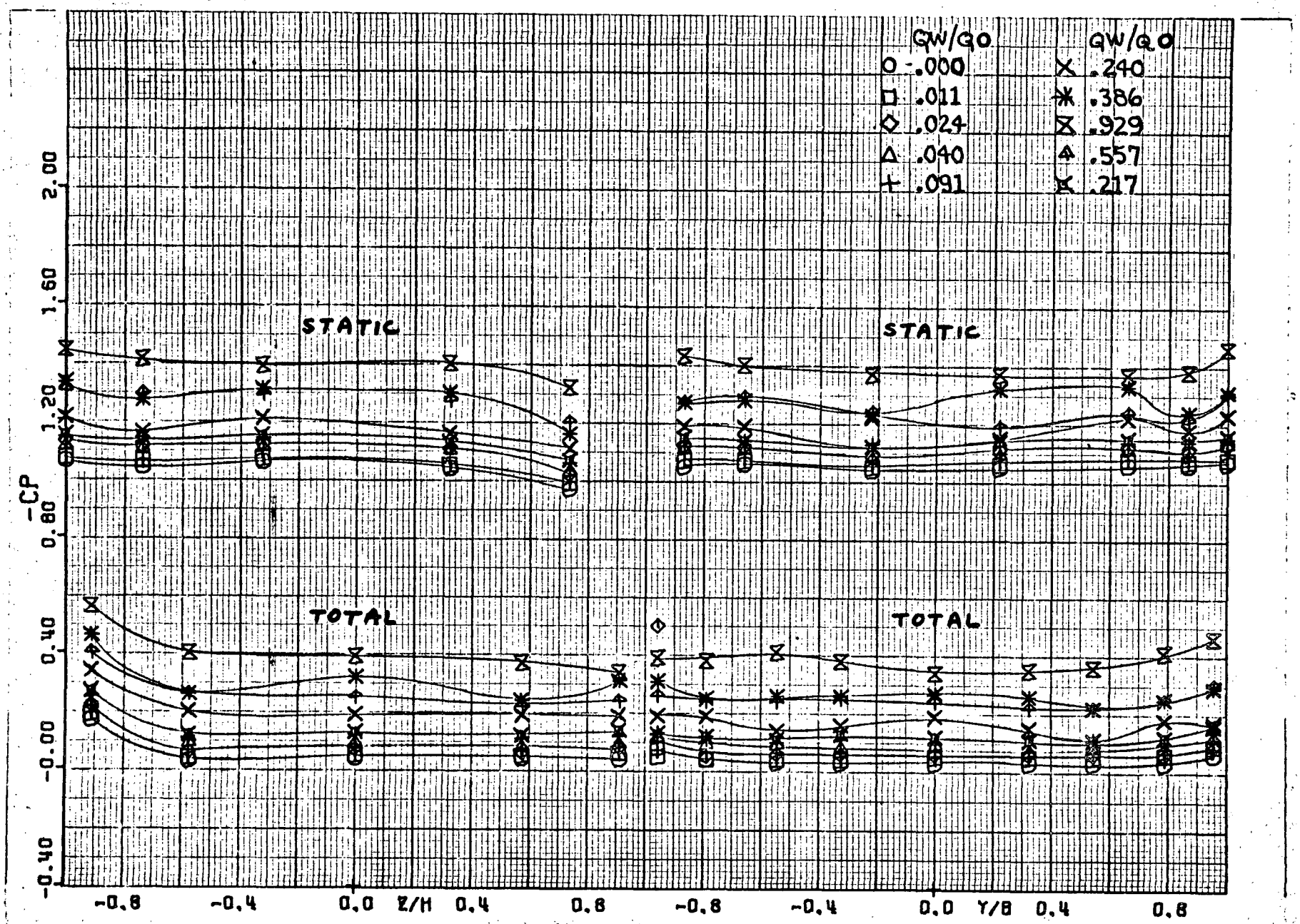

(d) $\psi = -135°$.

Figure 12.- Continued.

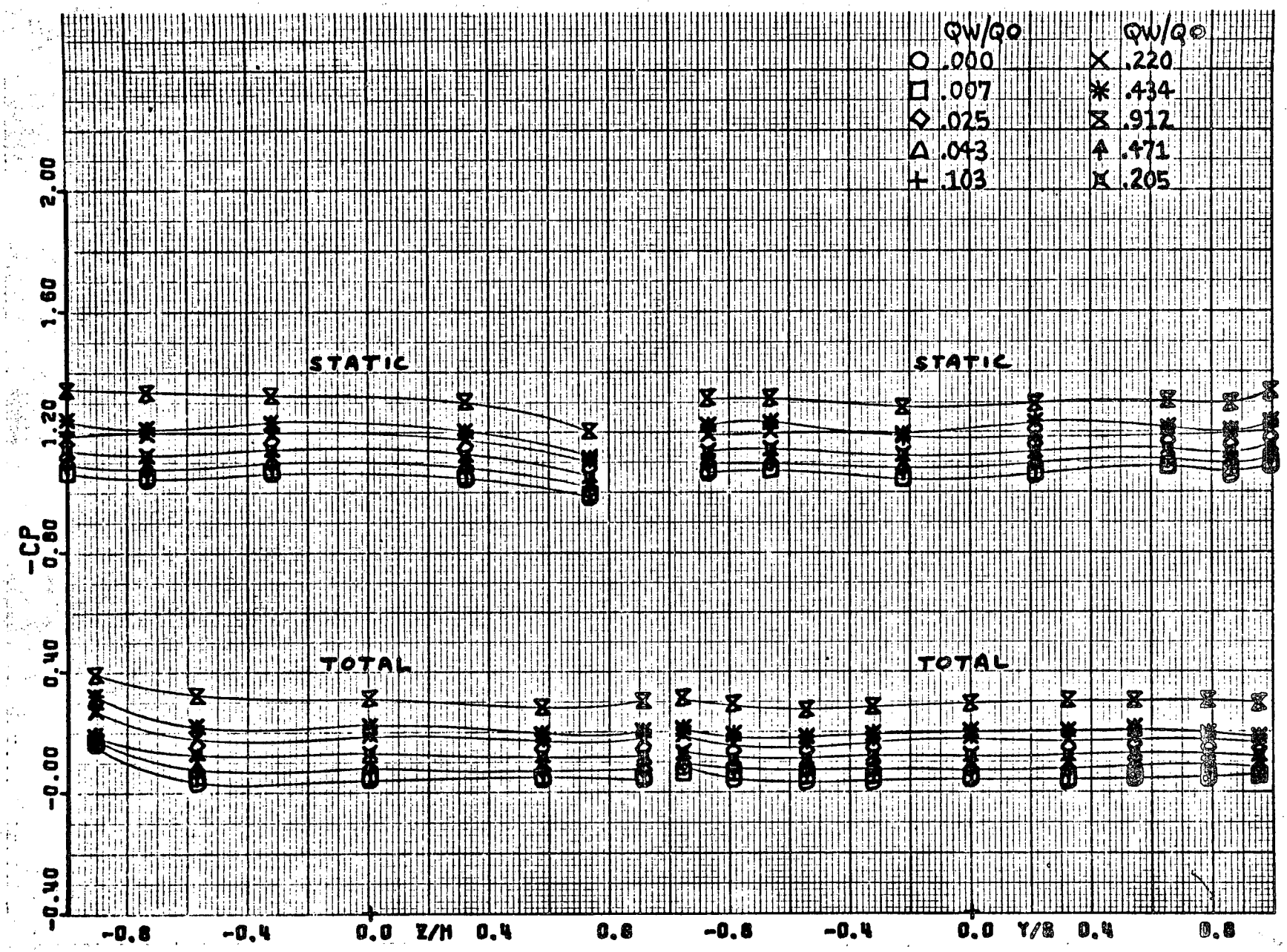

(e) $\psi = 180°$.

Figure 12.- Concluded.

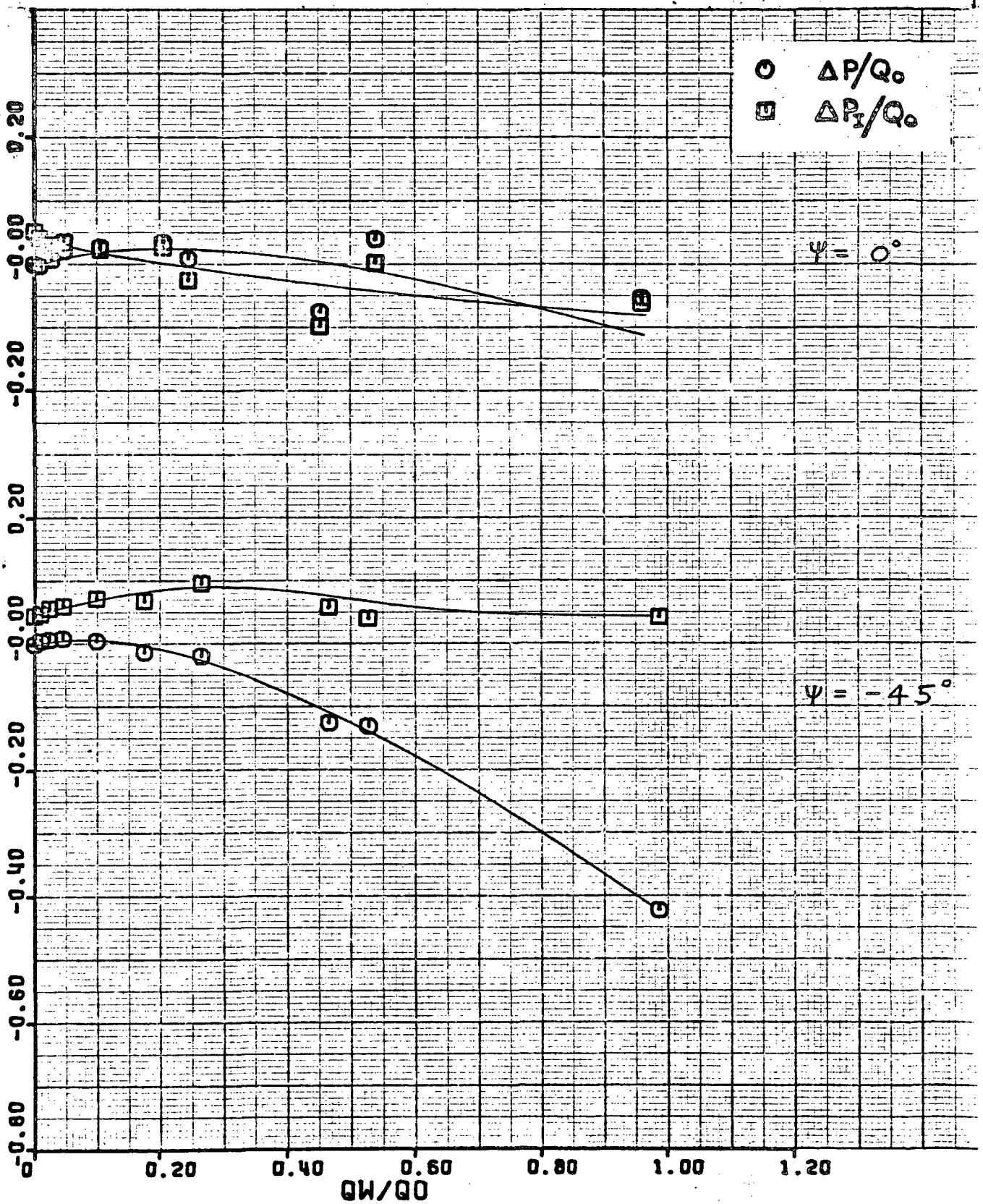

(a) $\psi = 0°$ and $-45°$.

Figure 13.- Pressure losses for model with small inlet screen.

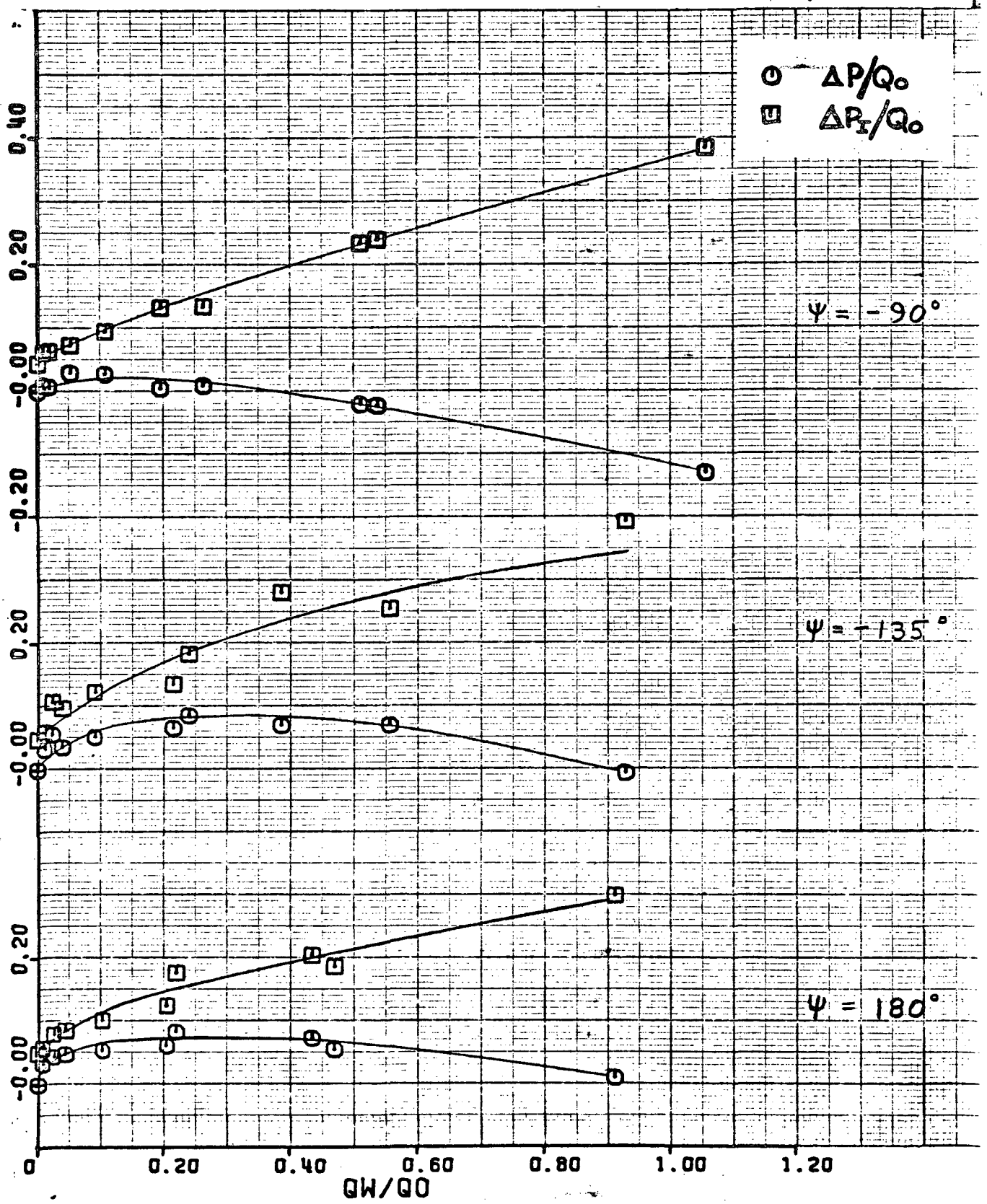

(b) ψ = -90°, -135° and 180°.

Figure 13.- Concluded.

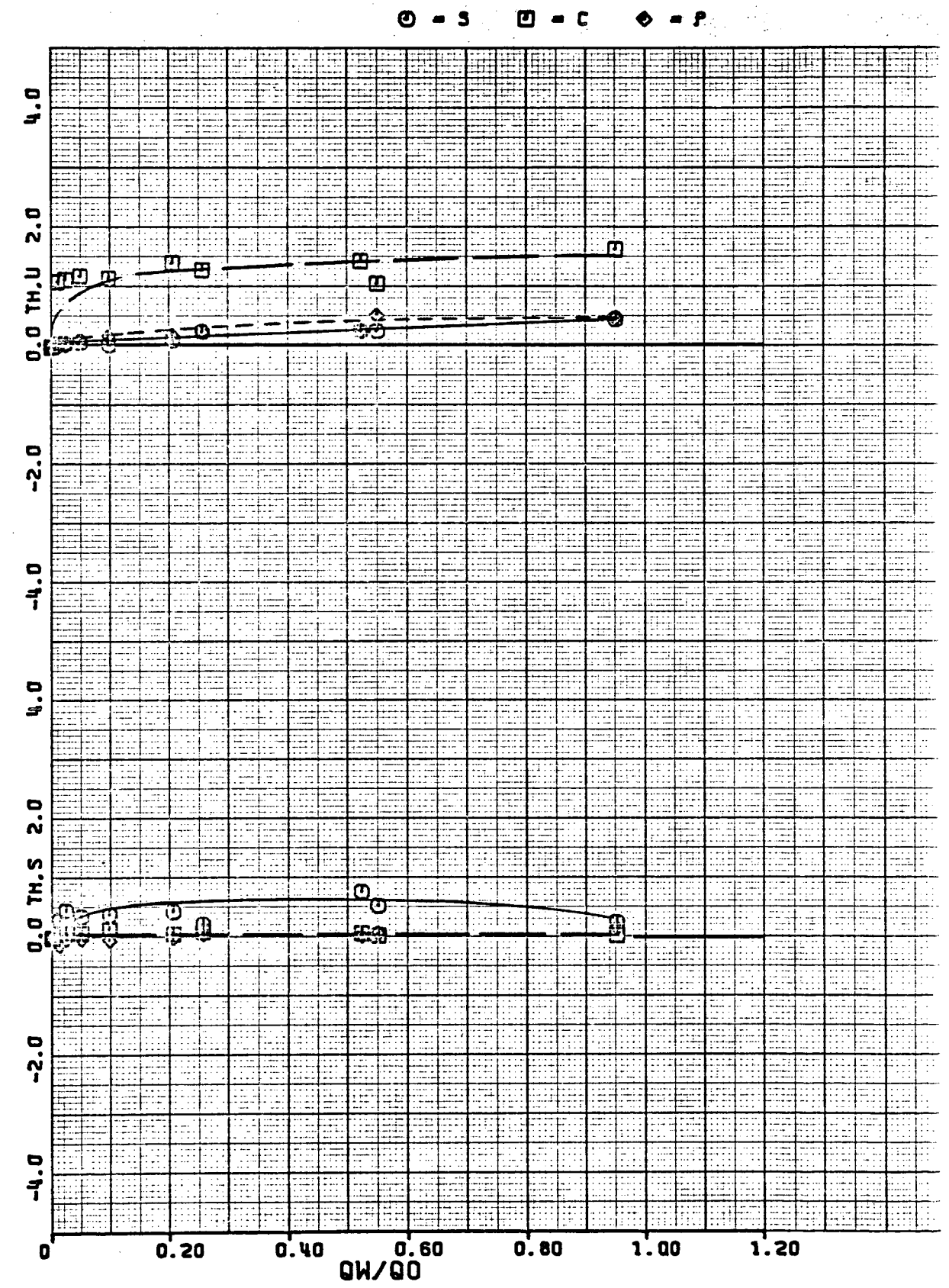

(a) $\psi = 0°$.

Figure 14.- Flow angularity for model with 4.8:1 contraction system.

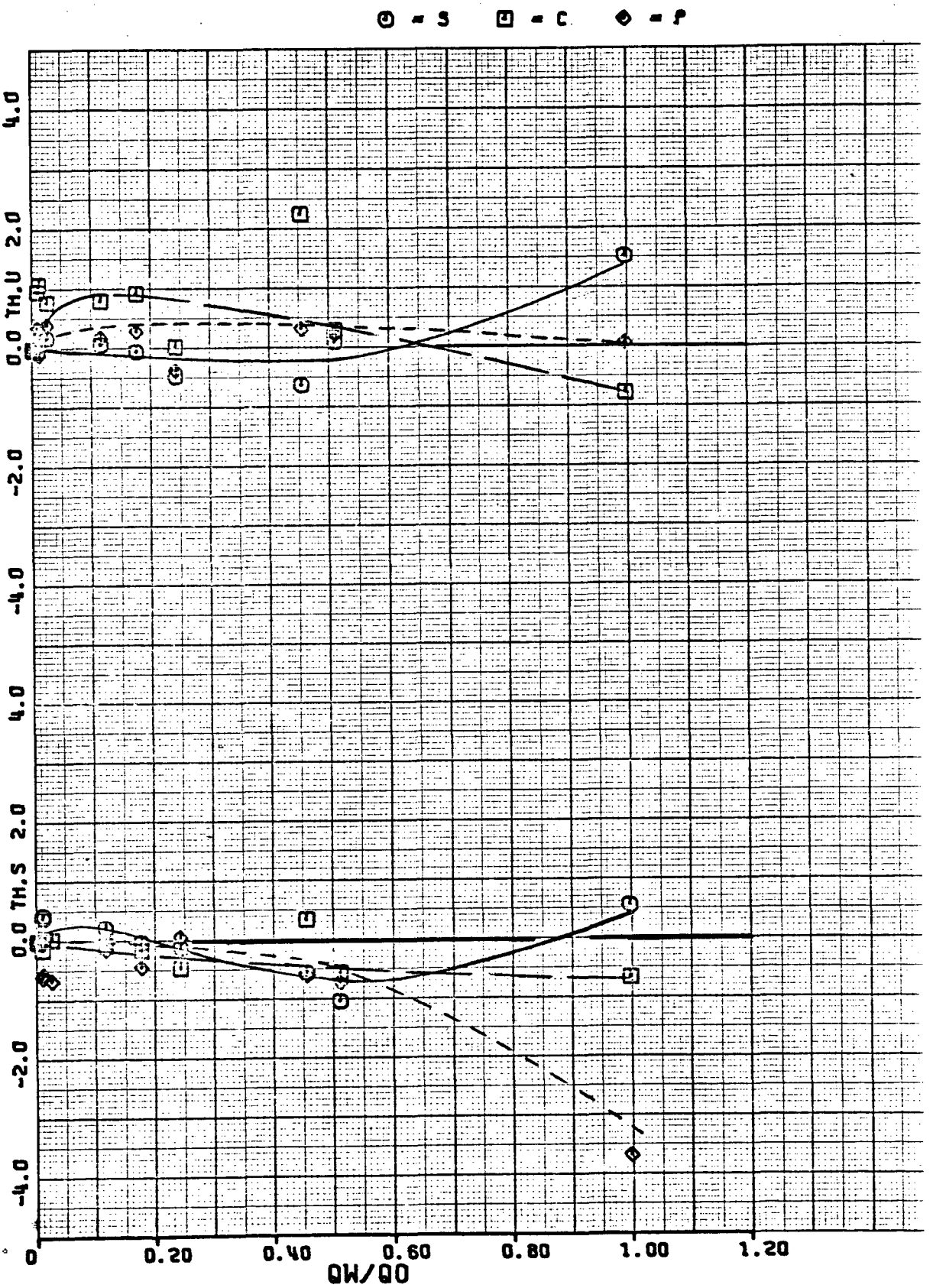

(b) $\psi = -45°$.

Figure 14.- Continued.

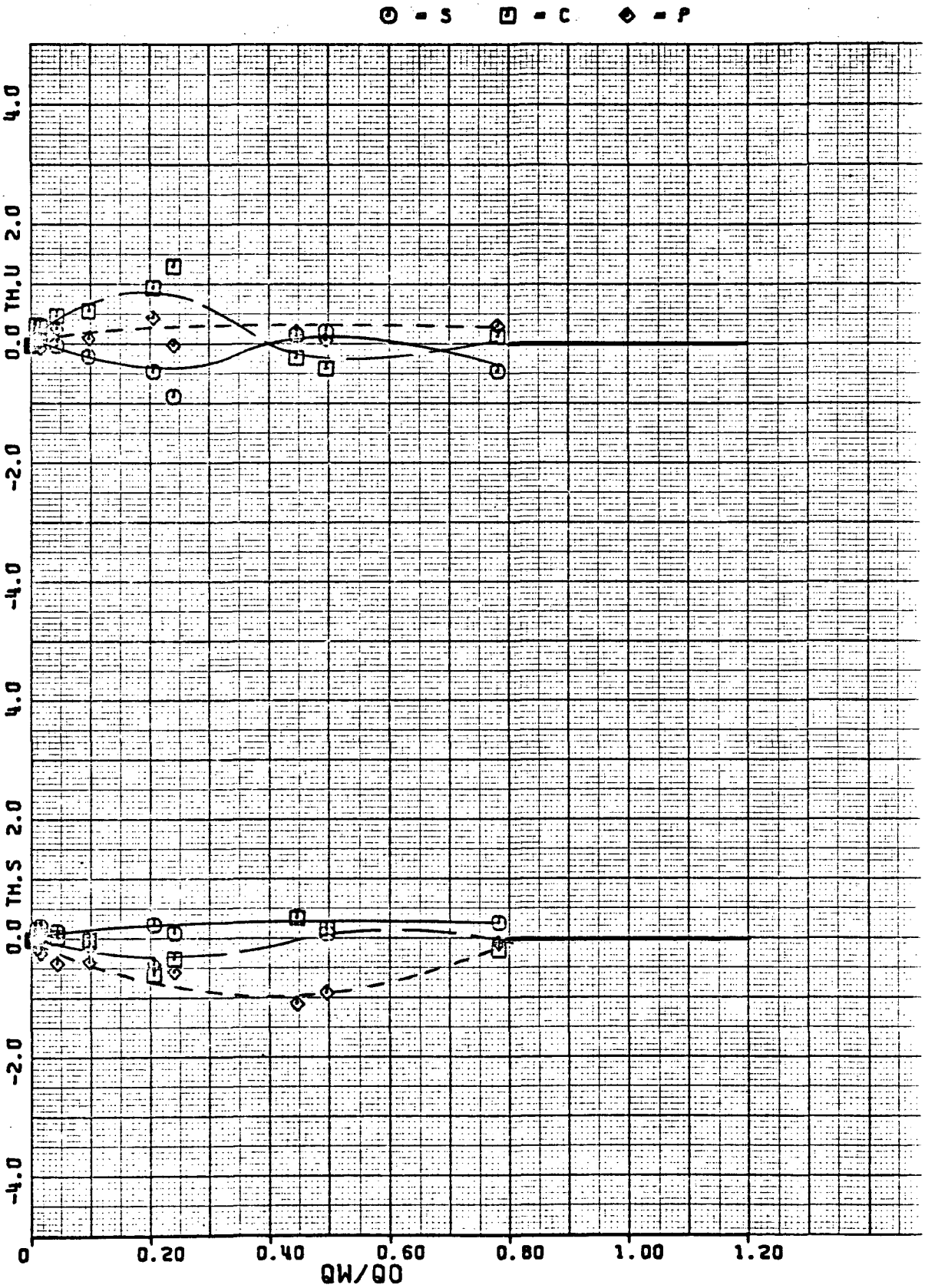

(c) $\psi = -90°$.

Figure 14.- Continued.

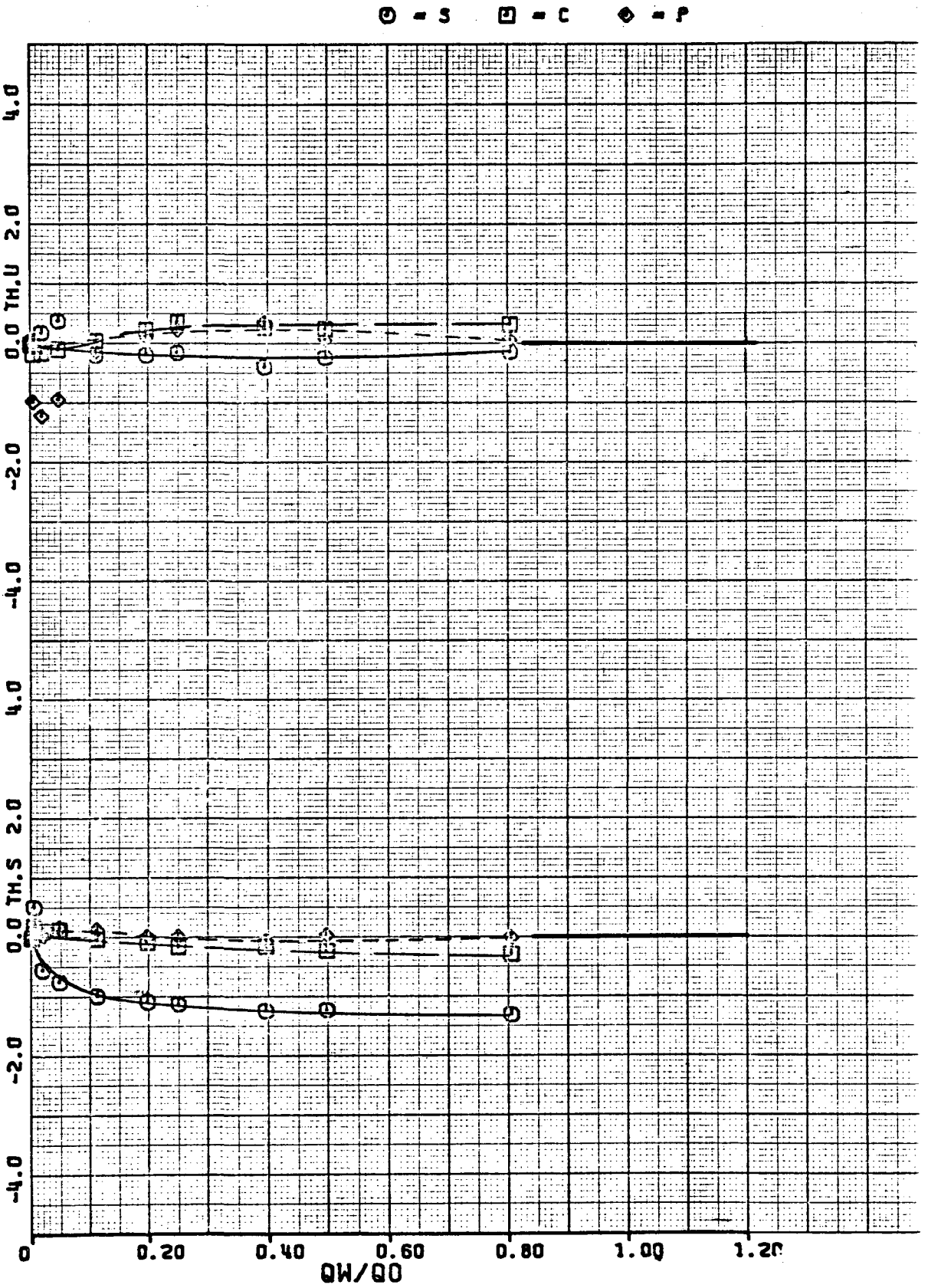

(d) $\psi = -135°$.

Figure 14.- Continued.

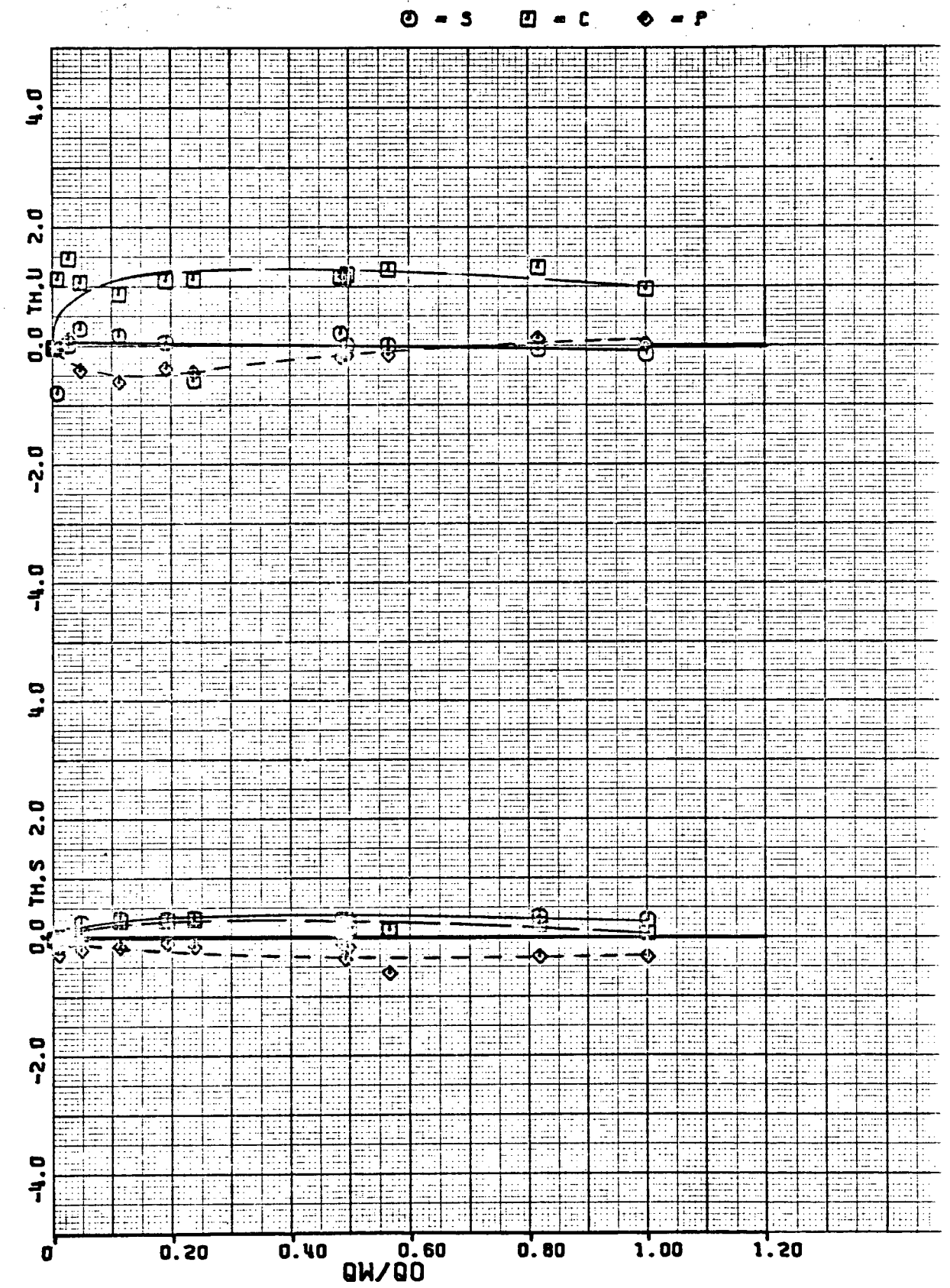

(e) $\psi = 180°$.

Figure 14.- Concluded.

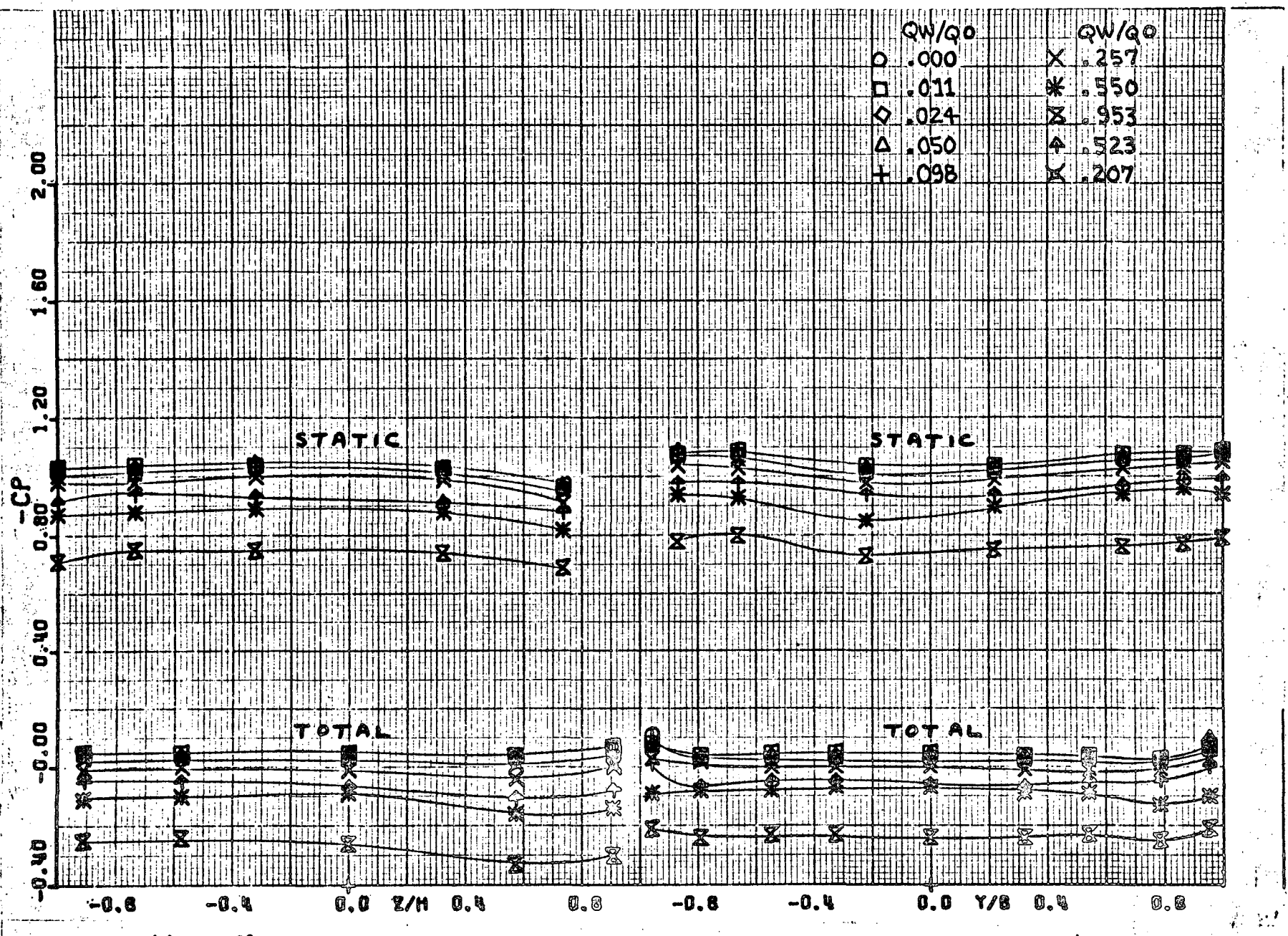

(a) $\psi = 0°$.

Figure 15.- Pressure coefficients for model with 4.8:1 contraction system.

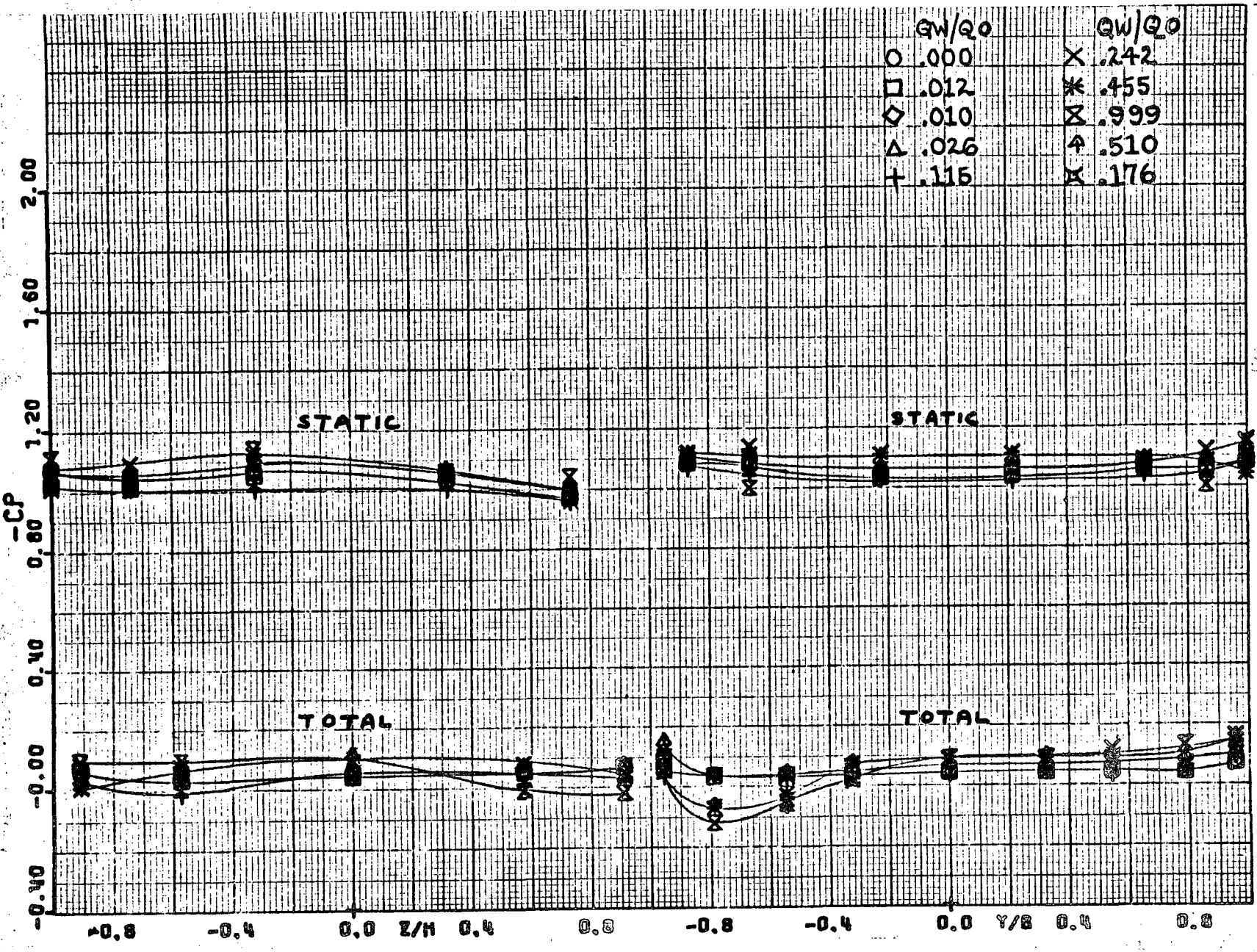

(b) $\psi = -45°$.

Figure 15.- Continued.

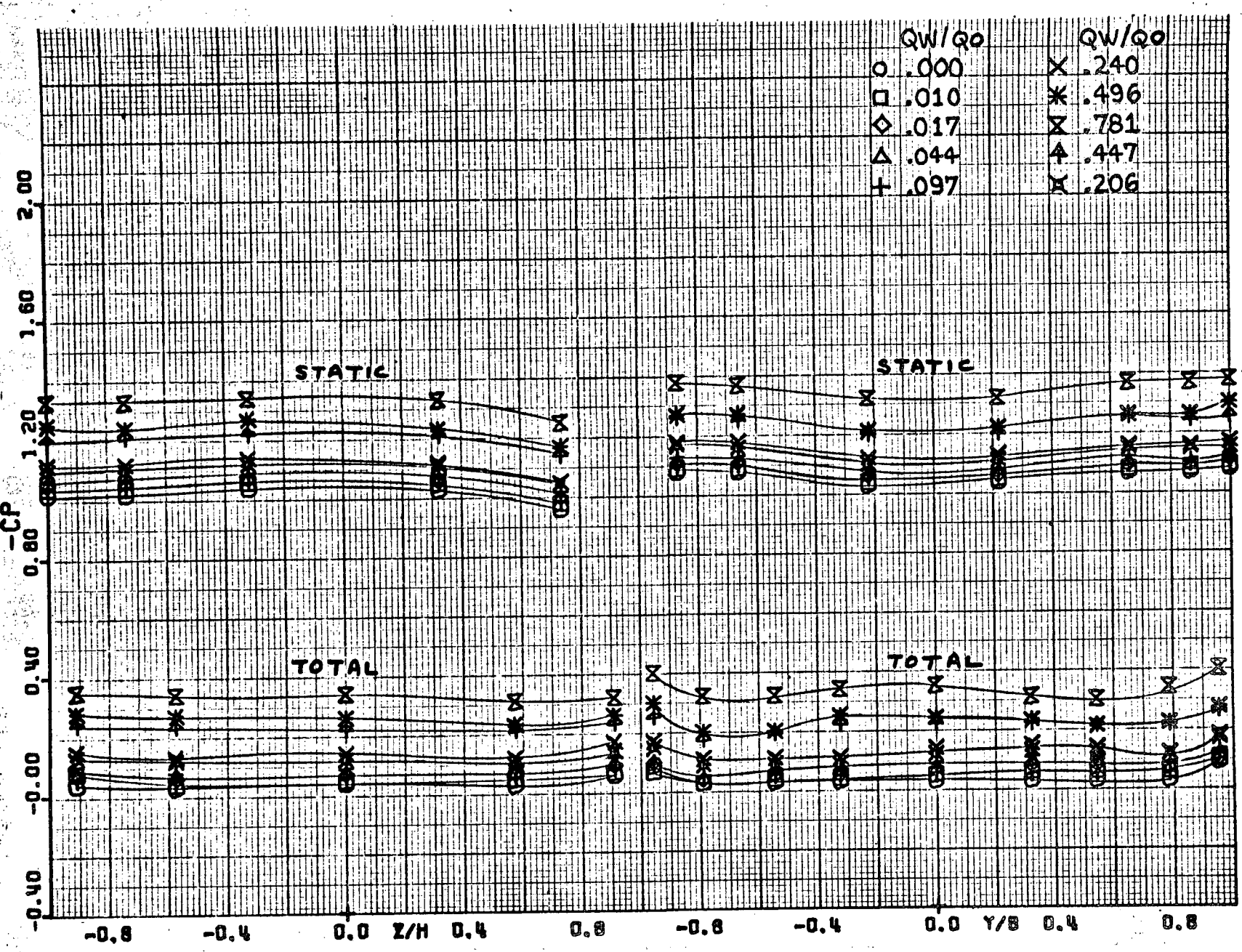

(e) $\psi = -90°$.

Figure 15.- Continued.

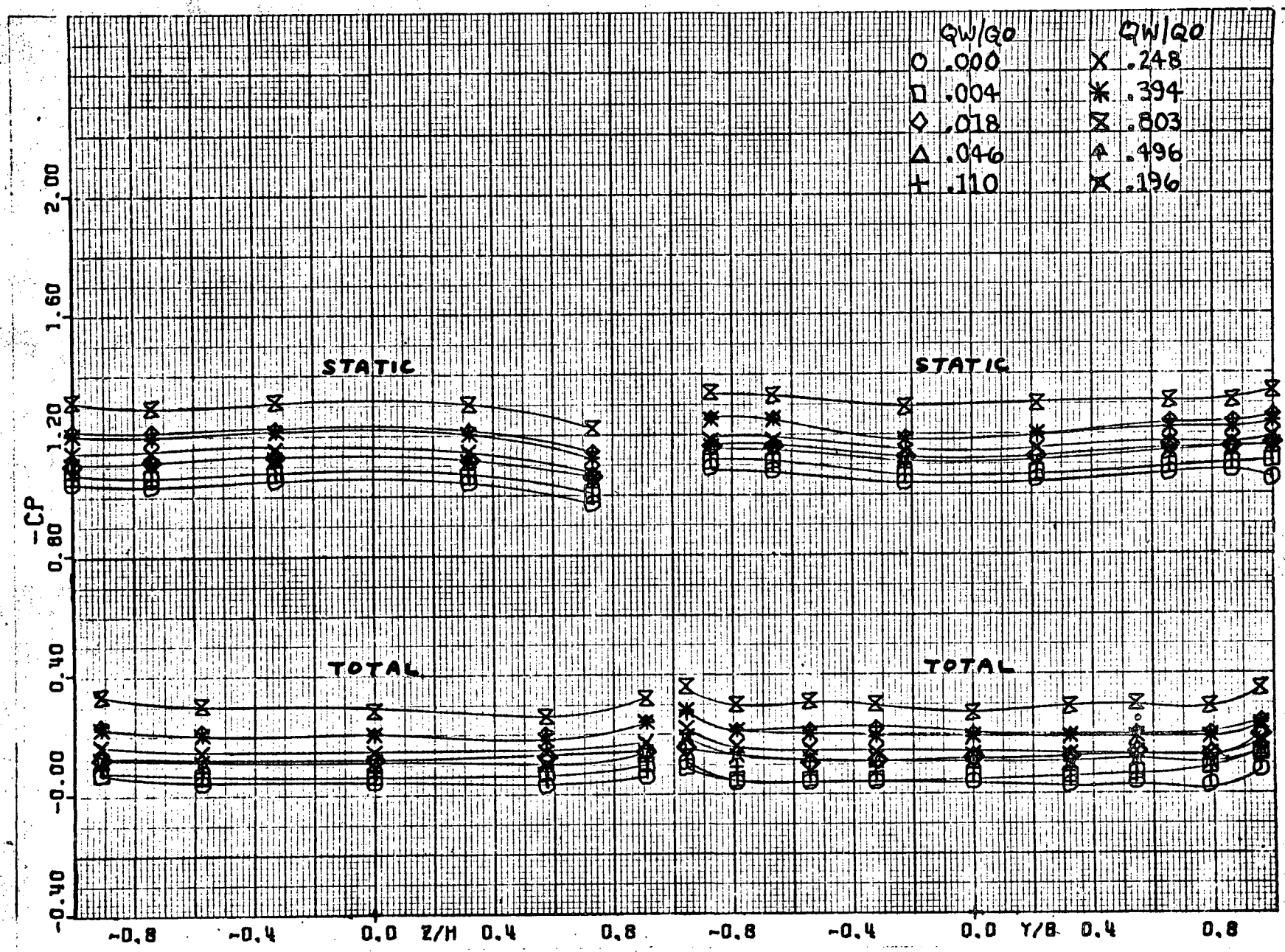

(d) $\psi = -135°$.

Figure 15.- Continued.

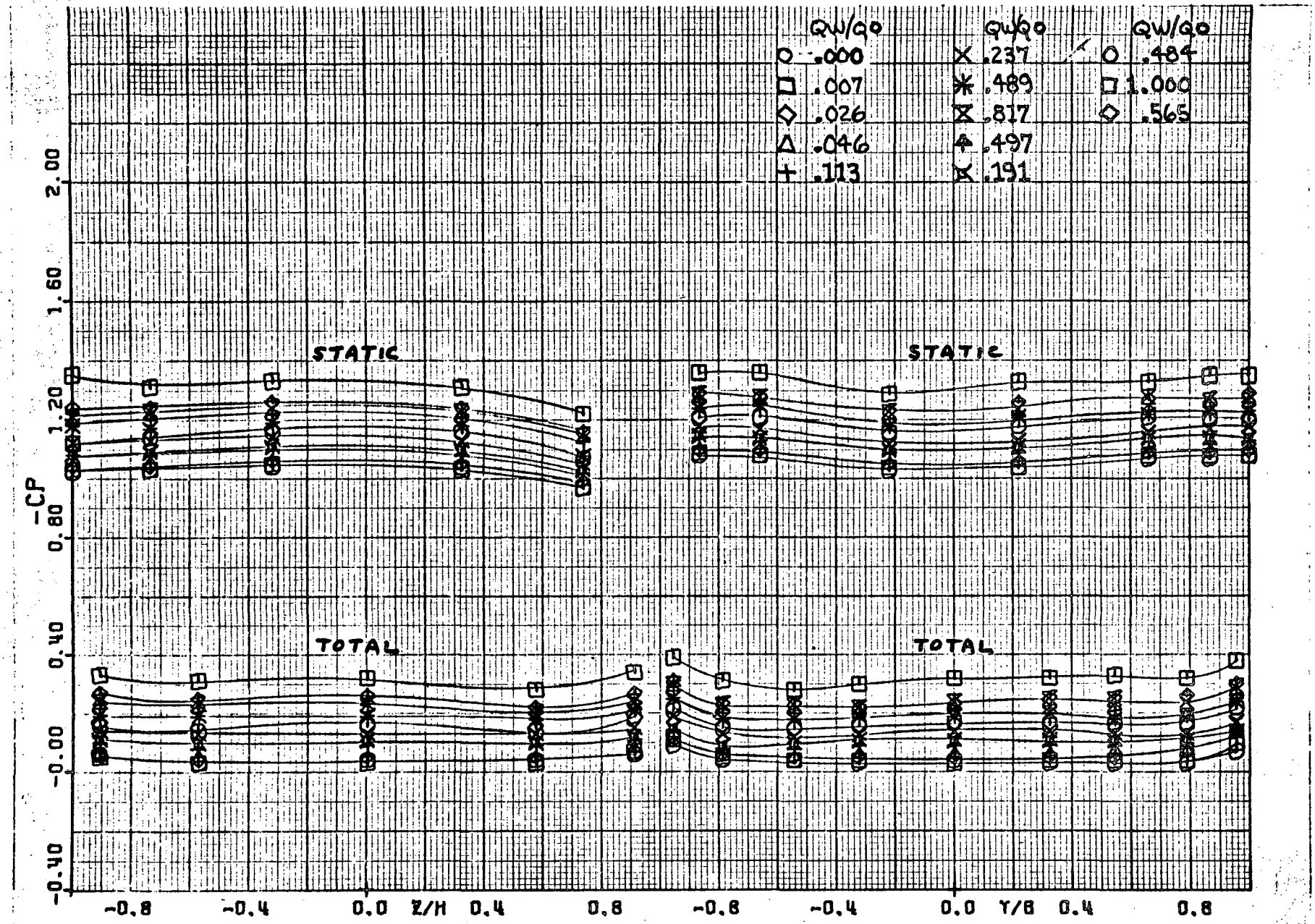

(e) $\psi = 180°$.

Figure 15.- Concluded.

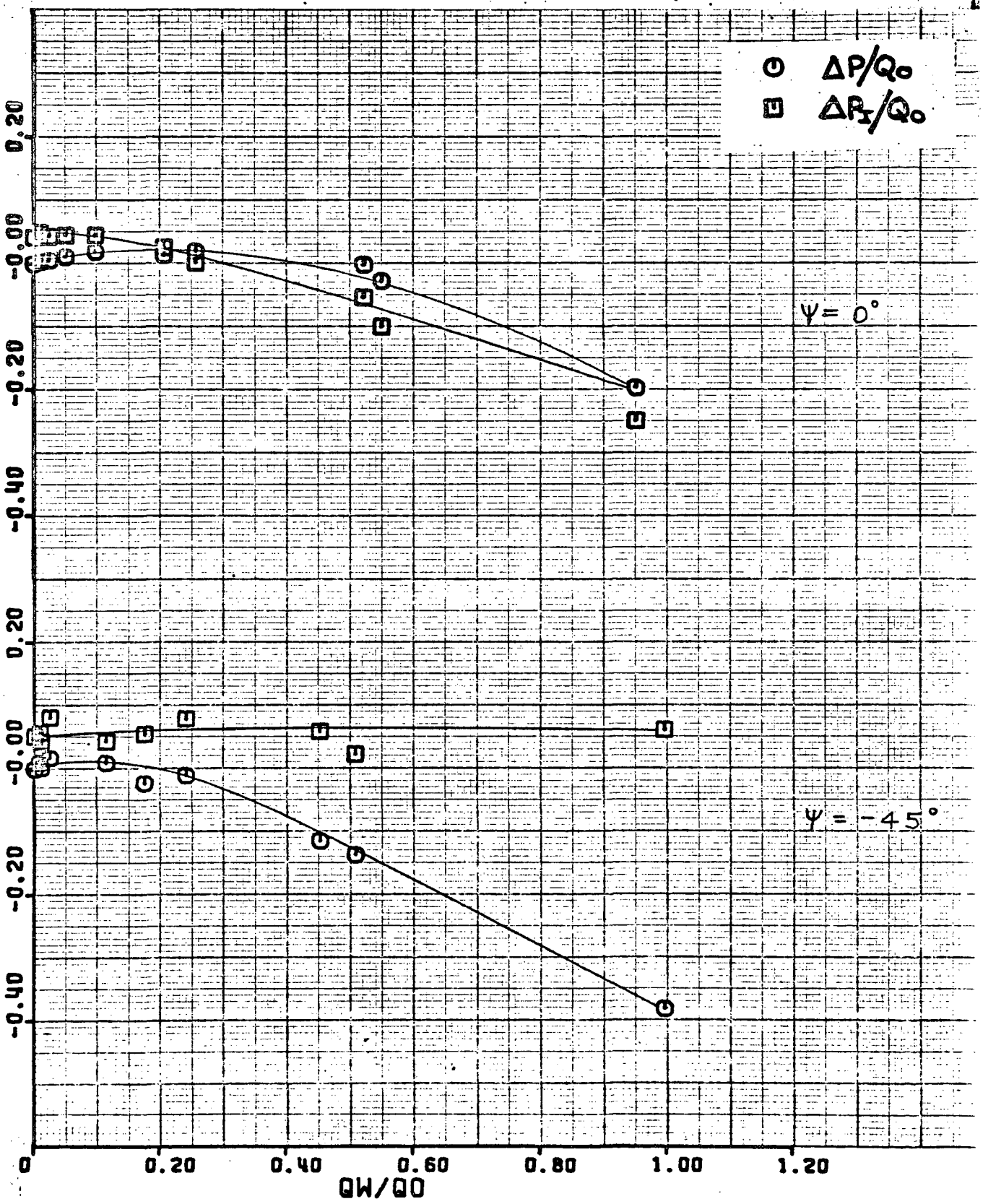

(a) $\psi = 0°$ and $-45°$.

Figure 16.- Pressure losses for model with 4.8:1 contraction system.

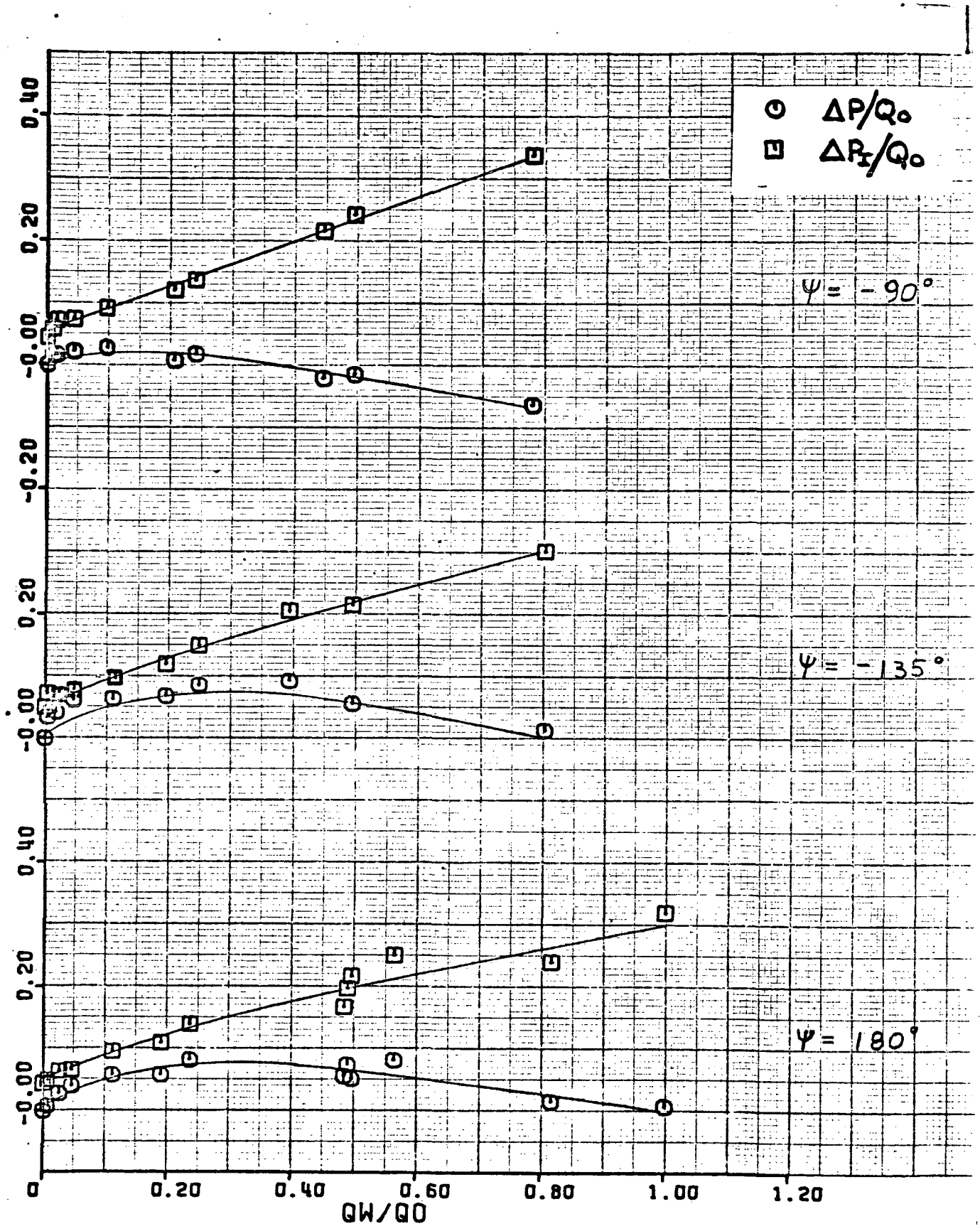

(b) ψ = -90°, -135° and 180°.

Figure 16.- Concluded.

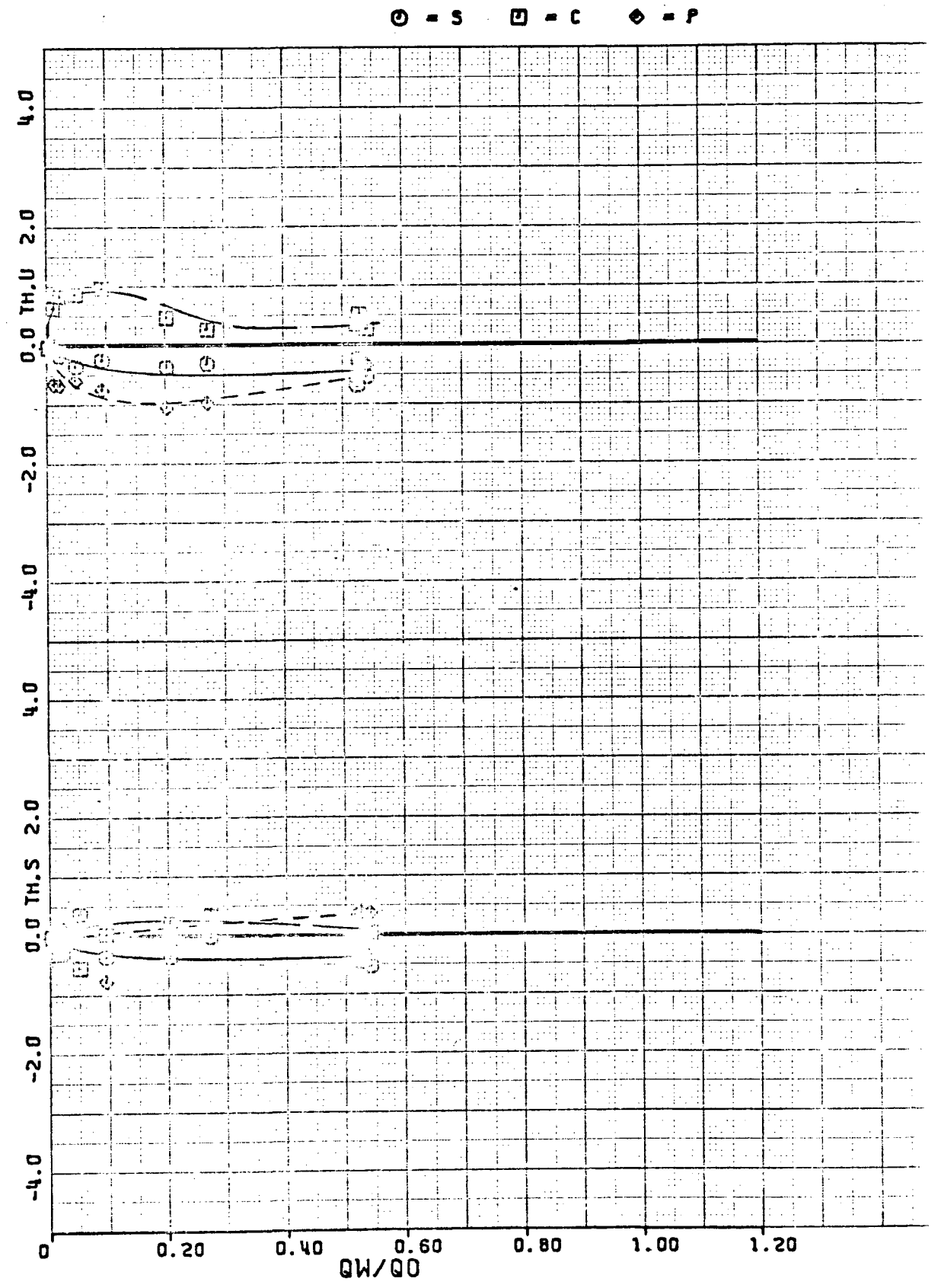

(a) Flow angularity.

Figure 17.- Model with 10.2 x 10.2 cm (4 x 4 in) flow straighteners, ψ = -90°.

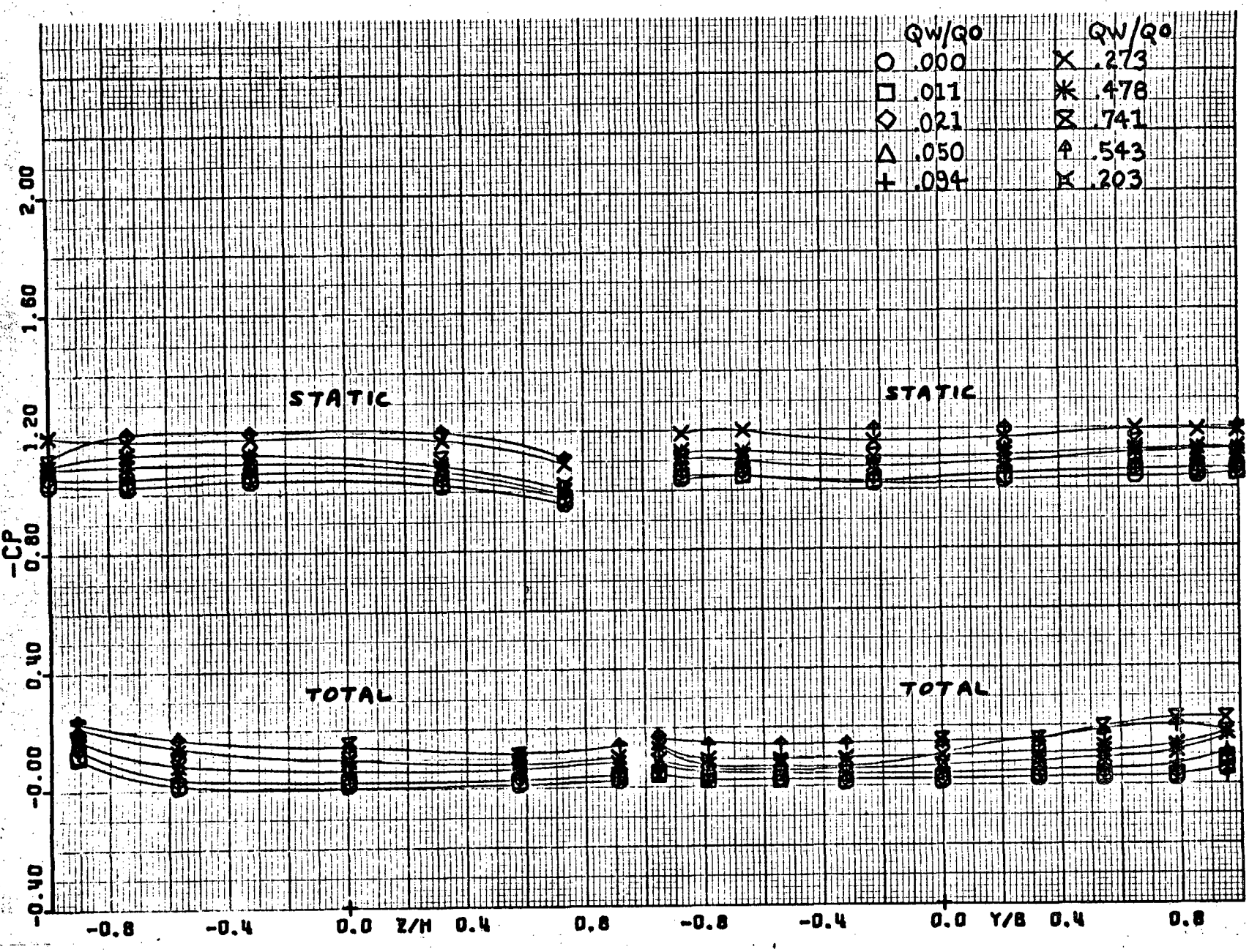

(b) Pressure coefficients.

Figure 17.- Continued.

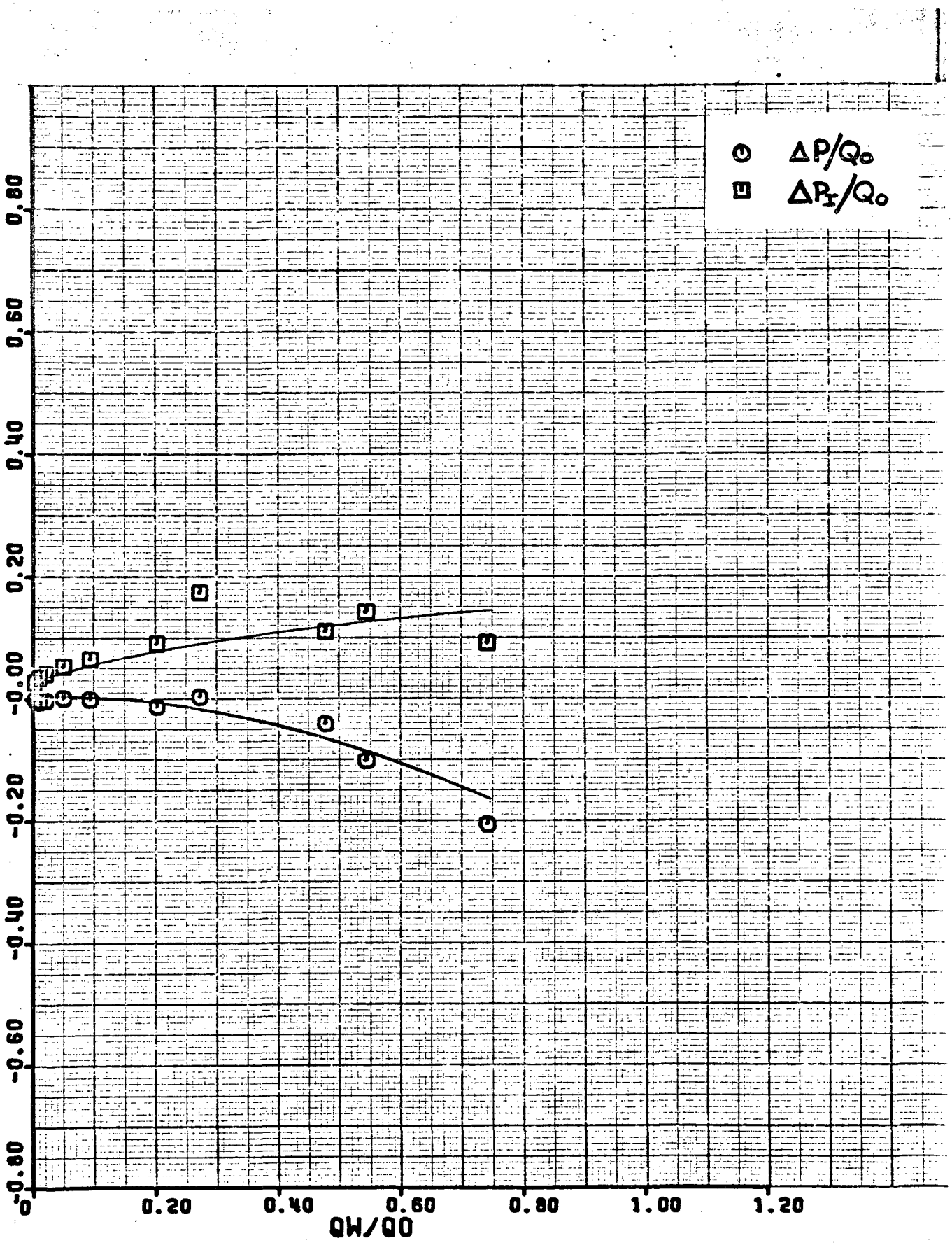

(c) Pressure losses.

Figure 17.- Concluded.

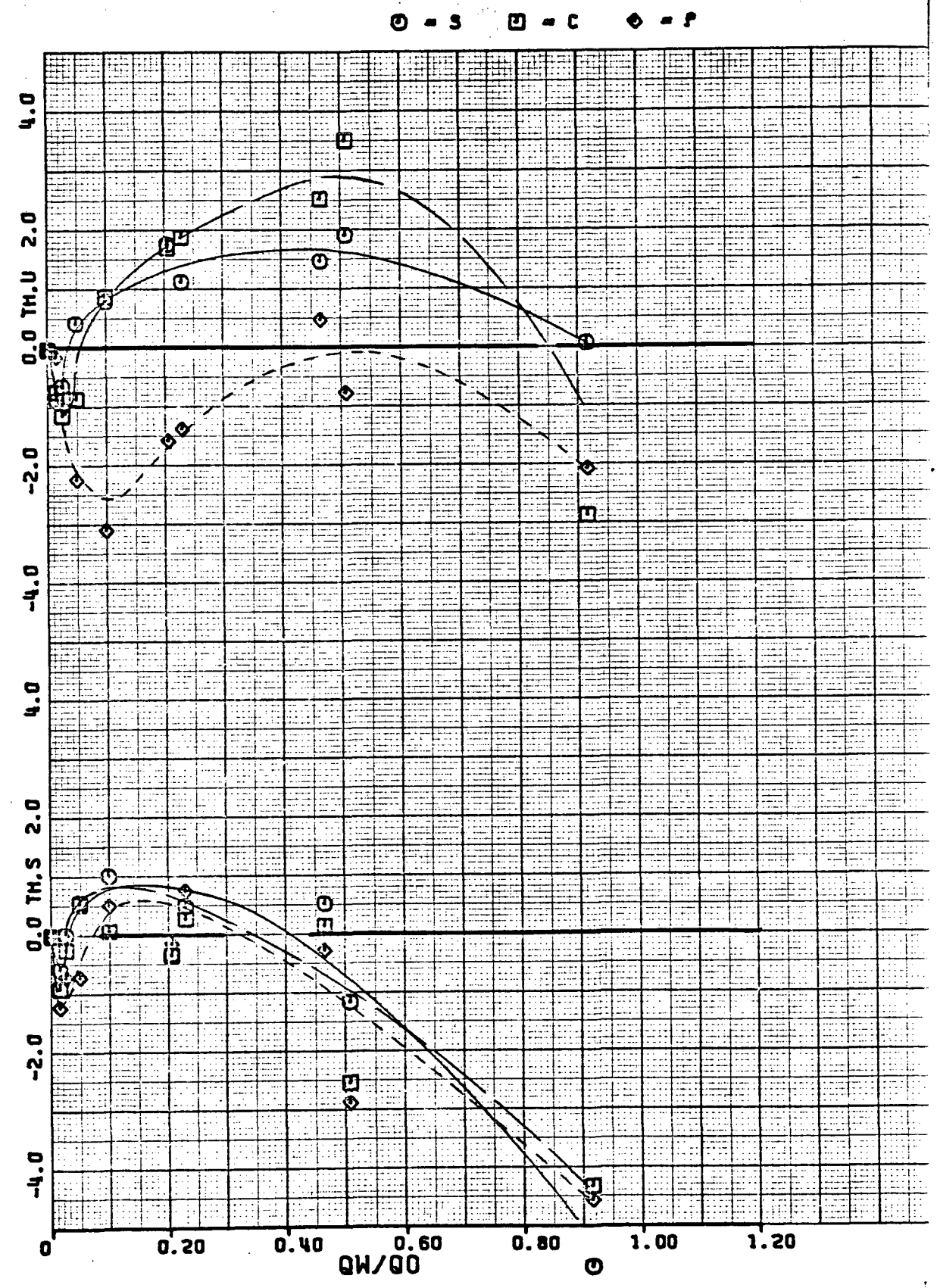

(a) Flow angularity.

Figure 18.- Model without flow straighteners, $\psi = -90°$.

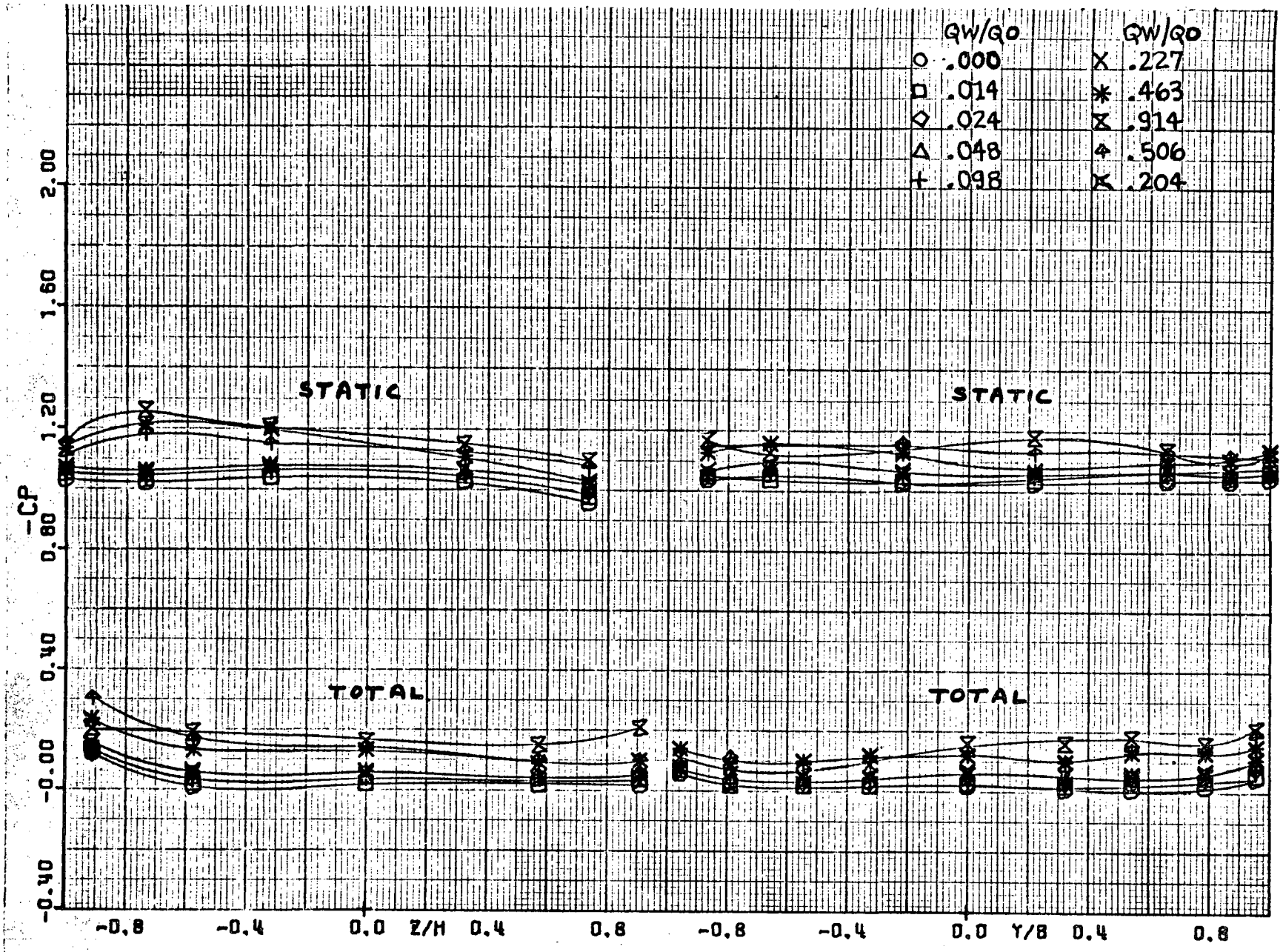

(b) Pressure coefficients.

Figure 18.- Continued.

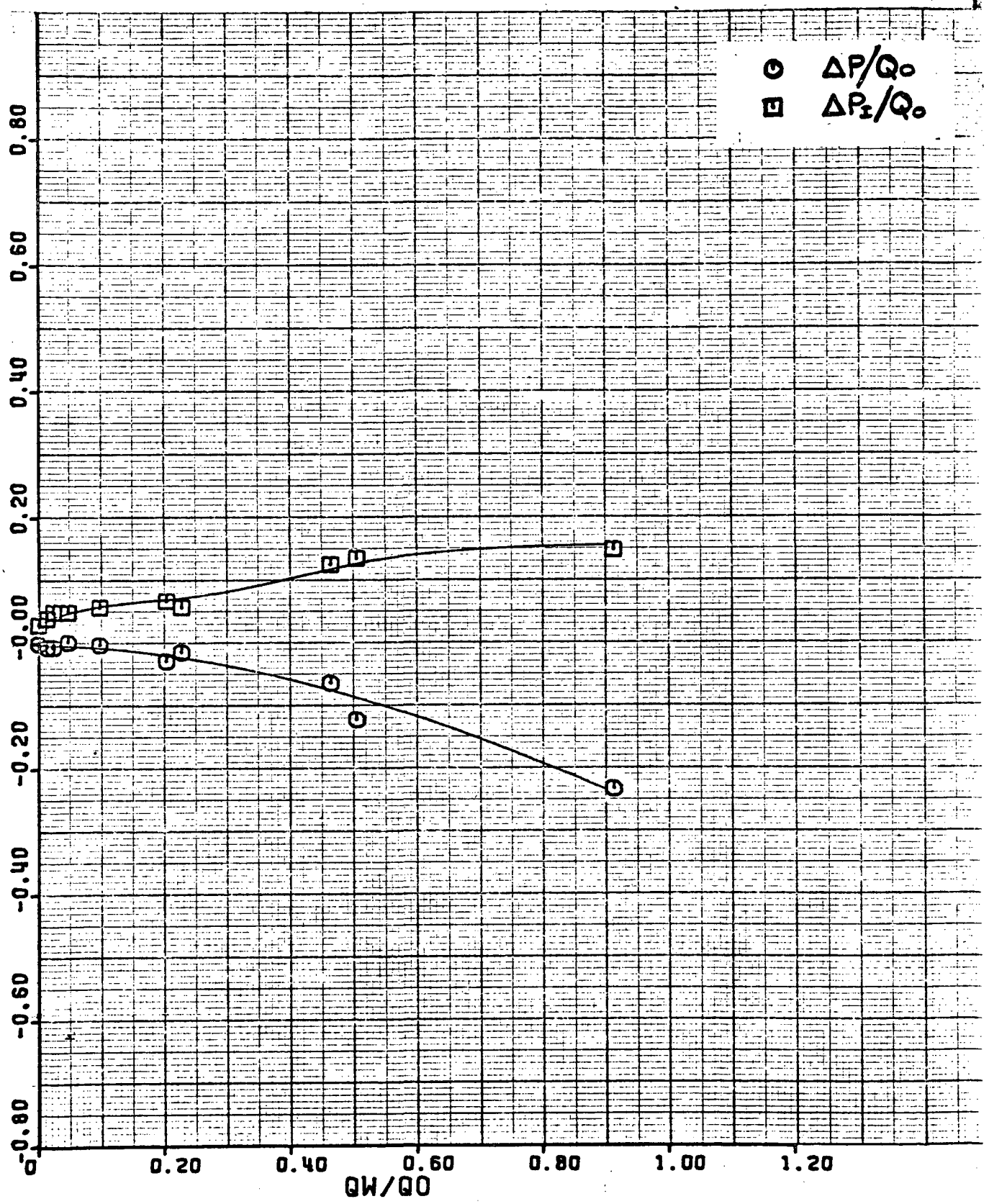

(c) Pressure losses.

Figure 18.- Concluded.

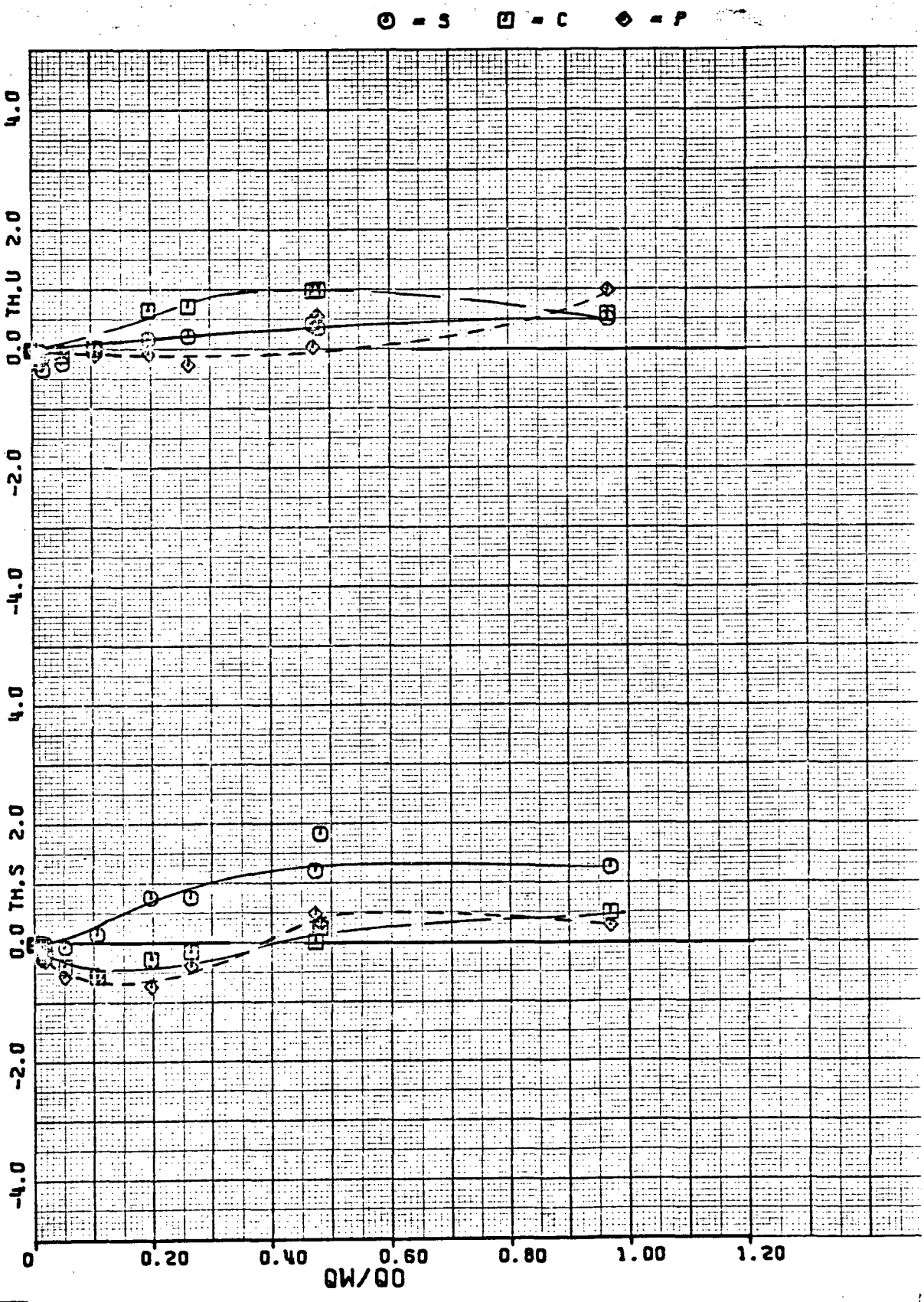

(a) Flow angularity.

Figure 19.- Model with 185 cm (73 in) contraction length, $\psi = -90°$.

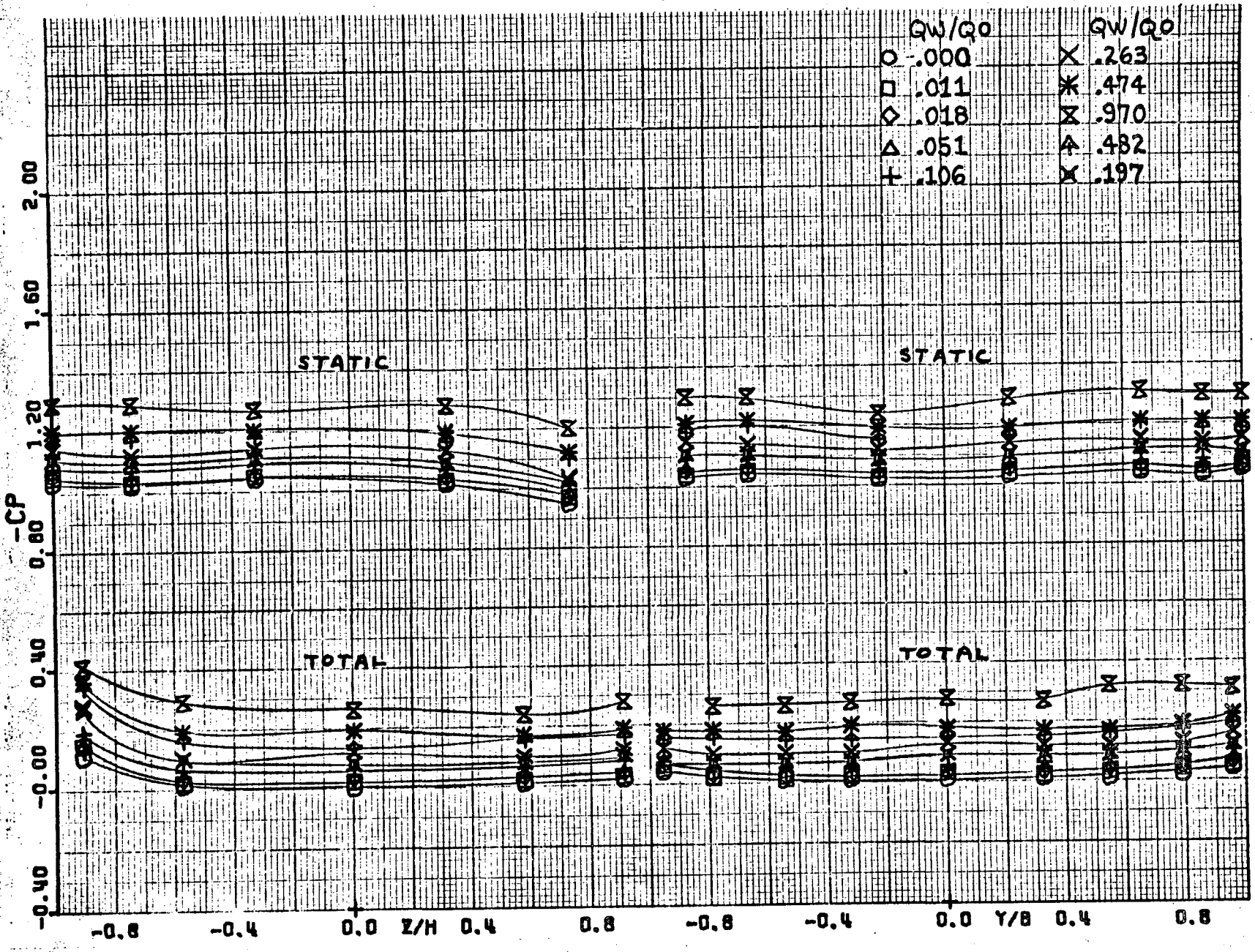

(b) Pressure coefficients.

Figure 19.- Continued.

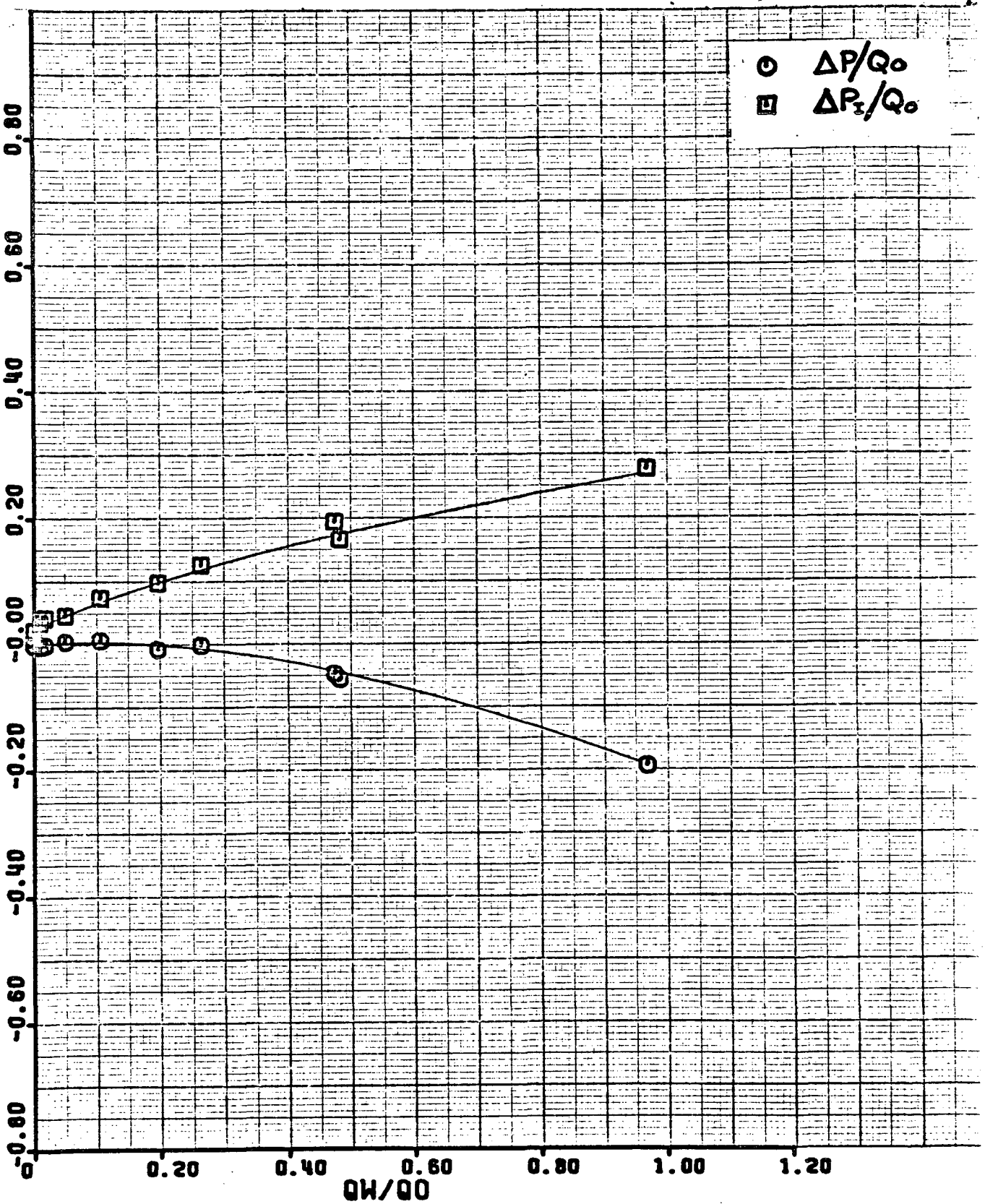

(c) Pressure losses.

Figure 19.- Concluded.

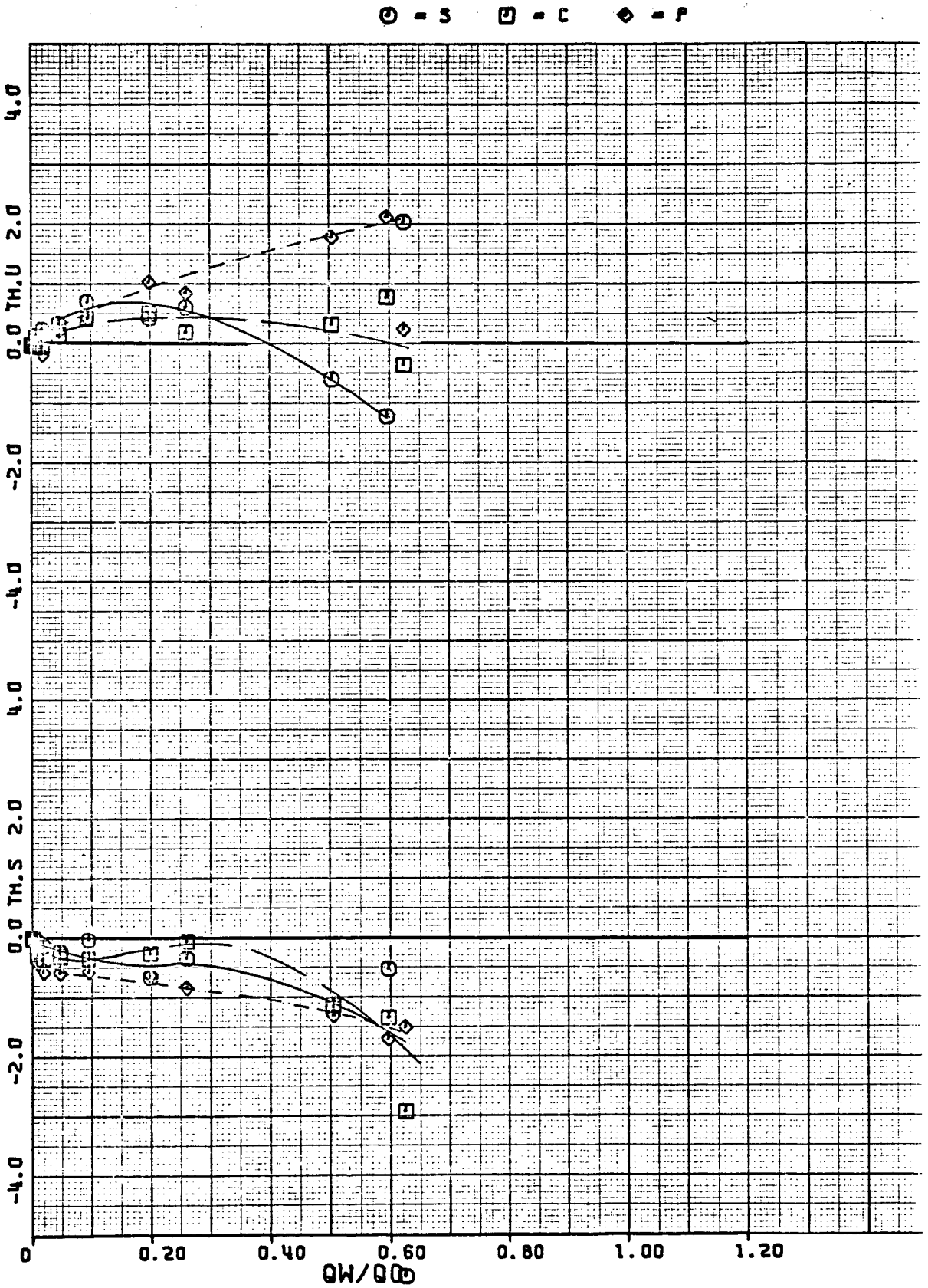

(a) Flow angularity.

Figure 20.- Model with 4.8:1 contraction system without inlet screen, ψ = -90°.

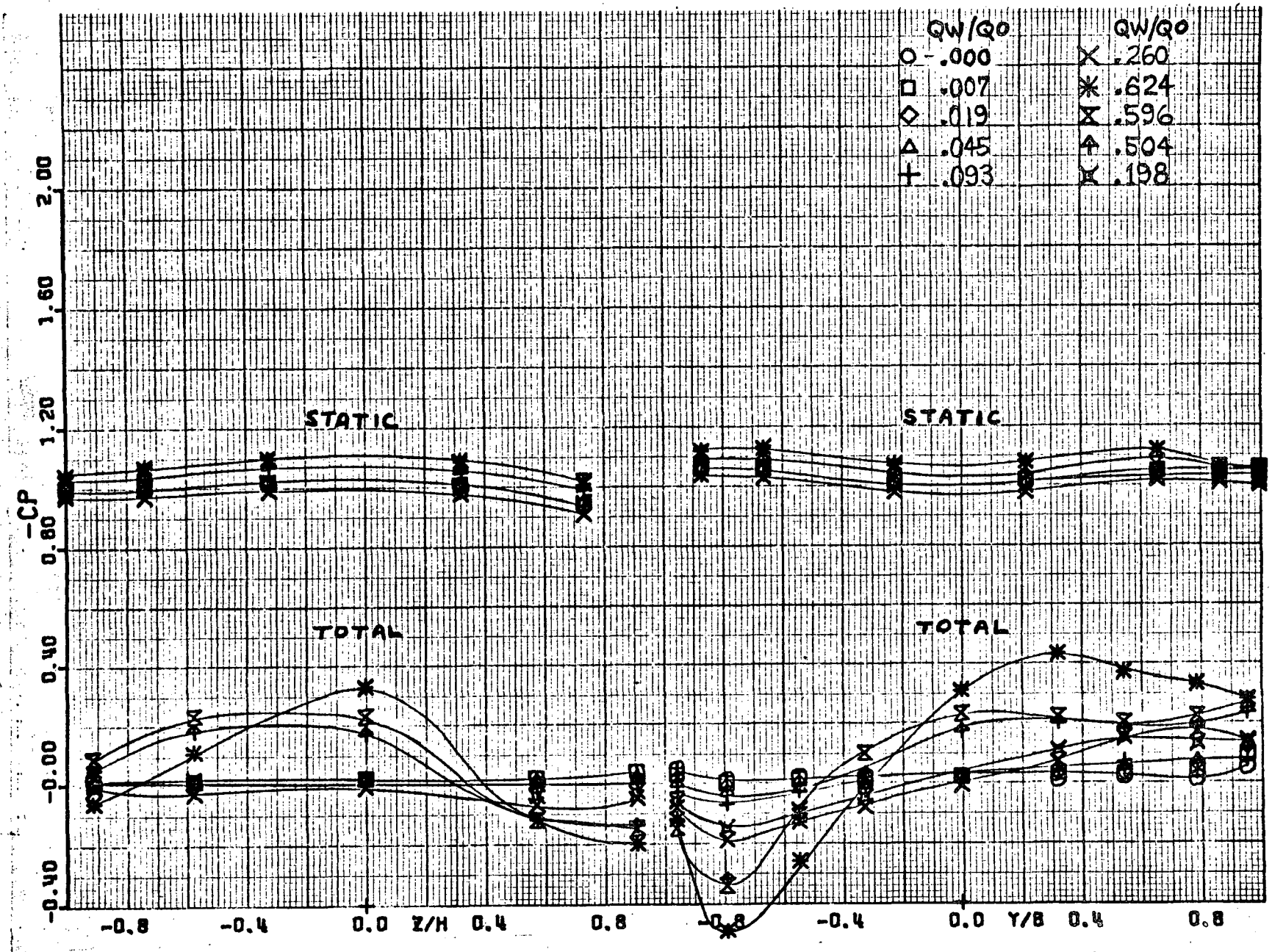

(b) Pressure coefficients.

Figure 20.- Continued.

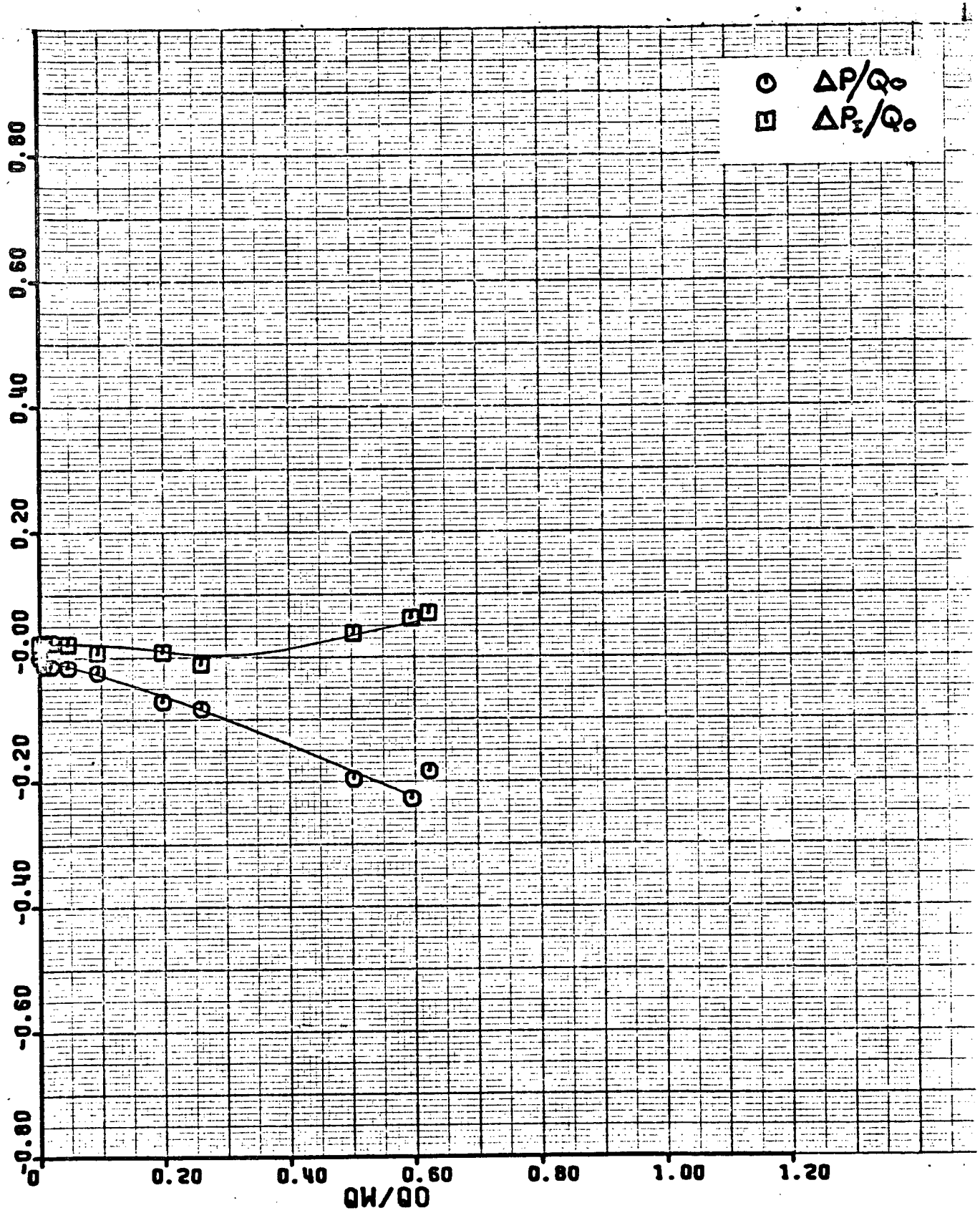

(c) Pressure losses.

Figure 20.- Concluded.

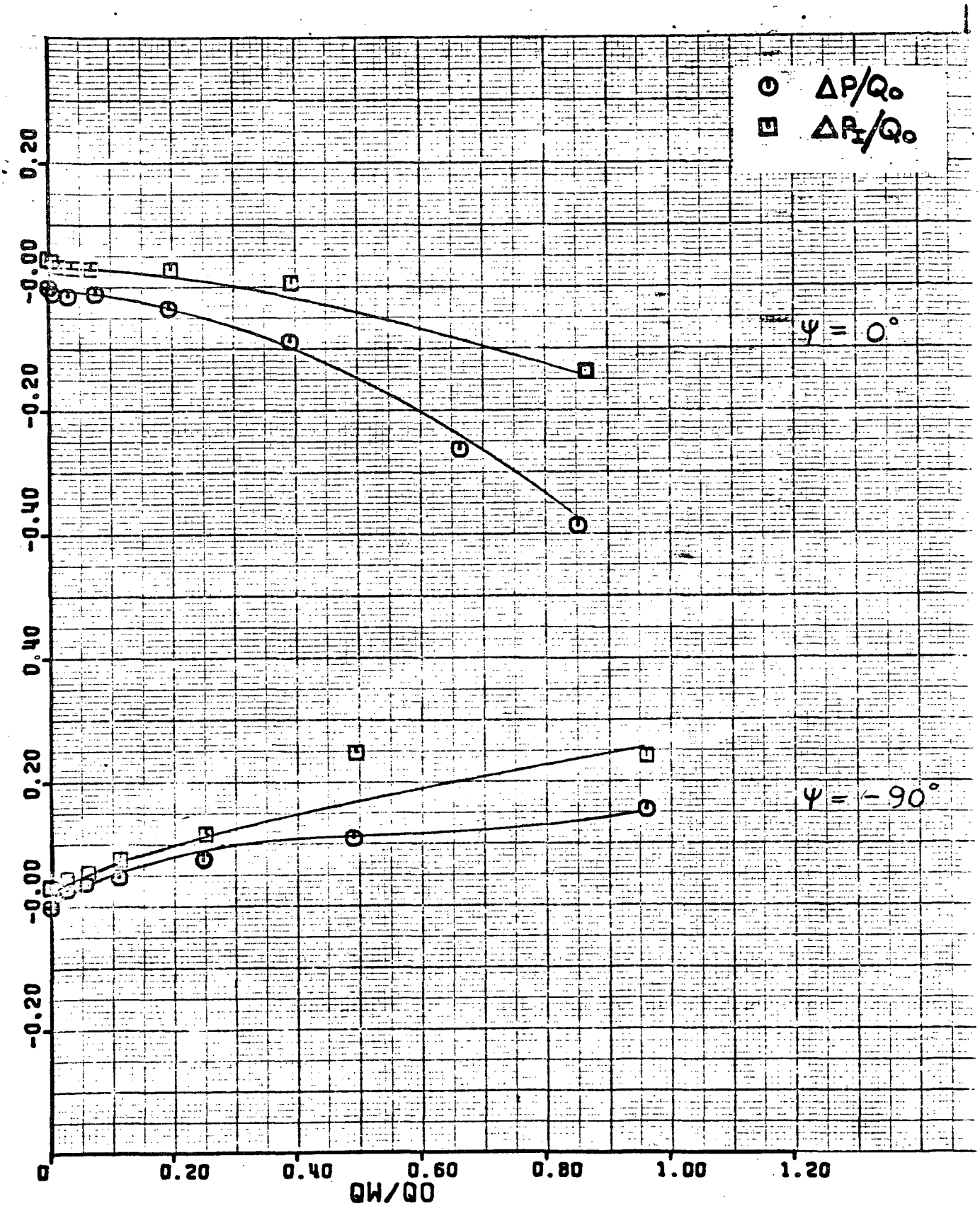

(a) ψ = 0° and -90°.

Figure 21.- Pressure losses for model with horizontal exit.

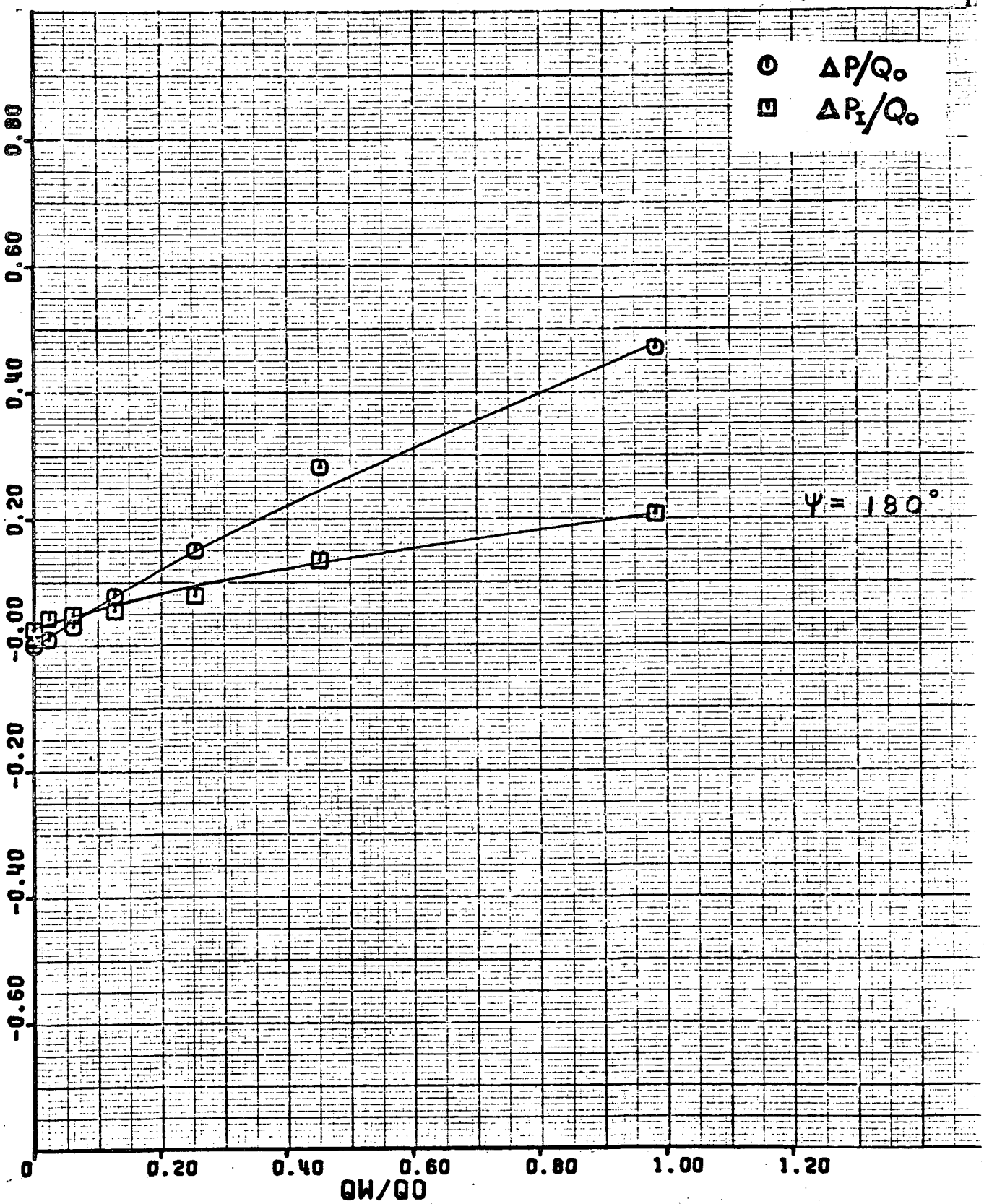

(b) $\psi = 180°$.

Figure 21.- Concluded.

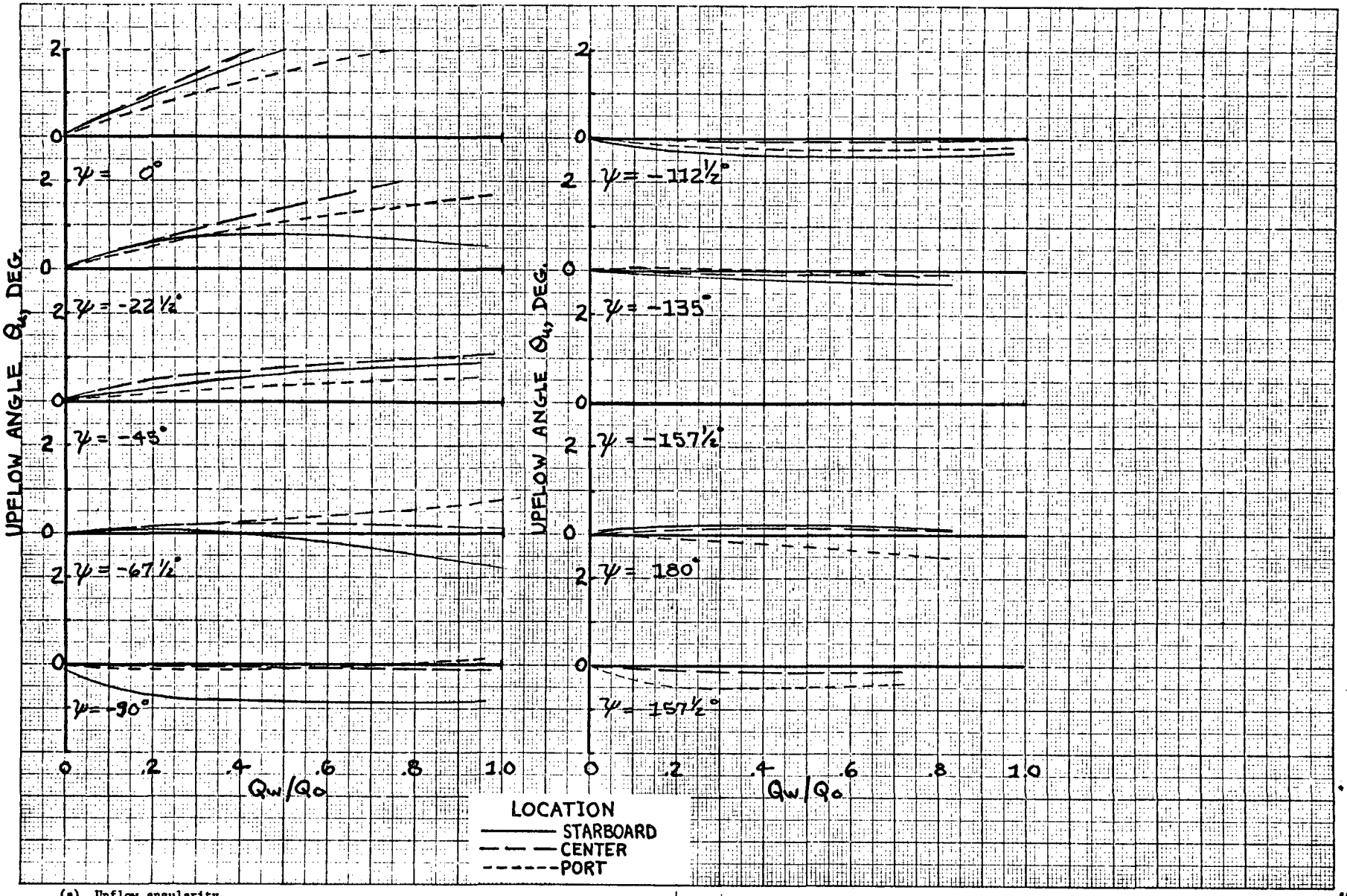

(a) Upflow angularity.

Figure 22.- Effect of azimuth angle variation on basic configuration.

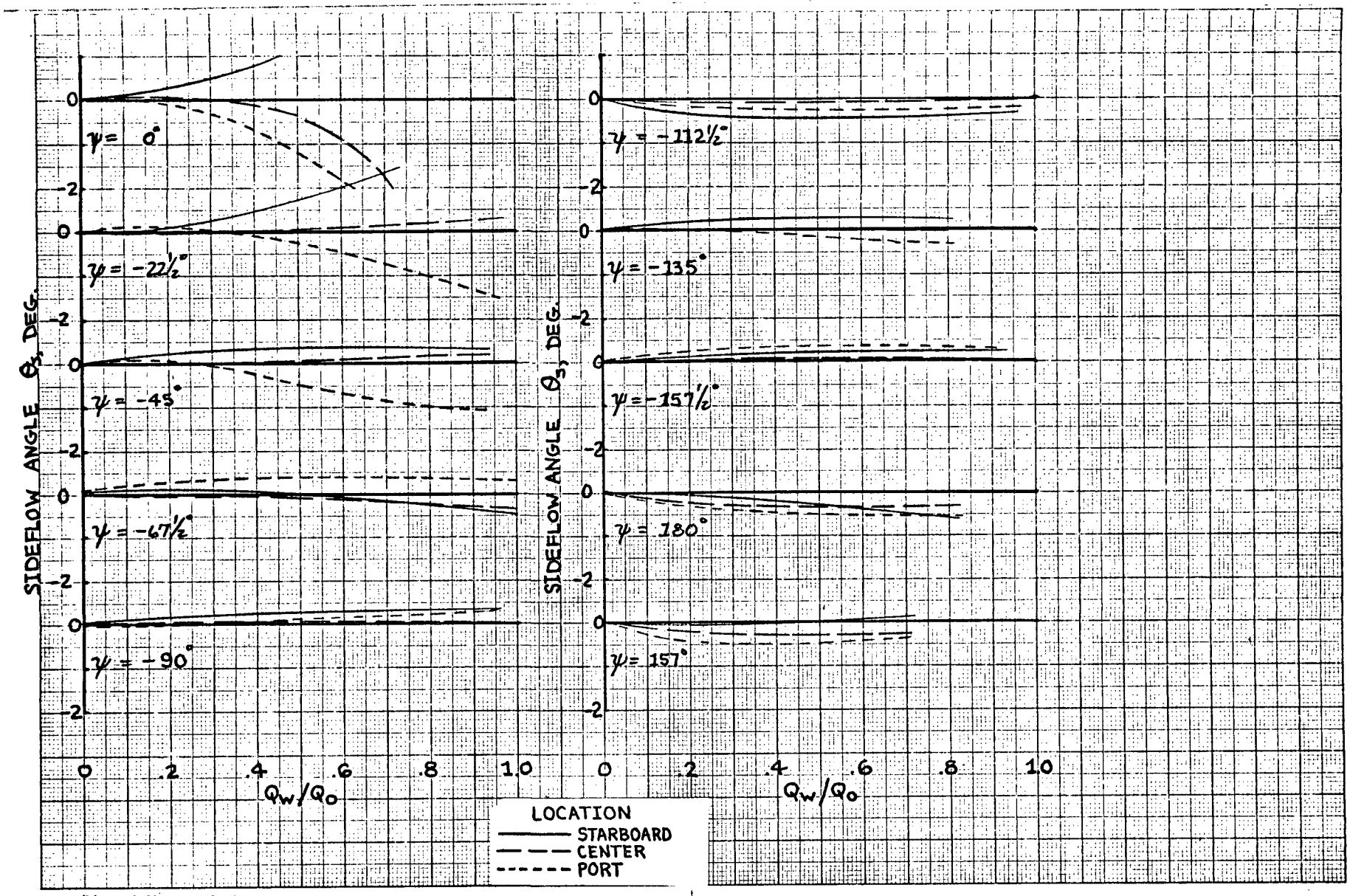

(b) Sideflow angularity.

Figure 22.- Continued.

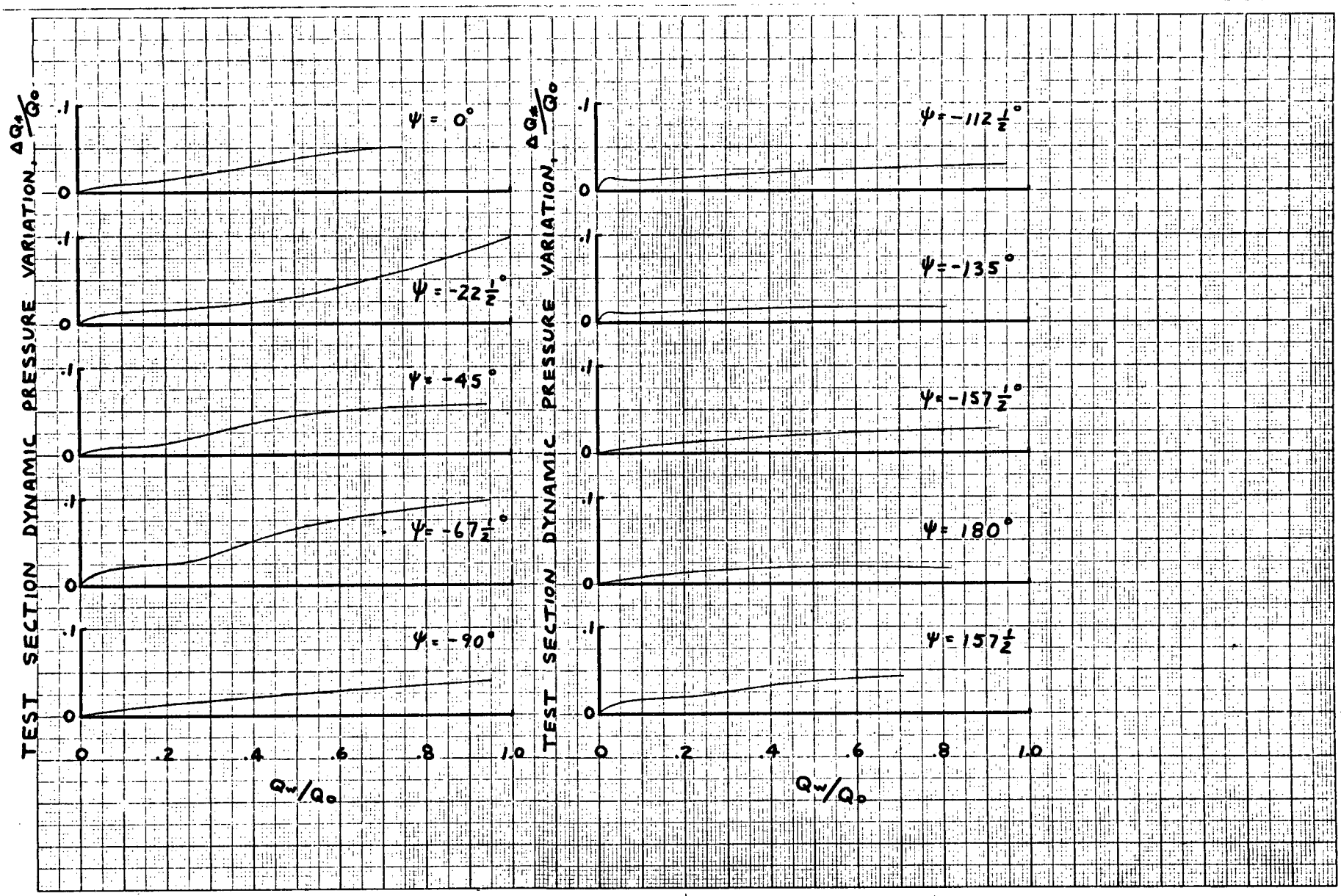

(c) Test section dynamic pressure variation.

Figure 22.- Continued.

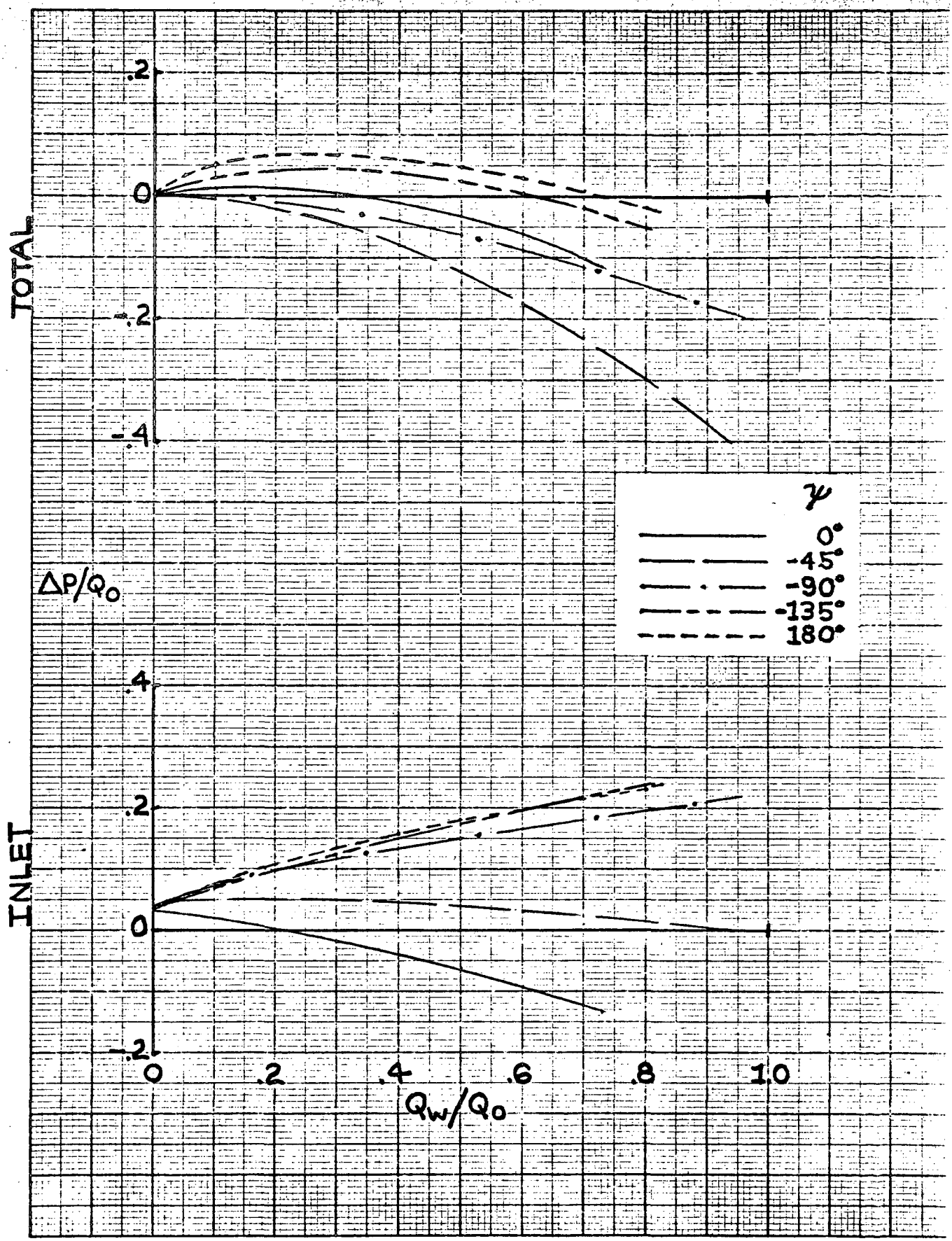

(d) Pressure losses.

Figure 22.- Concluded.

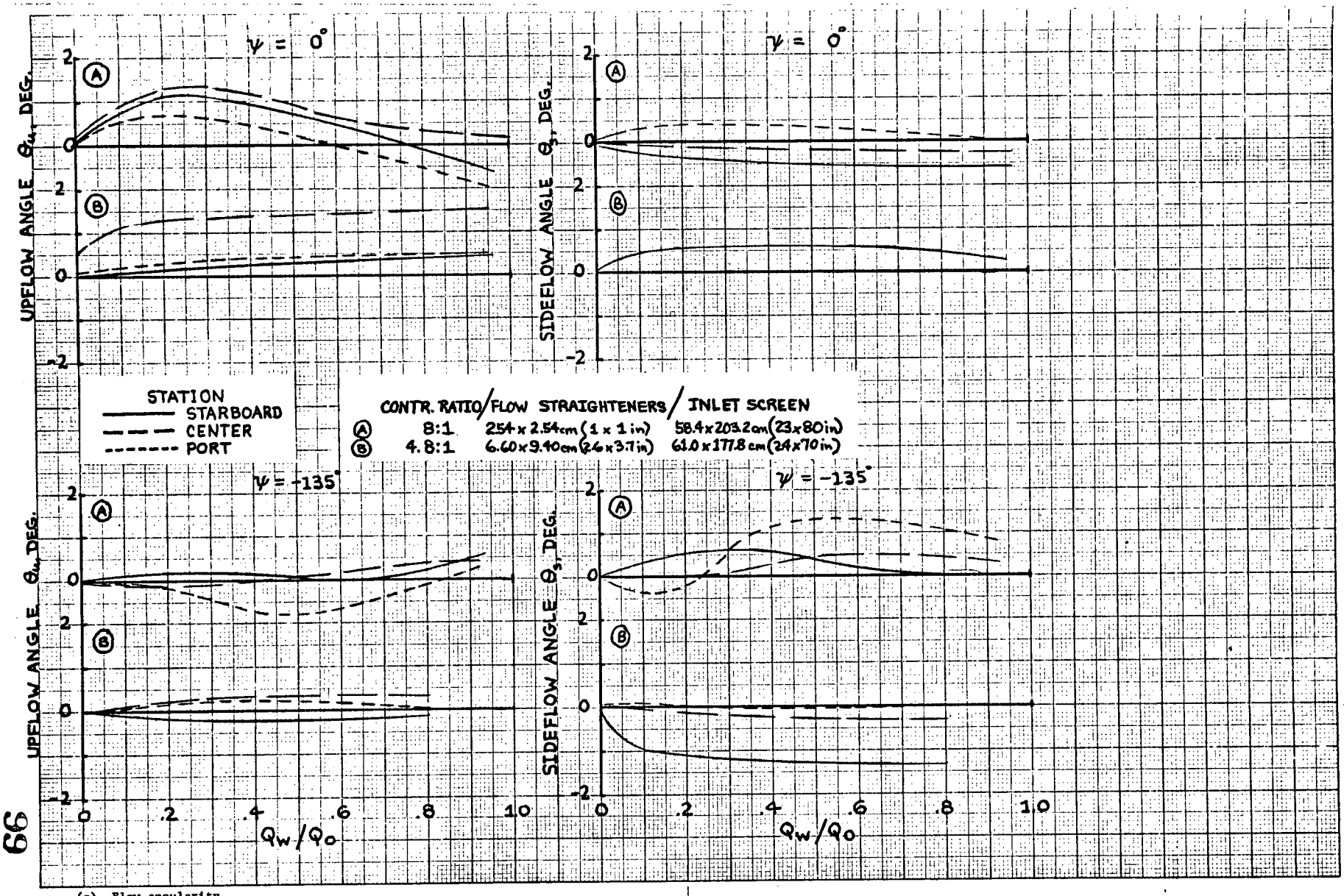

(a) Flow angularity.

Figure 23.- Comparison of contraction-ratio systems.

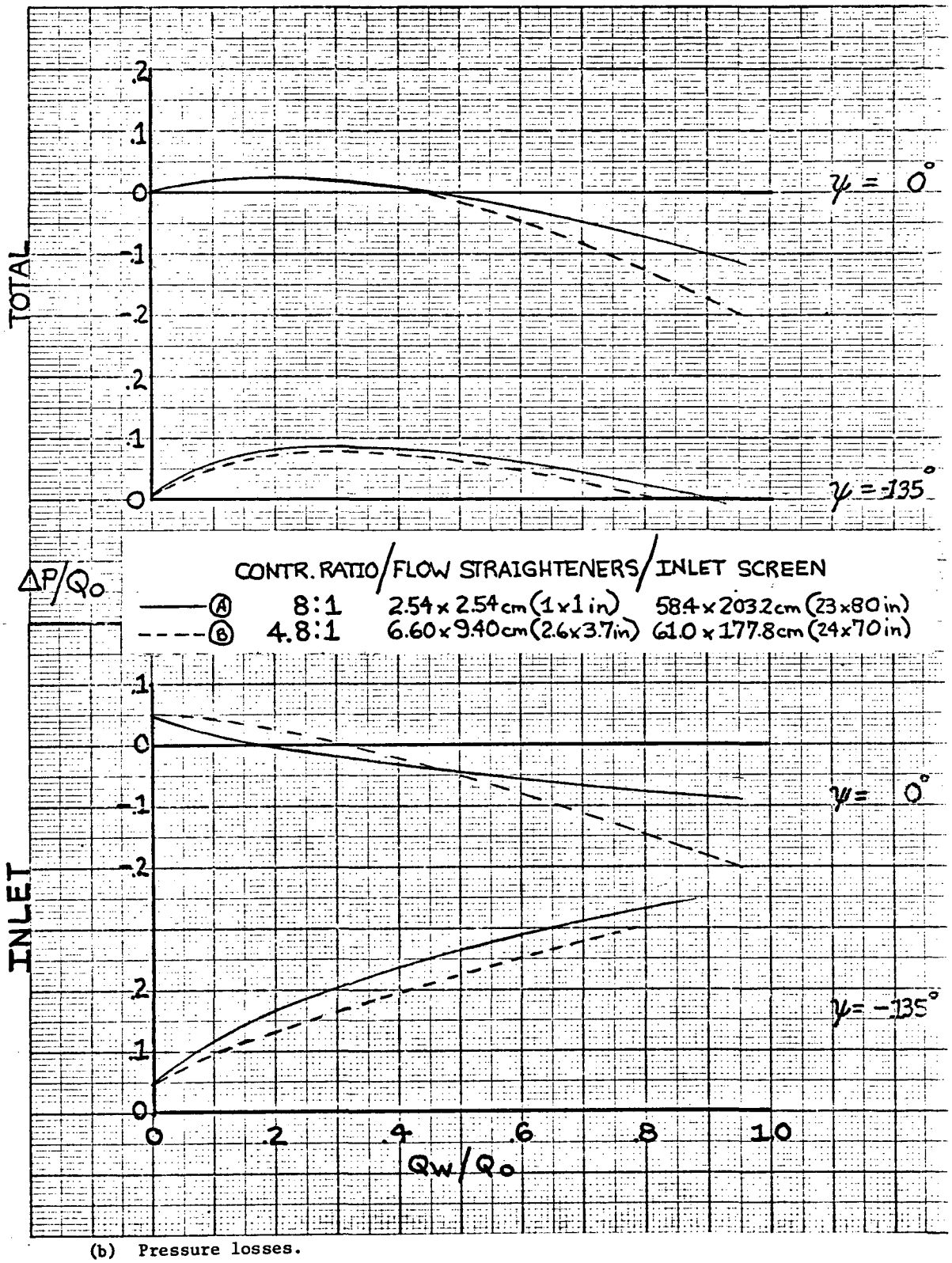

(b) Pressure losses.

Figure 23.- Concluded.

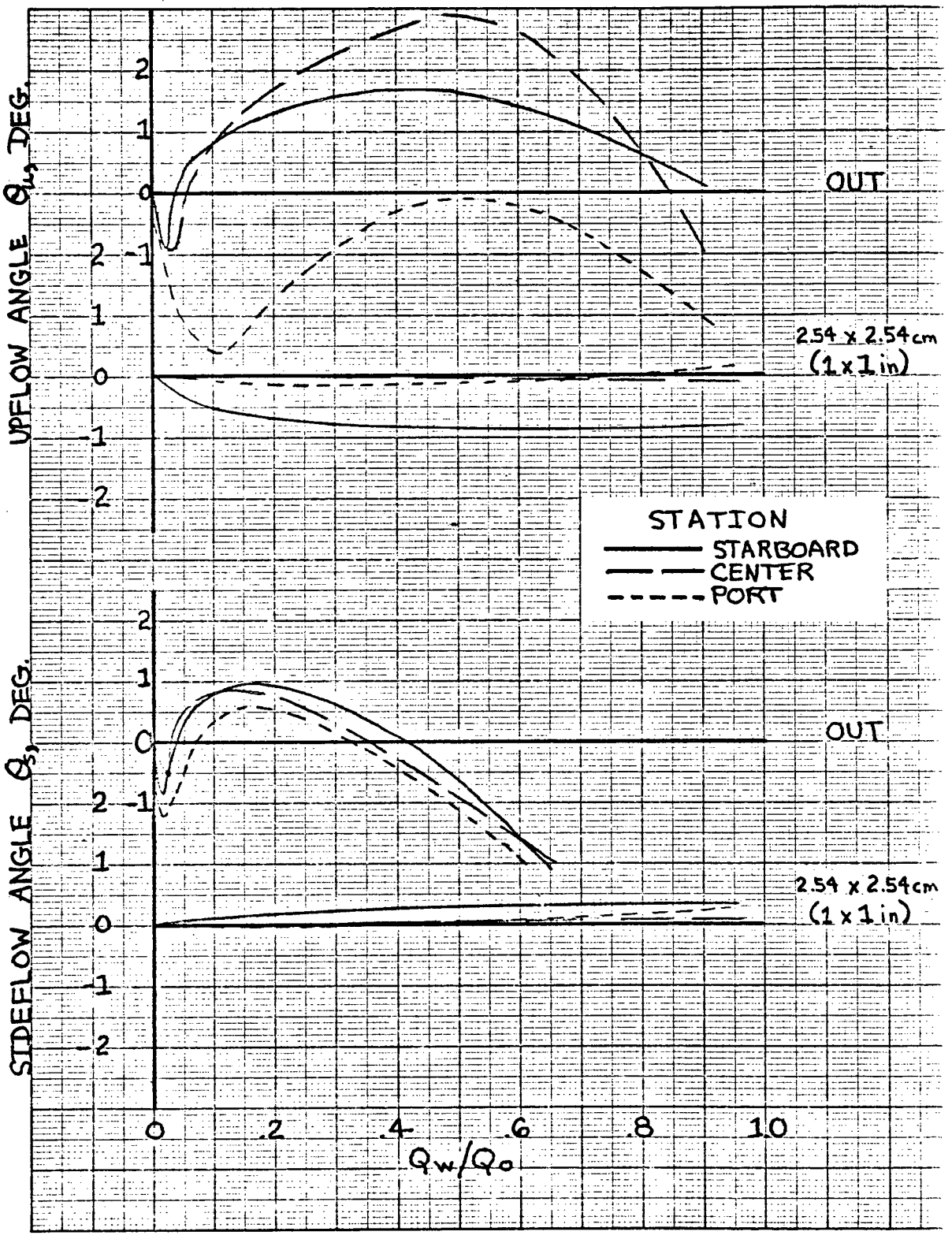

(a) Flow angularity with and without straighteners; inlet posts in.

Figure 24.- Effect of flow straighteners; $\psi = -90°$.

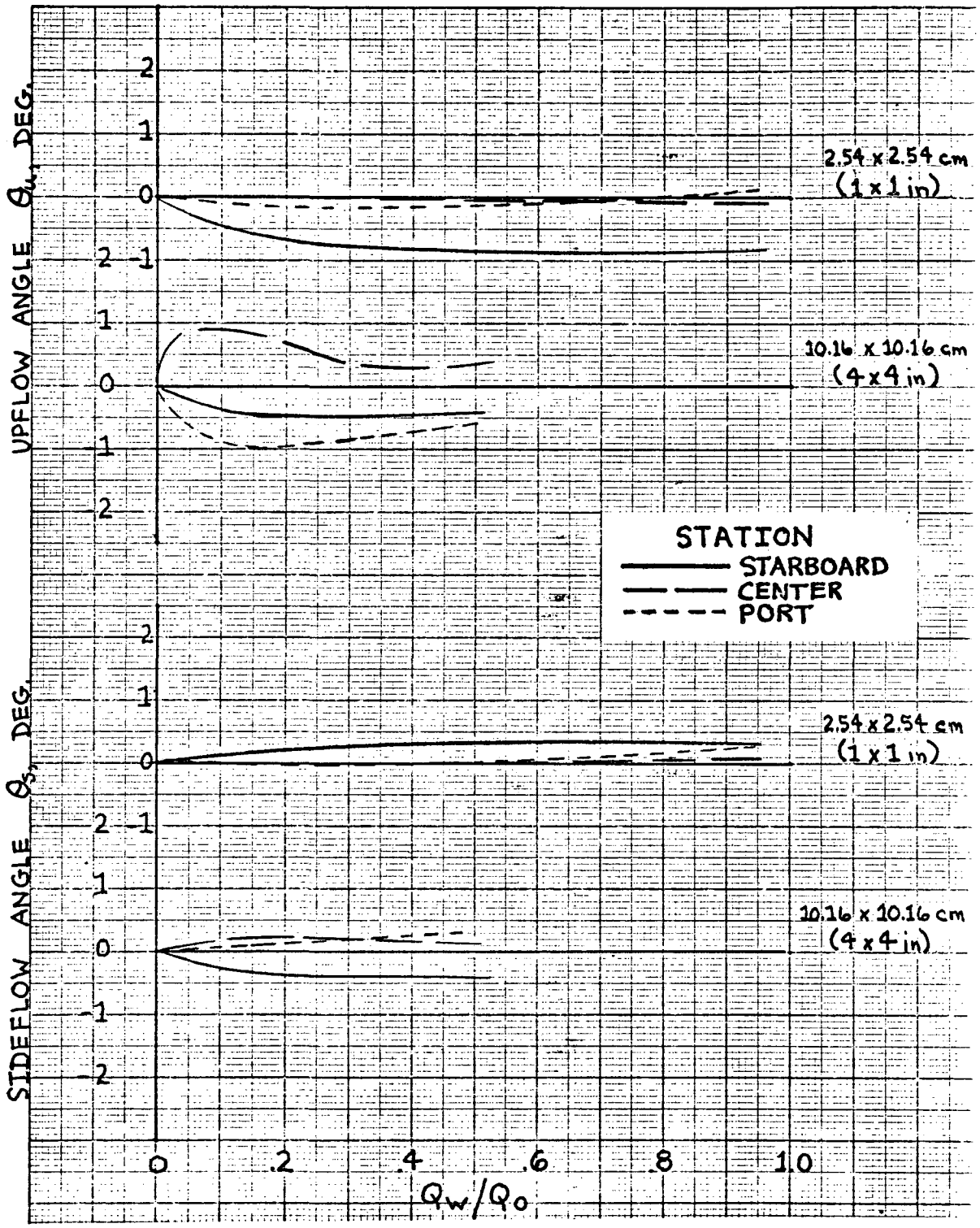

(b) Flow angularity for two different straightener sizes; inlet posts out.

Figure 24.- Continued.

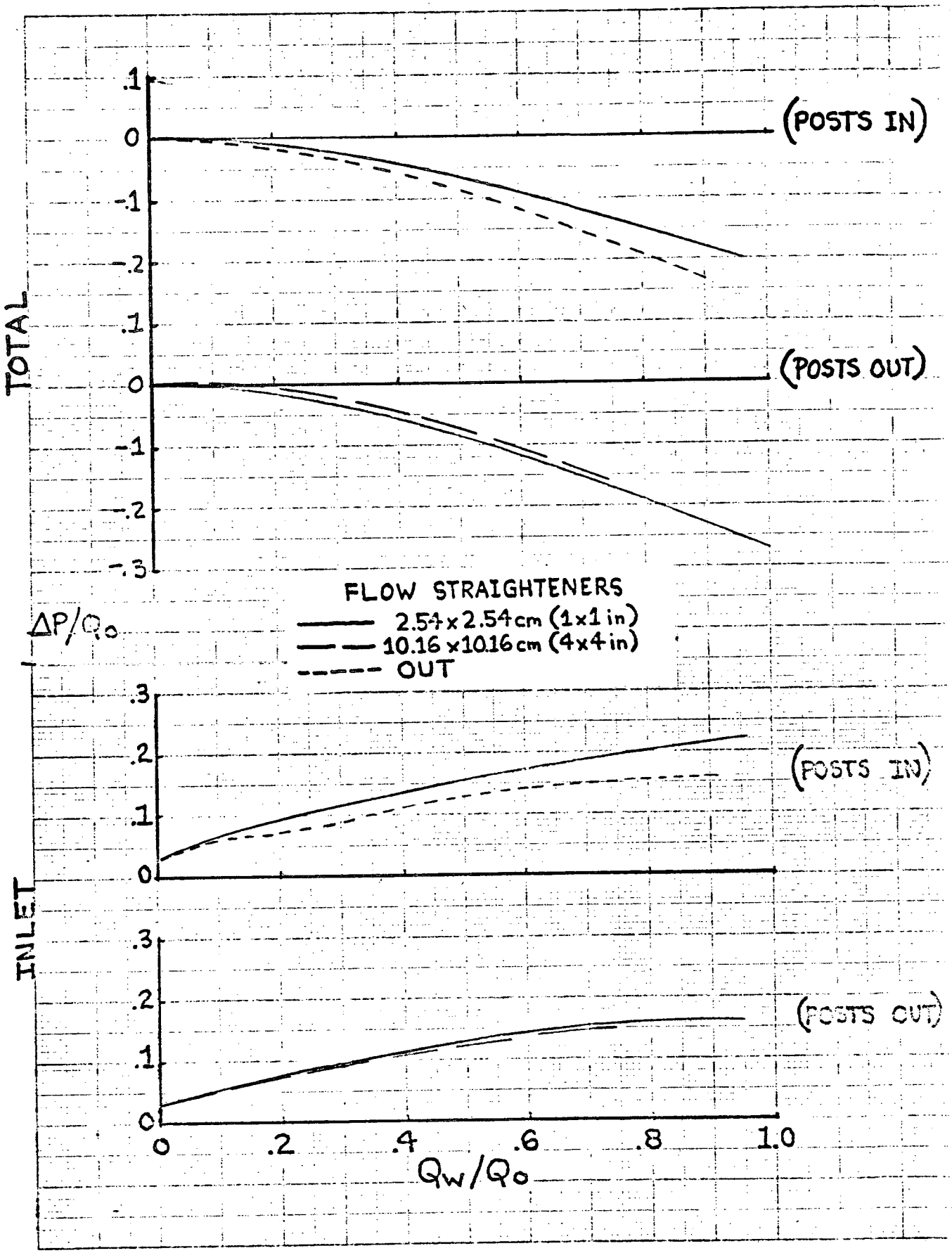

(c) Pressure losses.

Figure 24.- Concluded.

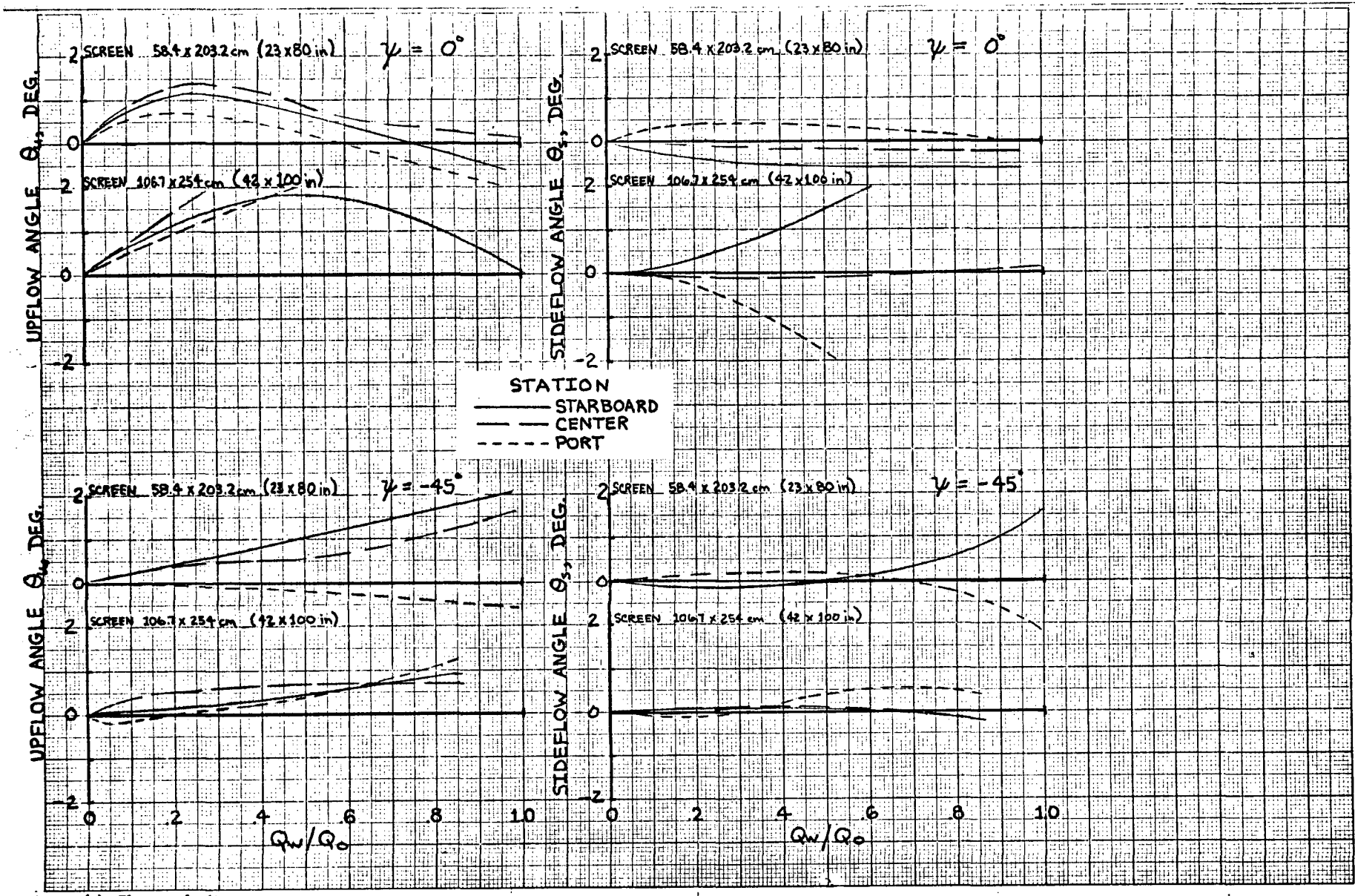

(a) Flow angularity.

Figure 25.- Effect of inlet screen size.

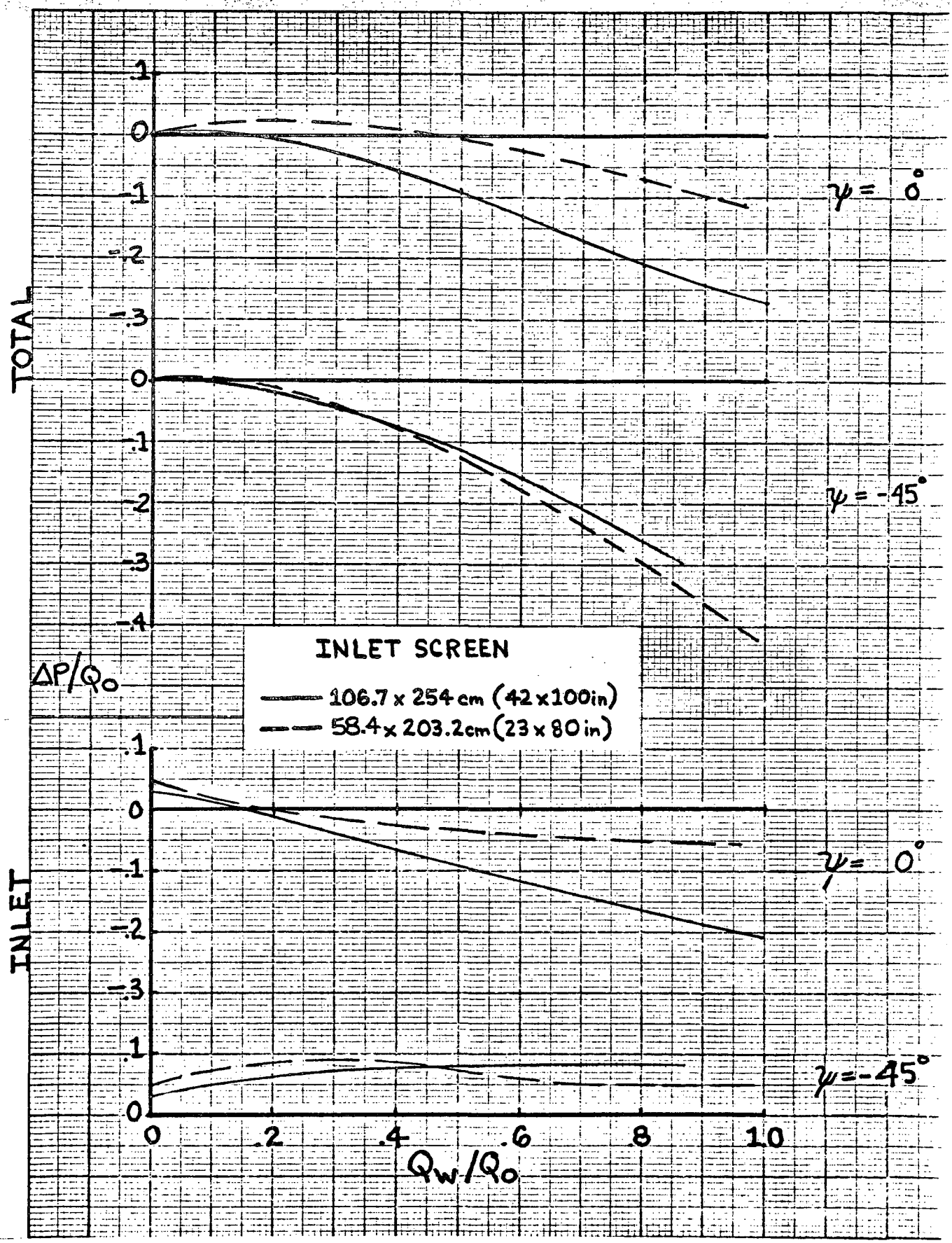

(b) Pressure losses.

Figure 25.- Concluded.

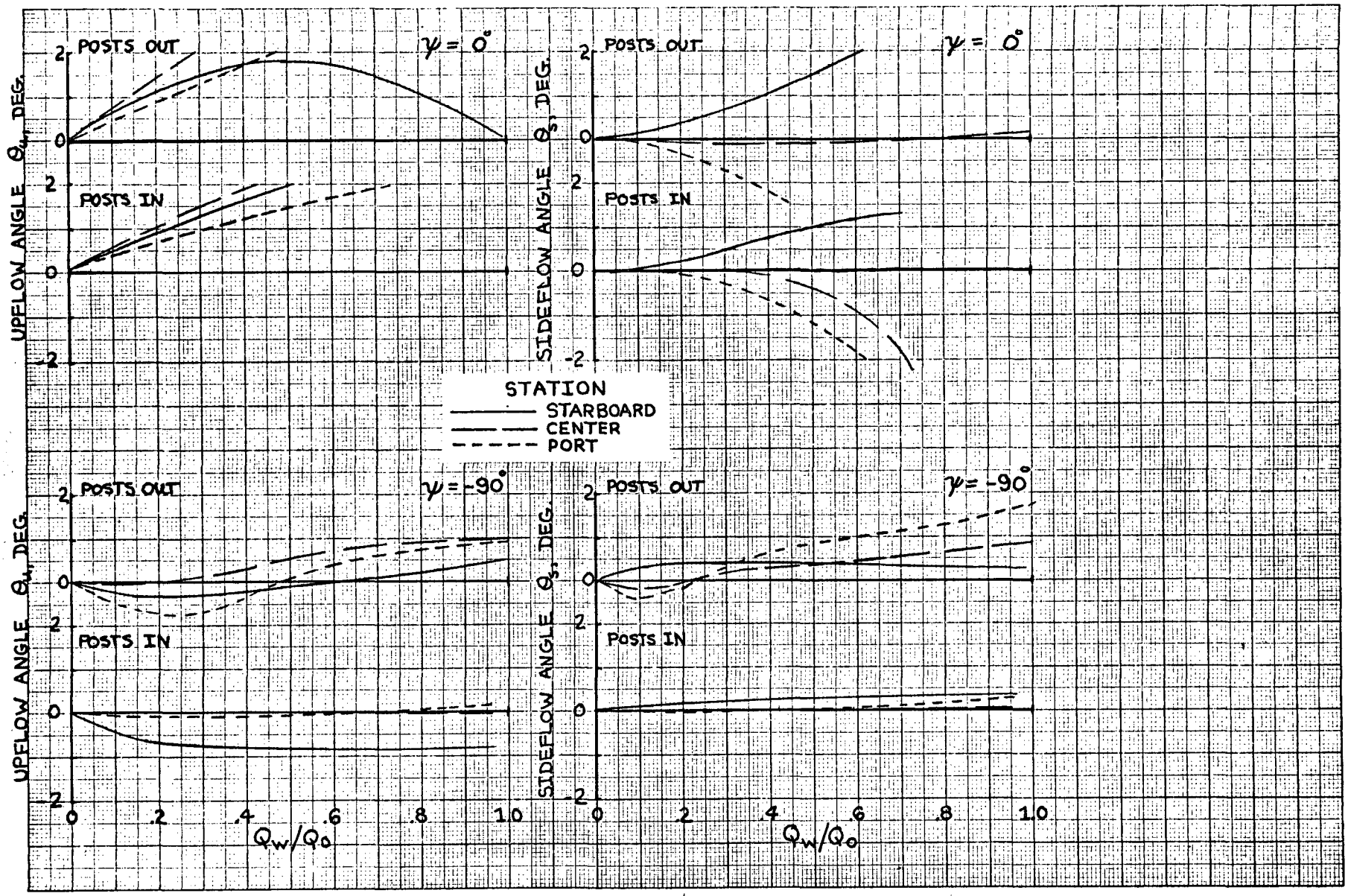

(a) Flow angularity.

Figure 26.- Effect of inlet roof support posts.

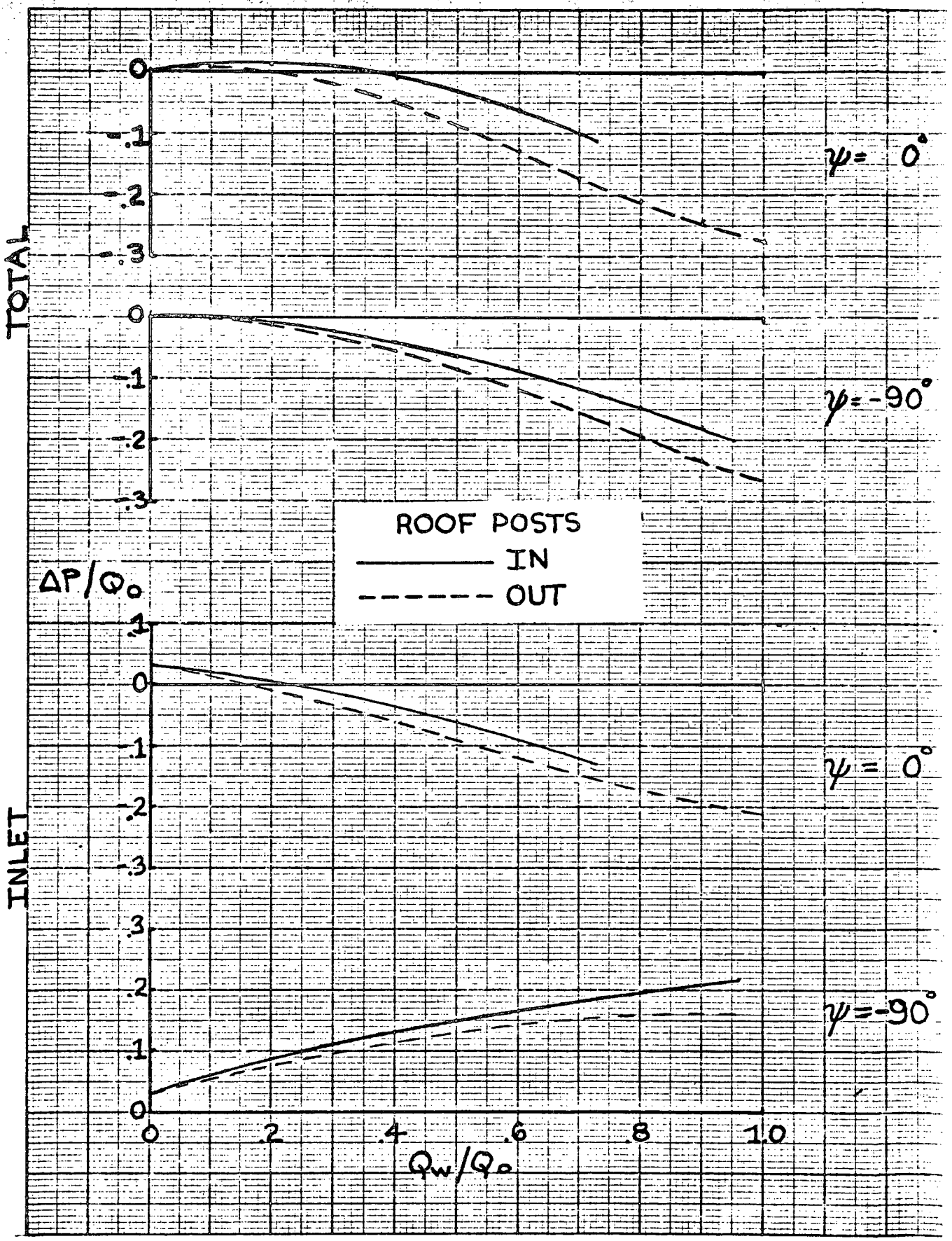

(b) Pressure losses.

Figure 26.- Concluded.

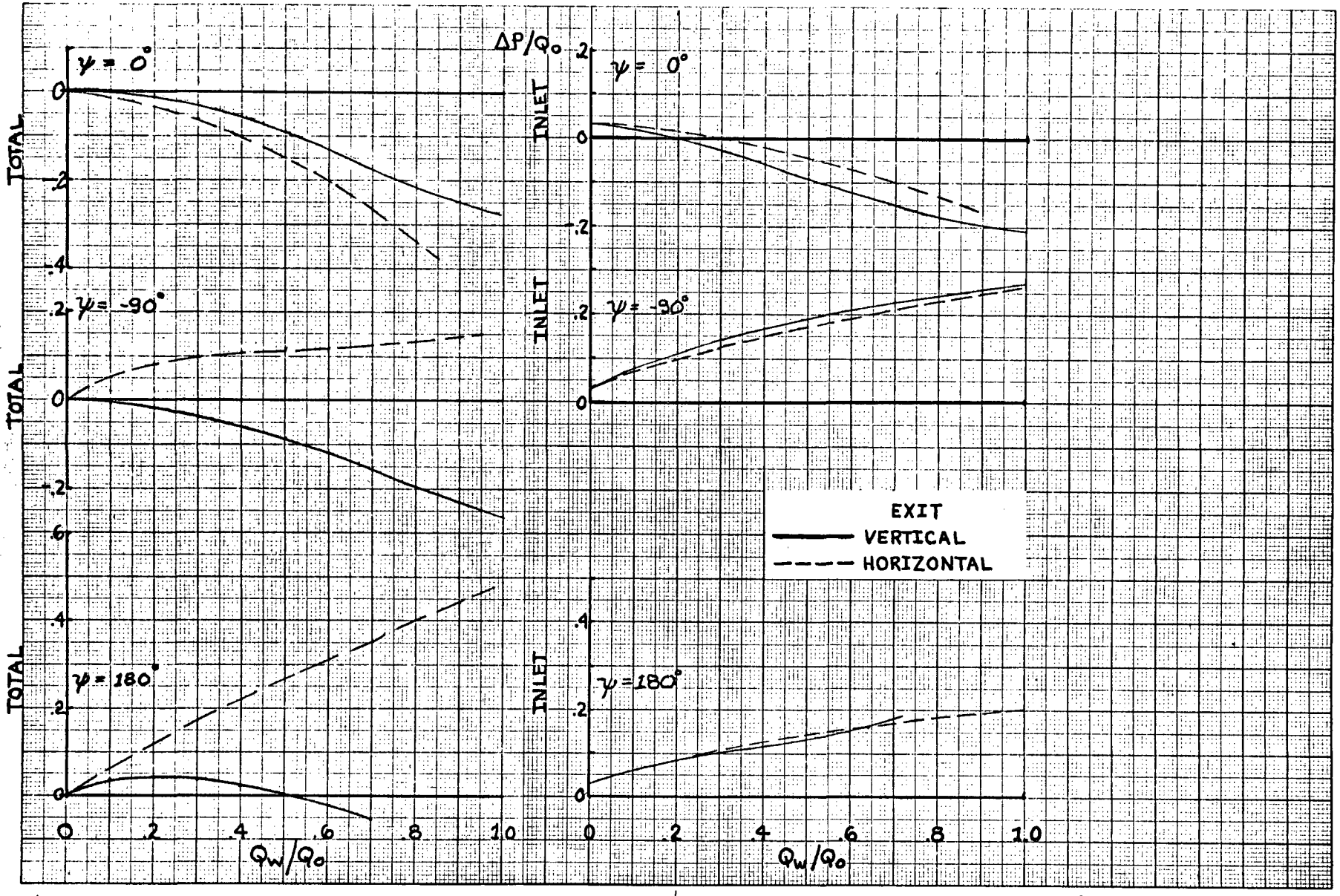

Figure 27.- Effect of exit type.

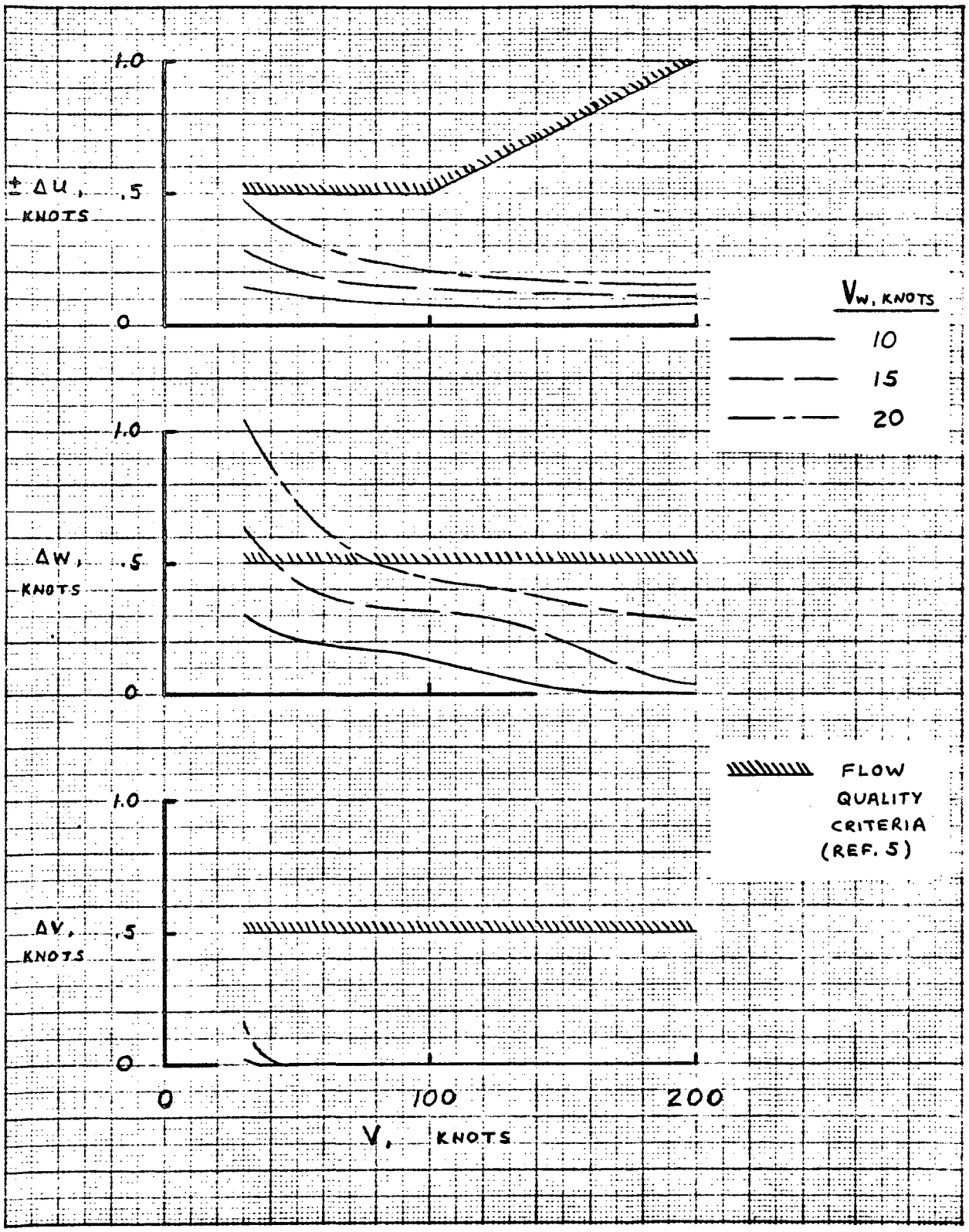

(a) Effect of wind magnitude; $\psi = 0°$.

Figure 28.- Flow quality evaluation for basic configuration.

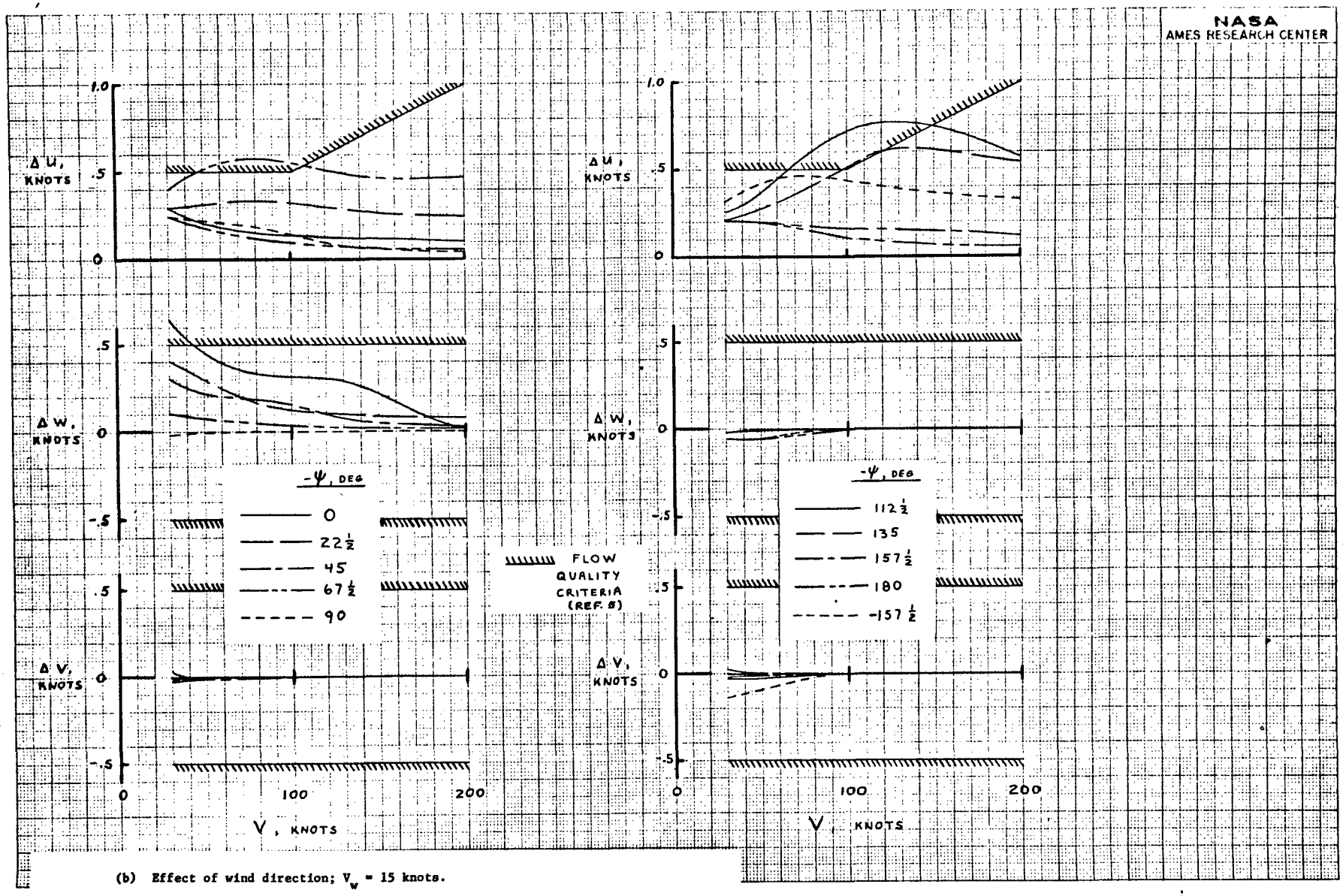

(b) Effect of wind direction; V_w = 15 knots.

Figure 28.- Concluded.